KU LEUVEN

FACULTEIT INGENIEURSWETENSCHAPPEN

Probit function analysis of blast effects on human beings

The Flemish 40 mbar overpressure criterion

ir. Jeroen Debroey

Thesis submitted for the degree of Master of Science in Safety Engineering, option Prevention

Thesis supervisor:
dr. ir. Filip Van den Schoor

Assessors:
Prof. dr. ir. John Vantomme
Prof. ir. Jan Van Peteghem

Academic year 2015 – 2016

Preface

Although writing my master's thesis has surely been an exacting exercise, lonesomely performed after my professional duties and parental activities, it can under no circumstances be considered as an individual achievement.

I owe indeed a debt of gratitude to quite a number of people. Some of them have enabled me to dedicate sufficient time to fulfil the task, others have excited me intellectually to pursue perfection, still others have enthusiastically encouraged me on the sidelines. Supported by all these contributions, I am able to proudly present to you, respected reader, this master's thesis on secondary blast effects on human beings.

In the first place, I would like to express my sincere gratitude to dr. ir. Filip Van den Schoor, promoter of this master's thesis. His fascinating classes on consequence modelling have incited me to explore this topic more thoroughly, and his readiness to follow up on my research has encouraged me to aim for the moon.

Special acknowledgement goes to Prof. dr. ir. John Vantomme, Head of the Civil and Materials Engineering Department of the Royal Military Academy. Due to his intervention, I was able to enrol in the Advanced Master programme of KU Leuven, allowing me to enlarge my skills in the field of Safety Engineering and Prevention. I am proud that he accepted to join in as an assessor for my master's thesis. As such he gave me the green light to organise a real scale explosion campaign with human resources, logistic means and financial support from his Department.

I cannot cite all personnel involved during the explosion testing for there are too many. But it goes without saying that I am indebted to all of them for their contribution to the successful outcome. I do thank Bruno, Bachir and Peter (COBO), Elie and Alain (ABAL), and Jan and Mark (CC R&A) explicitly and sincerely for sharing their experience and expertise with me.

Completing this work would have been all the more difficult were it not for the support and friendship provided by my colleagues at the Laboratory of Materials. I would particularly like to thank my direct superior, Prof. dr. ir. Luc Rabet, for his patience and credit. I will always acknowledge what a pleasure and privilege it has been for me to work as his teaching assistant and intimate during my term at the Royal Military Academy.

Finally, and most importantly, I would like to express my deepest gratitude and admiration to my beloved wife. Dear Laurence, I can only imagine the trying times you had to go through during your last months of pregnancy with our second baby girl and your first months as a mother of two while dad was spending most of his free time behind his laptop. Therefore, this master's thesis is as much your achievement as it is mine, if not more. I lovingly dedicate it to you as a symbol of appreciation for all the efforts and sacrifices you have unconditionally made, so that I was able to complete this assignment in the best possible conditions.

ir. Jeroen Debroey
Leuven, June 2016

Abstract

Large-scale industrial premises conducting potentially hazardous operations within the EU are required to quantitatively assess the external human risk they create, in compliance with *Seveso-III-Directive 2012/18/EU*.

This research focusses on the Flemish probit function that is used to estimate lethal response to sudden overpressure caused by an explosion. It is published by the Safety Reporting Division of the Flemish Department of Environment, Nature and Energy.

Although its use is mandatory, the true origin of the Flemish probit function is only vaguely described. In this master's thesis, the hypotheses that were made during its development are successfully traced.

In the low overpressure region, personal harm from window breakage is the essential injury mechanism that is considered. In the high overpressure region, fatalities from structural collapse become more likely, resulting in a gradual shift in the injury mechanism.

In order to be able to evaluate the pertinence of the 1 % probability of lethal injury criterion, associated with an overpressure of 40 mbar, methods are reviewed to predict the blast resistance and failure mechanisms of window glazing.

In order to comprehend the potential harm from flying glass and structural debris, injury models are reviewed for skin penetration, blunt trauma and skull fracture.

It is concluded that the original assumptions of the Flemish probit function are rather conservative, compared to modern circumstances. A tentative modification is therefore suggested.

As the process industry would benefit from a substantiated mitigation of the current overpressure criterion, it could be worthwhile to bring the findings of this master's thesis to the attention of the Safety Reporting Division of the Flemish Department of Environment, Nature and Energy.

List of symbols

Latin symbols upper-case

A	surface area	m^2
A_f	fragment presented area	m^2
B	bending stiffness of a plate (cf. equation 3.17)	N·m
C_1,C_2	constants for linear curve fit	-
C_D	drag coefficient	-
D	dynamic strength of windows	Pa
Du	ductility ratio	-
E	YOUNG's modulus of elasticity	Pa
E_λ	energy of a photon with wavelength λ	J
F	cumulative frequency of accident scenarios involving at least N fatalities	p.a.
$F(t)$	force associated with pressure history $P(t)$	N
F_0	force associated with ambient pressure P_0	N
F_{max}	force associated with dynamic peak load P_{so^+}	N
F_{st}	distributed static force	N
G	shear modulus	Pa
ΔH_x	combustion or explosion heat of substance x	$J \cdot kg^{-1}$
I	impulse associated with force F	N·s
$\bar{I}$	scaled impulse (w.r.t. P-I diagram)	-
K	linear spring stiffness	$N \cdot m^{-1}$
$K(z)$	non-linear spring stiffness	$N \cdot m^{-1}$
K_c	fracture toughness	$Pa \cdot m^{1/2}$
K_{Ic}	plain strain fracture toughness (mode I)	$Pa \cdot m^{1/2}$
L_w	blast wavelength	m
M_i	Mach number of incident wave	-
N	number of fatalities	-
$\mathcal{N}(0,1)$	standard normal distribution	-
$P(t)$	pressure i.f.o. time	Pa
$\bar{P}$	scaled pressure (w.r.t. P-I diagram)	-
P_0	ambient pressure	Pa
P_r	reflected (over)pressure	Pa
P_s	incident (over)pressure	Pa

P_{so^+}	side-on overpressure of positive phase	Pa
P_{so^-}	side-on overpressure of negative phase	Pa
P_{st}	static pressure due to static force F_{st}	Pa
Pr	probit value	-
Q	dynamic wind pressure	Pa
Q_D	dynamic drag pressure	Pa
Q_s	peak dynamic wind pressure (cf. equation 2.6)	Pa
R	radial stand-off distance	m
$\bar{R}$	scaled stand-off distance ($= Z$)	$\mathrm{m{\cdot}kg^{-1/3}}$
S	(localised) static strength (i.e. pressure at failure)	Pa
S_{center}	pressure in the center of a failing window pane	Pa
S_{corner}	pressure in the corner of a failing window pane	Pa
T	absolute temperature	K
T_g	glass temperature	K
T_m	melting temperature	K
U	shock velocity	$\mathrm{m{\cdot}s^{-1}}$
V	volume	$\mathrm{m^3}$
W_x	charge weight of explosive substance x	kg
Y	geometrical constant for fracture toughness K_c	-
Z	scaled stand-off distance ($= \bar{R}$)	$\mathrm{m{\cdot}kg^{-1/3}}$

Latin symbols lower-case

a	characteristic length of a crack, or	m
	ply width (or longest dimension)	m
a_c	critical crack length for failure	m
b	Friedlander's waveform parameter, or	-
	ply height (or shortest dimension)	m
c	speed of sound in vacuum	$\mathrm{m{\cdot}s^{-1}}$
d	ply thickness	m
d_a	air space thickness	m
d_{eq}	equivalent ply thickness	m
d_i	inner ply thickness	m
d_l	interlayering ply thickness factor	-
d_o	outer ply thickness	m
e	Euler's number	-
f_1	lowest (first mode) natural frequency	$\mathrm{s^{-1}}$
f_i	accident frequency	p.a.
f_n	natural frequency	$\mathrm{s^{-1}}$
g	constant of gravitational acceleration	$\mathrm{m{\cdot}s^{-2}}$
h	Planck's constant	J·s
i	impulse	Pa·s
$\bar{i}$	scaled impulse	$\mathrm{Pa{\cdot}s{\cdot}kg^{-1/3}}$

i_{s^+}	specific impulse of positive phase	Pa·s
i_{s^-}	specific impulse of negative phase	Pa·s
k_r	reflection coefficient (cf. equation 2.7)	-
m	mass	kg
n	refractory index	-
n_i	number of fatalities associated with an accident	-
p	probability	-
p_f	probability of failure	-
p_h	probability of being hit	-
p_i	probability of injury	-
p_p	risk mitigation factor	-
p_{tot}	probability of injury due to structural failure	-
r	radius of spherical charge	m
t	time	s
$\bar{t}$	scaled time	$\mathrm{s{\cdot}kg^{-1/3}}$
t_{0^+}	duration of positive phase	s
t_{0^-}	duration of negative phase	s
t_a	arrival time	s
t_d	duration of linear decay	s
t_{max}	time at maximum dynamic displacement	s
v	velocity	$\mathrm{m{\cdot}s^{-1}}$
v_0	impact velocity	$\mathrm{m{\cdot}s^{-1}}$
v_{50}	ballistic limit	$\mathrm{m{\cdot}s^{-1}}$
v_D	drag velocity	$\mathrm{m{\cdot}s^{-1}}$
v_p	blast wind (particle) velocity	$\mathrm{m{\cdot}s^{-1}}$
z	score of standard normal distribution $\mathcal{N}(0,1)$	-
$z(t)$	(vertical) displacement i.f.o. time	m
$z_{max,dyn}$	maximum dynamic displacement	m
z_{st}	static displacement due to F_{max}	m
$\dot{z}(t)$	velocity	$\mathrm{m{\cdot}s^{-1}}$
$\ddot{z}(t)$	acceleration	$\mathrm{m{\cdot}s^{-2}}$

Greek symbols

α	thermal expansion coefficient	$\mathrm{K^{-1}}$
β	angle of incidence	°
β_{lim}	limit angle of incidence	°
γ	isotropic coefficient	-
$\delta(P_{st})$	deflection due to uniform static pressure P_{st}	m
δ_{cr}	critical deflection (cf. equation 3.15)	m
ϵ	strain	-
ϵ_{el}	elastic strain	-
ϵ_f	elongation at break	-

$\dot{\epsilon}$	strain rate	s^{-1}
ζ	Fourier series factor (cf. equation 3.10)	-
η	explosion yield factor	-
θ	angle subtended by a fragment	$^\circ$
λ	thermal conductivity	$W{\cdot}m^{-1}{\cdot}K^{-1}$
μ	dynamic viscosity	Pa·s
ν	Poisson's ratio	-
ρ	density	$kg{\cdot}m^{-3}$
ρ_D	spatial density of fragments	m^{-2}
σ	stress	Pa
σ_1,σ_2	principle (tensile) stresses	Pa
σ_c	critical stress for crack propagation	Pa
σ_f	fracture strength	Pa
σ_{fl}	flexural strength	Pa
σ_{UCS}	ultimate compressive strength	Pa
σ_{UTS}	ultimate tensile strength	Pa
σ_Y	tensile yield strength	Pa
τ	natural period of free vibration	s
χ	causative factor (cf. equation 4.6)	$J{\cdot}m^{-2}$
$\Psi(z)$	cumulative distribution function of $\mathcal{N}(0,1)$	-
ω_n	natural angular frequency	s^{-1}

Acronyms

AASTP	Allied Ammunition Storage and Transport Publication
ACMH	Advisory Committee on Major Hazards
AMINAL	*Administratie Milieu-, Natuur-, Land- en waterbeheer*
ANG	annealed glass
ASTM	American Society for Testing and Materials
BIN	*Belgisch Instituut voor Normalisatie*
BLEVE	boiling liquid expanding vapour explosion
CEN	European Committee for Standardization
`ConWep`	conventional weapons effects calculations from TM5-855-1
CWE	conventional weapons effects
CPIC	continuous probability of injury criterion
DoD	U.S. Department of Defence
DLF	dynamic load factor (cf. equation 3.7)
ECS	energy consumption survey
EPR	explosion pressure resistance
EVA	ethylene-vinyl acetate
EXR	explosion resistance - range test
FEM	Finite Element Method
`FRAGHAZ`	fragment hazard computer programme
FSL	facility security level

FTG	fully tempered glass
GSA	U.S. General Services Administration
HC	hydrocarbon
HE	high explosive
HOB	height of burst [m]
HSE	U.K. Health and Safety Executive
HSG	heat-strengthened glass
IBD	inhabited building distance
IGU	insulating glass unit
INERIS	*Institut National de l'Environnement et des Risques*
IRC	iso-risk contour
ISC	Interagency Security Committee
ISO	International Organisation for Standardization
LAEE	Laboratory for Analysis of Effects of Explosions
LNE	*Leefmilieu, Natuur en Energie*
LOC	loss of containment
MSIAC	Munitions Safety Information Analysis Center
NBN	*Bureau voor Normalisatie*
PGS	*Publicatiereeks Gevaarlijke Stoffen*
PML	Prins Maurits Laboratory
PTSD	post traumatic stress disorder
PVB	polyvinyl butyral
QRA	quantitative risk analysis
RMA	Royal Military Academy
RPT	rapid phase transition
SDOF	single-degree-of-freedom
SES	socio-economic survey
SIF	stress intensity factor [$Pa \cdot m^{1/2}$]
SLG	soda-lime-silicate glass
SWA	*Samenwerkingsakkoord*
TNO	The Netherlands Organisation of Applied Scientific Research
UFC	Unified Facilities Criteria
VCE	vapour cloud explosion
WBDG	Whole Building Design Guide

Conversion factors metric $\leftrightarrow$ U.S.

Mass	1 kg	=	2.20462 lb	1 lb	=	0.4535929 kg
Length	1 m	=	3.28083 ft	1 ft	=	0.3048 m
	1 mm	=	0.0393701 inch	1 inch	=	25.4 mm
Velocity	1 $m \cdot s^{-1}$	=	3.28083 $ft \cdot s^{-1}$	1 $ft \cdot s^{-1}$	=	0.3048 $m \cdot s^{-1}$
Force	1 N	=	0.2248089 lbf	1 lbf	=	4.448222 N
	1 kN	=	0.2248089 kips	1 kip	=	10^3 lbf
Energy	1 J	=	0.7375597 ft-lbf	1 ft-lbf	=	1.355818066 J
Pressure	1 kPa	=	0.1450377 psi	1 psi	=	6.8947570 kPa
	1 bar	=	14.50377 psi	1 psi	=	0.068947570 bar
Impulse	1 kPa·ms	=	0.1450377 psi·ms	1 psi·ms	=	6.8947570 kPa·ms

---

Source: MAYS et al. (2009) [43] pp. 323 (appendix D)

Table of contents

There can be no greater legacy than saving lives.

Leon E. Panetta
U.S. Secretary of Defence, 2012

Chapter 1

Introduction

The continuous endeavour for technological innovation and progress has led to the existence of an inexhaustible list of potential anthropogenic hazards. The discipline of Safety Engineering consequently covers a considerable set of safety topics, including personal health considerations, environmental impact, economic loss and structural integrity issues. Its rationale consists basically in the determination of the most efficient way to effectively eliminate or reduce to an acceptable level the risks associated with hazardous unit operations and equipment. This is achieved by performing an iterative optimisation process, formally known as a risk assessment.

The practical output of a risk assessment consists of an enumerated list of the hazards identified in relation to their likelihood to cause harm and the extent thereof. This is evaluated against criteria of acceptance. Risk reducing strategies are then developed if needed.

The systematic application of risk assessment techniques, in combination with top management practices to participate in loss prevention in its broadest sense, is referred to as risk management. The successive steps of the risk management process are illustrated in figure 1.1 on page 1.

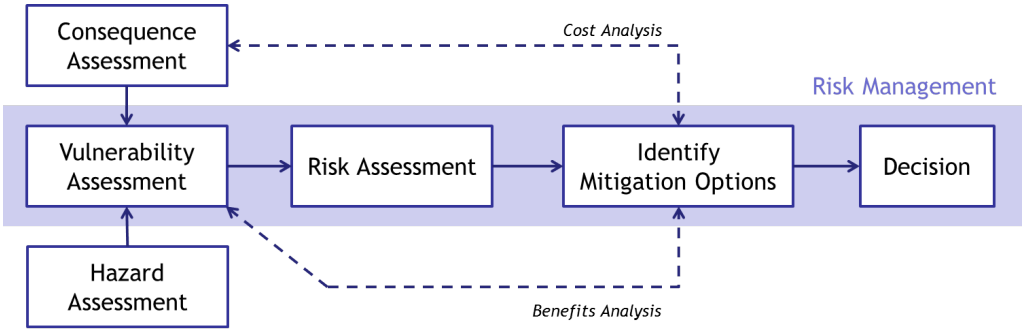

Figure 1.1: Risk management process [24]

Two important items can hinder or at least influence the risk management process.

a. The first item obviously concerns company budget allocated to safety. Cost-benefit analysis is quite narrowly connected to any risk assessment study. Clearly, finding a suitable compromise between effectiveness and efficiency can be challenging and will sometimes put a spanner in the works of the safety department.

b. The second item is related to the applicable law. Companies performing hazardous activities are obliged to report about the risks associated with their activities. They need to give proof of legal compliance in order to receive a permit to operate. This means that regulations exist which quantitatively stipulate the maximum allowable risk that is still considered to be acceptable by the public. These legal targets are referred to as risk acceptance criteria. Risk acceptance criteria are expressed for two types of risks, namely location-based (or individual) risk and societal (or group) risk, and always pertain to persons external to the company (in a physical sense). Hence, the term external human risk is more generally applied to cover each of these two types of risk.

QRA in Flanders

The aim of a quantitative risk analysis or QRA is to generate numerical predictions for the external human risk associated with industrial activities. For the scope of this master's thesis, QRA application must be situated in the frame of the European *Seveso-III-Directive 2012/18/EU* [61], which has repealed the *Seveso-II-Directive 96/82/EC* since June 1, 2015.

Seveso-III [61] principally aims to prevent major accidents involving dangerous substances. However, as accidents may nevertheless occur, it also aims at limiting their possible consequences. It covers establishments where dangerous substances may be present (e.g. during processing or storage) in quantities above a certain threshold. Depending on the amount of dangerous substances present, establishments are categorised in lower- and upper-tier establishments. Logically, the latter are subject to more stringent requirements.

One of the more stringent requirements for upper-tier establishments is the delivery of a safety report (cf. Art. 10 of *Seveso-III* [61]). One of the purposes of such a safety report is to demonstrate that major-accident hazards and possible major-accident scenarios have been identified and that the necessary measures have been taken to prevent such accidents from happening and to limit their consequences for human health and the environment. Practically this means that external human risk needs to be determined quantitatively as a combination of the estimated frequency of an accident with the likelihood that this accident will lead to a particular effect outside the fence of the establishment following a specific scenario.

In Belgium, translation of the European Directive to national legislation is assured by means of a document entitled *Samenwerkingsakkoord (SWA)*. *SWA3*, which pertains to *Seveso-III* [61] and must as such succeed and replace *SWA2*, was officially published on August 20, 2015 *(BS 54074)*. The approval process, involving the Federal government and the three Regional governments, has entered its final phase. Meanwhile, *SWA2* is still in force and transitional measures apply.

Both *SWA2* (Art. 12) and *SWA3* (Art. 8) include the upper-tier operator's obligation from *Seveso-III* [61] to produce a safety report. The competent authority responsible of ensuring that all regulations of the Directive are respected is situated on a regional level. In Flanders this is the Safety Reporting Division of the Department of Environment, Nature and Energy (Dept LNE).

Clearly, the performance of a full QRA for an upper-tier establishment can be a rather extensive activity. In order to avoid time-consuming QRA studies of accident scenarios with limiting effects, selection criteria exist that dissociate between so-called relevant scenarios and scenarios which can be ignored in the external human risk assessment. In Flanders, a scenario is considered as relevant from an external human risk point of view when its effect outside the installation's premises is at least equal to a 1 % lethal response. This must be assessed in three ways as will be explained further in this section.

In figure 1.2 on page 3, the sequence of a full QRA is presented schematically. Notice the presence of the 1 % lethal response threshold adhered to in Flanders in order to limit the number of accident scenarios that have to be developed in detail. The different items of the scheme will be discussed in this section, and particular emphasis will be put on the situation in Flanders. As an exception, the initial step, which is the hazard identification is not elaborated below. Logically, any quantitative risk analysis will first explore which installations contain some form of dangerous products, capable of causing harm upon uncontrolled release, and perform brainstorming sessions to determine the possible accident scenarios that can be associated with these installations.

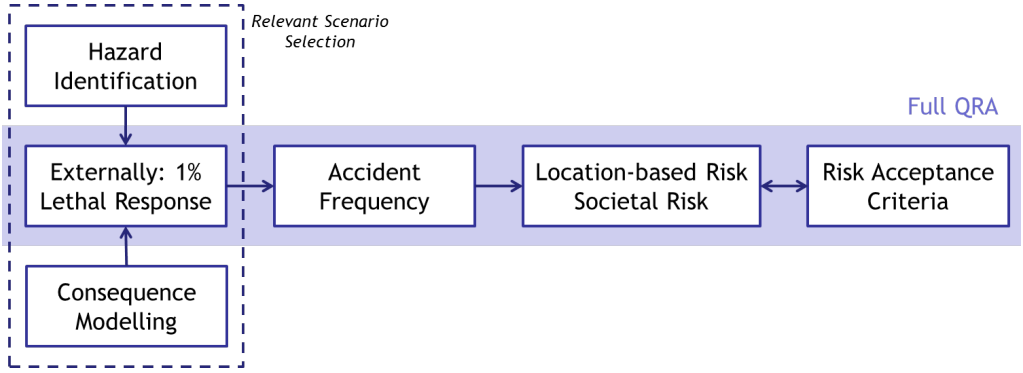

Figure 1.2: Full QRA process for external human risk in Flanders (www.lne.be)

Consequence modelling

The consequences of the accident scenarios identified are calculated in detail using consequence models. Escalation scenarios, accounting for possible event changes in time, give rise to deviations in the consequence outcome. This is best seen from the scheme in figure 1.3 on page 4 which sums up the successive steps in the consequence modelling process. It originates from a given release scenario and results in an estimation of the adverse effects to humans (or to infrastructure or to the environment). If the latter is assessed outside the installation's premises, it can be compared to the 1 % lethal response scenario selection criterion adhered to in Flanders.

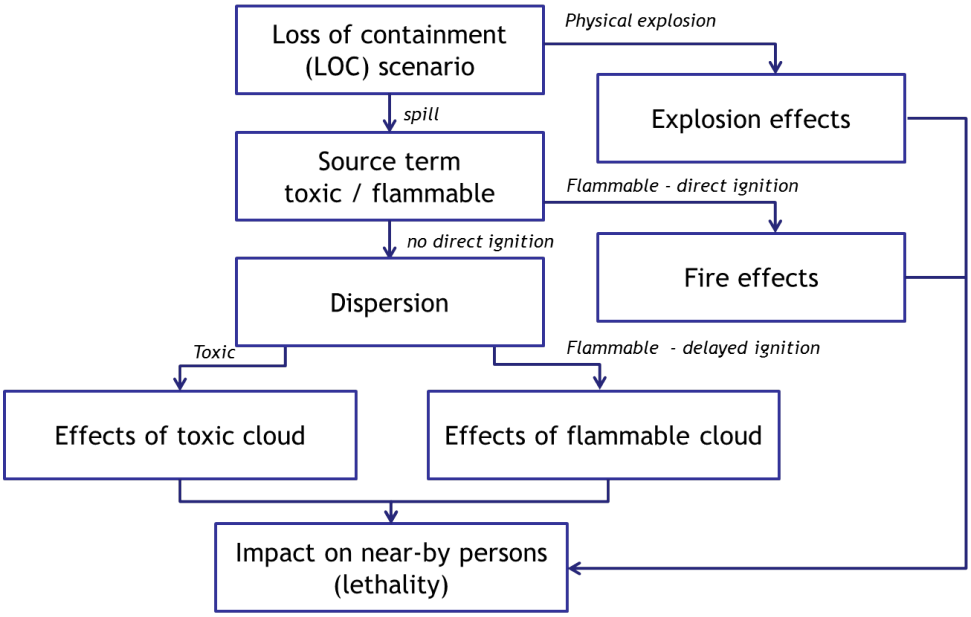

Figure 1.3: Successive steps in the consequence modelling process [76]

Loss of containment scenario describes the circumstances of a release (e.g. position and dimensions of the orifice and maximum duration of the release).

Source term modelling covers the quantity and physical properties of a discharge expected for a given loss of containment scenario.

Dispersion modelling predicts the dispersion and dilution with time of a plume, jet or cloud in the surrounding air taking into account the release momentum, buoyancy, atmospheric turbulence, terrain characteristics, wind speed and wind direction. In the case of a toxic release, this means the extent of a plume with a specific harmful concentration is estimated. For flammable gases, the range is determined where the upper and lower flammability limits are reached.

Fire modelling predicts the flame characteristics and the heat release rate of a fire event such as a pool fire or a jet fire.

Explosion modelling predicts the shock wave properties at a given location away from the burst center of a physical or a chemical explosion.

Damage modelling leads to the determination of the lethal response to the physical effects (e.g. toxicity, heat radiation, overpressure, fragmentation) of a major accident. Other consequences such as structural damage or a specific non-lethal response could be the subject of damage modelling as well. Probit functions are a popular tool in QRA to express stochastic cause-effect relations.

The probit function

The harm caused by an industrial accident, be it personal, structural, environmental, economical even, will always be probabilistic of nature. Indeed, both cause and effect are governed by a vast set of variables and many of them are difficult to control or to assess. After all, no incident is identical really, nor is a plant lay-out, let alone a human being. Consequence modelling therefore relies on a number of hypotheses, based on accident investigation reports and experimental field work, on what the probability for damage of some kind might be under particular circumstances.

From the assumptions that the response to a stimulus can only take two values (e.g. fatality: yes or no) and obeys a normal distribution, the use of so-called probit functions or probability unit functions has become a widespread method in QRA to relate damage being less than or equal to a given definition to a probability.

A probit function is a statistical construction where a probit value Pr which is coupled to a probability value p, is equal to the z-score of the cumulative distribution function $\Psi(z)$ of the standard normal distribution $\mathcal{N}(0,1)$ associated with the same probability value, given by the area under the bell curve delimited by the z-score. The idea to use it for dose versus response prediction was first introduced by Bliss (1934) and later carried forward by Finney (1947) who tabled probit values, while adding a value of 5, to avoid having to work with negative probits (cf. table 1.1 on page 6). The former solution is usually implemented in computational solvers whereas the latter solution is more popular when calculations are performed by hand using tabulated results.

In equations 1.1a, 1.1b, and 1.1c, the concept is shown for the 1 % criterion, where it is known from table values of $\mathcal{N}(0,1)$ that for a z-score of -2.33, a probability of 0.00990 is found, which is approximately equal to 1 %. According to Finney's adaptation, this corresponds to a probit value Pr equal to 2.67.

$$\Psi(-2.33) = 1 - \Psi(2.33) = 0.00990 \approx 1\% \tag{1.1a}$$

$$\text{(Bliss)} \quad Pr(1\%) = -2.33 \tag{1.1b}$$

$$\text{(Finney)} \quad Pr(1\%) = -2.33 + 5 = 2.67 \tag{1.1c}$$

Table 1.1: Finney's relation between probit value Pr and probability p

All values can be generated with Excel using the `Norm.S.Inv` function

%	0	1	2	3	4	5	6	7	8	9
0		2.67	2.95	3.12	3.25	3.36	3.45	3.52	3.59	3.66
10	3.72	3.77	3.82	3.90	3.92	3.96	4.01	4.05	4.08	4.12
20	4.16	4.19	4.23	4.26	4.29	4.33	4.36	4.39	4.42	4.45
30	4.48	4.50	4.53	4.56	4.59	4.61	4.64	4.67	4.69	4.72
40	4.75	4.77	4.80	4.82	4.85	4.87	4.90	4.92	4.95	4.97
50	5.00	5.03	5.05	5.08	5.10	5.13	5.15	5.18	5.20	5.23
60	5.25	5.28	5.31	5.33	5.36	5.39	5.41	5.44	5.47	5.50
70	5.52	5.55	5.58	5.61	5.64	5.67	5.71	5.74	5.77	5.81
80	5.84	5.88	5.92	5.95	5.99	6.04	6.08	6.13	6.18	6.23
90	6.28	6.34	6.41	6.48	6.55	6.64	6.75	6.88	7.05	7.33

%	0.0	0.1	0.2	0.3	0.4	0.5	0.6	0.7	0.8	0.9
99	7.33	7.37	7.41	7.46	7.51	7.58	7.65	7.75	7.88	8.09

Scenario selection criteria

For each potential accident in a major hazard establishment, consequence modelling can be performed in order to calculate the so-called maximum consequence distance wherein serious injuries or fatalities can occur. It is usually relating to a particular expected (accepted) mortality rate for people in the surroundings other than the employees of the establishment present inside the company's fence. At the maximum consequence distance, the external human risk is equal to zero.

In Flanders all accident scenarios within an upper-tier Seveso establishment provoking a 1 % expected lethal response outside its premises must be retained for a full QRA study in order to assess the associated location-based and societal risk. As announced, the determination of the lethal response to a particular exposure event involves assessment of three physical effects. Indeed, estimations of toxicity, heat radiation and overpressure need to be calculated. They are translated into lethality probabilities by means of imposed probit functions given in reference [22]. The definition for each of the three 1 % lethality thresholds is given below.

Toxicity In the event of a release of a toxic substance or mixture, consequence distances are calculated related to a lethal concentration level at which 1 % of the exposed population will die upon constant inhalation during a time lapse of 30 minutes.

Heat radiation In case of fire, the 1 % fatality criterion is related to the distance at which a heat flux of 9.8 kW/m^2 is felt during a 20 seconds exposure duration.

Overpressure The overpressure due to an explosion is considered fatal down to 40 mbar which is assumed to be the overpressure related to window breakage causing a 1 % lethality due to flying glass sheds.

The 40 mbar overpressure criterion is the subject of study in this master's thesis. It is based on a 1993 study by PROTEC ENGINEERING NV for the Flemish government, ordered by the Environmental Administration (AMINAL) [3]. AMINAL was disbanded in 2006, after which Dept LNE took over its responsibilities.

As external human risk relates to exposure outside the fence, where the intensity of the shock wave from the explosion has already significantly decreased, the criterion is founded on lower overpressure (structural) damage phenomena. This will be elaborated throughout this master's thesis in a logical way, starting with a description of the causative element in chapter 2, which is an explosion with its particular characteristics. Next in chapter 3 the structural effects this can have on a glass window are considered, in order to finally assess the lethal response related to the fragments which are projected upon window breakage in chapter 4.

Accident frequency calculation

All the scenarios which are considered relevant according to the scenario selection criterion in force must be accorded a frequency of occurring. This is expressed in terms of a number of events per annum and depends on different parameters including the failure frequency of the equipment involved in the release and the likelihood associated with the escalation of events (e.g. the wind direction towards a populated area or the presence of an ignition source).

In order to align these values which are rather difficult to evaluate, governmental institutions issue guidelines containing generic events, based on the current state of the art. In Flanders the *Handbook Failure Frequencies* (2009) [21] is imposed as the official source of reference.

The *Handbook* provides generic failure frequencies for a selection of loss of containment scenarios involving different types of failures for different types of equipment and activities. It also contains generic event trees representing typical consequential event scenarios subsequent to a spill, such as ignition and explosion of a flammable vapour cloud. Probabilities for such events to happen, dependent of the sensitivity group of the substance under consideration, are also included.

In a QRA in Flanders all of these generic events relevant to the installation under study must be taken into account and the given generic failure frequency must be used. Only if an installation that is not described in the *Handbook* should turn out to be relevant to external safety, it should be included in the QRA and given a well-founded failure frequency that needs approval from the Safety Reporting Division.

External human risk and risk acceptance criteria

Again, the consequence distance found through consequence modelling is considered against third parties around major hazard establishments so with respect to people in the surroundings other than the employees of the establishment present inside the company's fence. This resulting third parties risk is referred to as the external human risk and comprises two different types of risk, namely location-based risk and societal risk. The former indicates how far the risk extends outside the company's fence whereas the latter can be thought of as a measure for the amount of neighbouring people that would suffer from the event.

Location-based risk (or individual) risk is calculated as the risk that a person who is continuously present and unprotected at a given location will die as a result of an accident within a major hazard establishment. It is expressed in terms of risk per annum.

Location-based risk is represented using iso-risk contours (IRC) which visualise the geographical distribution of risk for the establishment in question. As such it can be used to assess whether the risk individuals are exposed to is acceptable for any of the locations where they may spend time, independently from whether people are actually present or not. A generic example is given in figure 1.4 on page 8.

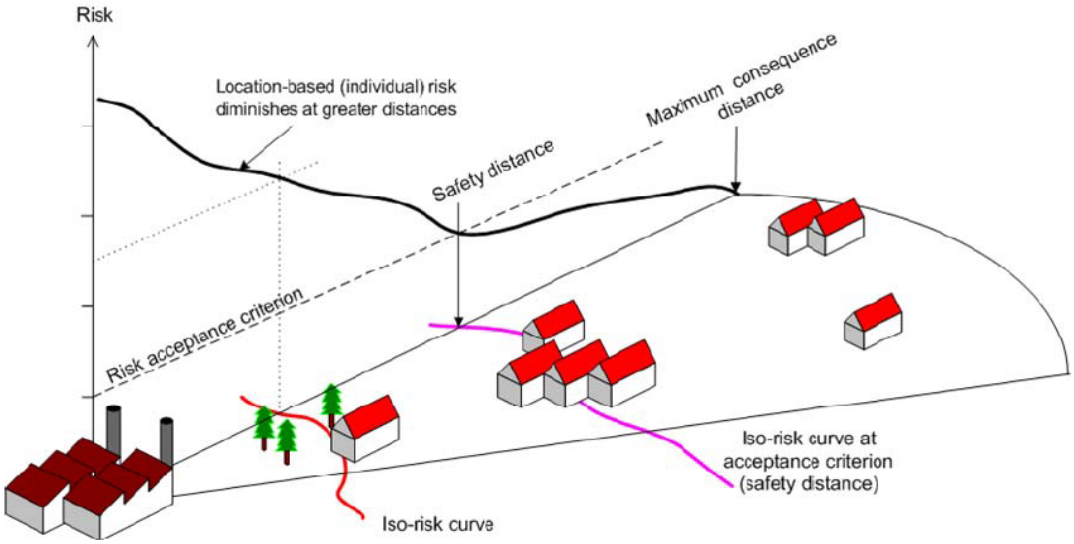

Figure 1.4: Example of iso-risk curves showing the distribution of location-based risk surrounding an establishment with respect to an acceptance criterion [23]

Criteria for location-based risk are used to determine areas which may not be used for residential or similar purposes. These are called risk zones. They further help to ensure that individuals are not exposed to excessive risk. The consequence distance where the acceptance criterion is met, is called the safety distance. In Flanders, three risk acceptance criteria for location-based risk are in force:

1a. A risk of 10^{-5} per year is accepted at the borders of the establishment.

1b. A risk of 10^{-6} per year is accepted for risk zones with a residential function.

1c. A risk of 10^{-7} per year is accepted for vulnerable sites such as schools and health care facilities.

Societal risk (or group) risk expresses the risk that a group of people is simultaneously exposed to the consequences of an accident. It is represented by means of a cumulative frequency consequence curve or $F - N$ curve visualising the relationship between the expected frequency f_i per annum of an accident scenario and the number of people n_i who will die as a result of this event.

Calculation of an $F - N$ curve takes into account the probability of a number of accident scenarios as well as the assessment of how many people might be exposed to consequences under these scenarios, based on population density (e.g. day/night situation or week/weekend regime), traffic circumstances and local protection (e.g. indoors or outdoors). In this way, the frequency F is the cumulative frequency of a type of accident involving more than N deaths.

Criteria for societal risk are used to ensure that locations where many people may assemble are not exposed to excessive risk of a major accident, even if they lie outside the risk zones. In figure 1.5 on page 10 a fictive $F - N$ curve as well as some interesting legal targets for societal risk are shown, including the following risk acceptance criteria imposed in Flanders:

2a. A risk of 10^{-4} per year is accepted for events with at least 10 fatalities.

2b. A risk of 10^{-6} per year is accepted for events with at least 100 fatalities.

2c. A risk of 10^{-8} per year is accepted for events with at least 1000 fatalities.

From acceptance criterion 2a and figure 1.5 (a) it follows that a societal risk of less than 10 fatalities is always tolerated in Flanders, no matter how high the likelihood for it to happen. On the other hand, if acceptance criterion 2c is studied using figure 1.5 (a) it is seen that a societal risk of more than 1000 fatalities can under no circumstances be tolerated.

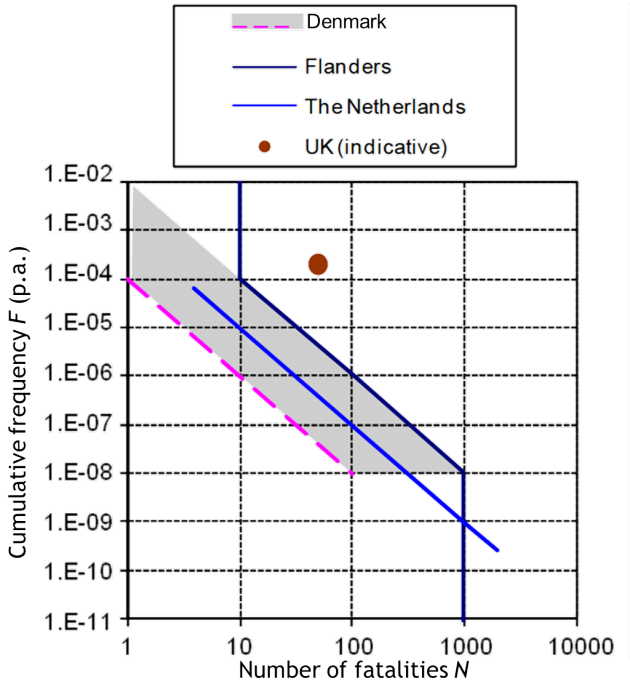

(a) Different societal risk acceptance criteria in Europe

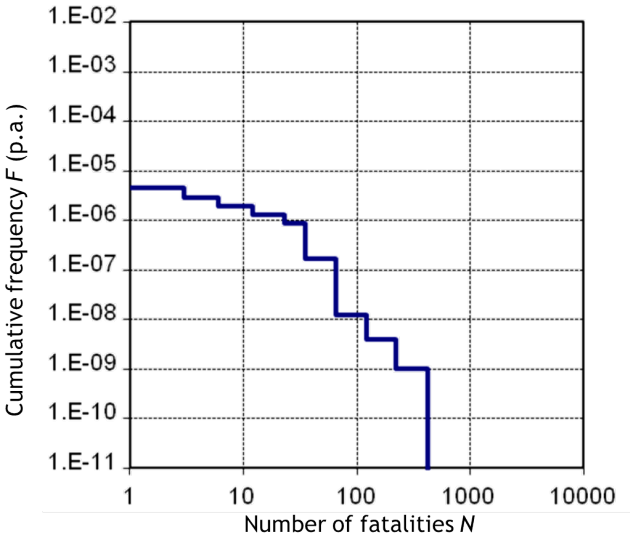

(b) Example of an $F - N$ curve

Figure 1.5: Graphical representation of societal risk [23]

Outline

This master's thesis consists of five chapters. Their mutual ordering respects the successive steps in the consequence modelling process as seen in figure 1.3 on page 4.

Chapter 1 provides background on the purposes to perform a quantitative risk analysis. It is seen that the European *Seveso-III-Directive 2012/18/EU* [61] obliges upper-tier establishments to deliver a safety report which includes calculations for the external human risk associated with the hazardous substances that are operated. In Flanders, the potential accident scenarios that must be submitted to a full QRA are those which engender a lethal response to the outside world of 1 % or more. By means of probit functions the lethal response is correlated with three physical effects, namely toxicity, heat radiation, and overpressure. The focus of this master's thesis lies with the probit relation that adheres a 1 % fatality to an overpressure of 40 mbar, associated with flying glass from breaking windows.

Chapter 2 introduces the explosion phenomenon in all its possible shapes. Gradually this is narrowed down to the idealised condensed phase chemical detonation in open air, characterised by the modified FRIEDLANDER wave form, which will be the explosion semblance mainly studied in this master's thesis. The most important explosion characteristics in terms of pressure-time history and release of energy are elaborated as they are needed to assess the destructive power of an explosion.

Chapter 3 is dedicated to the target material of the blast wave, which is glass. After thorough acquaintance with the physicochemical and mechanical properties of glass, the dynamic behaviour of window panes is studied. Some specific techniques are reported which are needed to account for the dynamic loading aspect of an explosion in the calculations and different solution models are given. Information on explosion-resistant glazing is included as well.

Chapter 4 discusses the lethal response of human beings to secondary fragments from a blast. Numerous models based on fragment mass and wounding ability are explored and compared to one another. This ultimately leads to the discovery of the assumptions made to establish the Flemish overpressure probit relation that includes the 1 % lethality prediction for a peak incident overpressure of 40 mbar. The probit function analysis of blast effects on human beings is concluded with a suggested modification based on selected best practice drawn from the different approaches studied.

Chapter 5 summarises the points of conclusion of this master's thesis regarding the history and actual legitimacy of the Flemish 40 mbar overpressure criterion, as well as a list of suggestions for the academic and legislative parties involved.

Additionally, it is worth mentioning that a real-scale experimental test campaign was organised by the Royal Military Academy (RMA) in support of this master's thesis. This opportunity imparted the author great knowledge and insight on the interaction mechanism between a blast wave and a modern window pane composed of single and double glazing. A separate report on the developed test protocol with a description of the results has been prepared for the RMA in the light of future research. In figure 1.6 on page 12 some images are shown in order to give the reader a small impression of this part of the study.

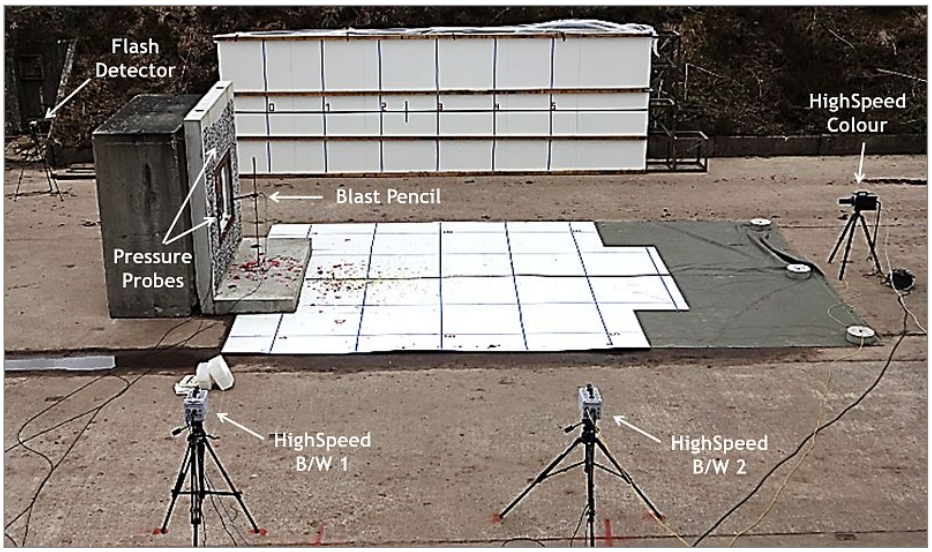

(a) Overview of the test set-up

(b) 0.100 kg C-4 at 3.33 m

(c) 0.155 kg C-4 at 4.24 m

Figure 1.6: Pictures taken during the experimental test campaign executed by the author in support of his master's thesis © RMA (2016)

References

[3, 10, 18, 20, 21, 22, 23, 24, 27, 58, 61, 76, 79]

Chapter 2

The explosion phenomenon

An explosion is generally defined as a violent release of energy, leading to a sudden increase in pressure which propagates to the surroundings in the form of pressure waves.

Explosions exist under many forms. It seems therefore appropriate to start this chapter with a brief introduction of the three main types of explosions. Their distinction is made by the underlying mechanism of the energy release being either physical, chemical or nuclear.

However it is clear that other parameters will influence the explosion behaviour as well. The velocity of the reaction front is a crucial one. It will dictate the nature of the explosion as being a deflagration or a detonation, which can be related to the brisance or the shattering effect of the explosion.

Furthermore, the surroundings the pressure waves are propagating to, will have an influence on the evolution of a pressure wave in time. Confinement creates reflections and turbulence leads to flame speed acceleration, two conditions able to change the nature of the explosion after its initiation.

Another significant feature to consider is the medium the pressure waves are propagating through. Underwater explosions or ground shock phenomena behave differently than the above ground explosion in open air where focus lies in this master's thesis.

2.1 Classification of explosions

The most straightforward approach to classify different types of explosions is to look at the origin of the energy which is being released. For ease of reference, a summary of the three main types of explosions is given in figure 2.1 on page 14.

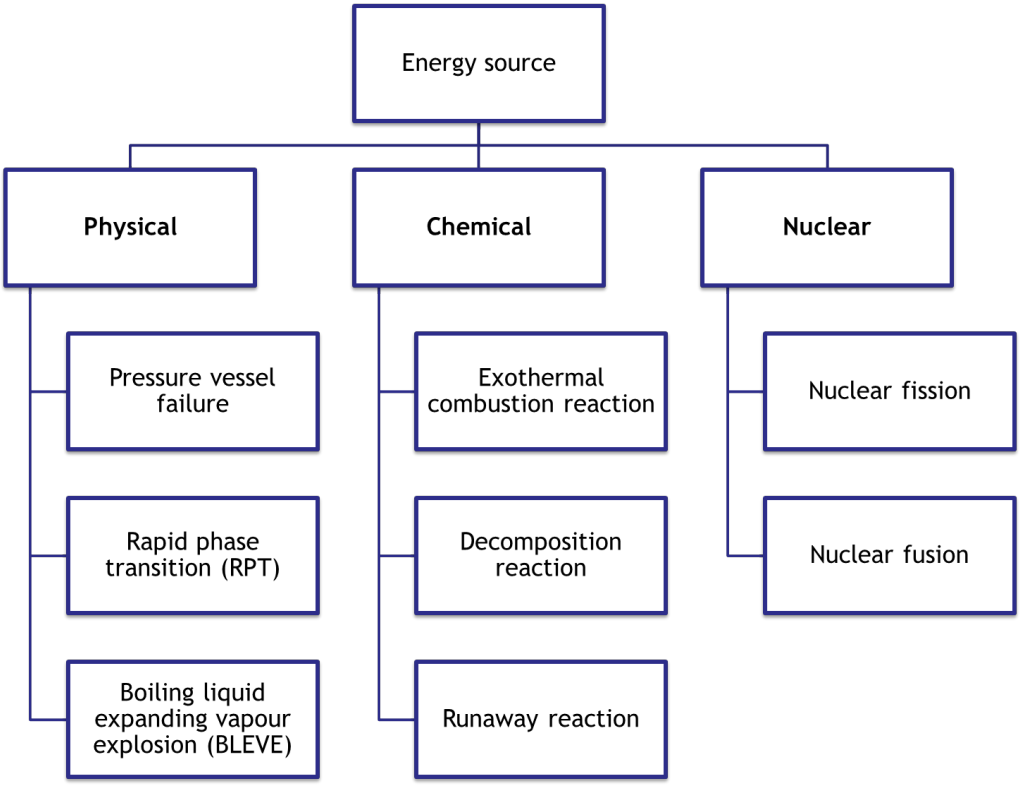

Figure 2.1: Explosion types [77, 78]

2.1.1 Physical explosions

For a first category of explosions, a large amount of internal energy is instantaneously released. This internal energy is due to the system's physical state.

Consider for instance a natural gas vehicle with a typical tank volume V of 75l containing compressed natural gas at a pressure P of 250 bar. Sudden vessel rupture would allow for the pressurized gas to expand to the environment, causing a so called physical explosion. In this example, the system's physical state is well intended, but the loss of vessel integrity is obviously not anticipated and should have been avoided.

Other situations exist where the initial physical state, which is considered as harmless, is disturbed by action from outside such as heating effect due to an external fire. The rapid phase transition of a superheated liquid and the phenomenon known as a boiling liquid expanding vapour explosion (BLEVE) are physical explosions where either a liquid or a pressure-liquefied gas all of a sudden exists above its boiling temperature, resulting in violent vapour production which can induce substantial pressure waves if set free.

2.1.2 Chemical explosions

When properly initiated, energetic materials undergo changes in chemical composition, creating expanding hot gases which are formed by the reaction products. This instantaneous release of chemical energy from a relatively small volume of reactant material can be viewed as an explosive event.

Chemical explosions include dust explosions and explosions due to the ignition of flammable gas clouds. These usually involve only rapid combustion or deflagration until the chemical reaction decelerates and eventually dies out. However if enough turbulence is created ahead of the combustion front, the reaction is likely to accelerate until a steady value has been reached. The combustion will then have developed to a detonation. It is noted that a condition of high confinement will give rise to higher initial reaction rates which could also result in detonating behaviour.

A second category of chemical explosions is associated with the energetic reaction of condensed phase chemicals, such as propellants and high explosives.

Propellants can be distinguished as the more energetic of the combustible materials. Needless to say that their main application lies within propulsive systems where they create a large amount of thrust upon deflagration. Propellants exist both in liquid (fuel) and solid (powder) form, or as a combination of both (gel). Propellants, as well as most of the light pyrotechnics, are referred to as low explosives after the rather low reaction rate, compared to the high explosives (HE).

High explosives are energetic materials which by their nature decompose so extremely fast that the chemical reaction process passes through the material at a supersonic speed. This gives rise to a shock front which is continuously nourished by the chemical energy that is being released. High explosives can be roughly grouped into two categories: military explosives and commercial explosives. Apart from their intended use, they are further distinguished by the fact that most commercial explosives exhibit non-ideal behaviour, in that their sensitivity and severity of explosion fall off rapidly with decreasing diameter and lack of confinement. Here sensitivity points to the ease of igniting. In this regard, high explosives are also often divided into primary explosives, which are easy to ignite, and secondary explosives, requiring an appropriate initiating charge of primary explosive. Some literature identifies a third group of even more insensitive explosives, called tertiary explosives, which rely on the explosive energy of a booster charge of secondary explosive to detonate.

The last category groups the thermal explosions. They originate from exothermic reactions which are either uncontrollable due to insufficient cooling capacity or not anticipated due to a lack of awareness of the chemical instability of the reactants used in the process. As temperature keeps rising, the reaction rate keeps growing, increasing the temperature even more until a runaway reaction is eventually established.

2.1.3 Nuclear explosions

The most devastating kind of explosions are the detonations which occur as a result of the rapid release of energy from a nuclear chain reaction.

Fission bombs work on the principle of induced fission. This is a reaction process where a very heavy nucleus, after absorbing additional light particles, splits into two or sometimes three pieces while releasing a large amount of reaction energy.

Nuclear fusion reactions where two light nuclei join to form a heavier one, with additional particles thrown off to conserve momentum, are currently not energetically viable. Thermonuclear weapons however, commonly referred to as hydrogen bombs, do realise (secondary) nuclear fusion reactions by using the energy from a primary nuclear fission reaction.

2.2 Explosion characteristics

After being introduced to the most common types of explosions which exist, one will surely comprehend that the characteristics of explosions can vary significantly, depending on their origin and evolution in time and space. Throughout this master's thesis, the study is mainly limited to chemical explosions. In this section, the most relevant variables required to define their effects are presented.

2.2.1 Reaction velocity

The reaction velocity is typically taken as an intrinsic property of a chemical substance. It mainly depends on the surrounding atmosphere and conditions wherein the substance reacts. There is a straightforward relationship between the reaction velocity and the significance of the effects as illustrated in figure 2.2 on page 16.

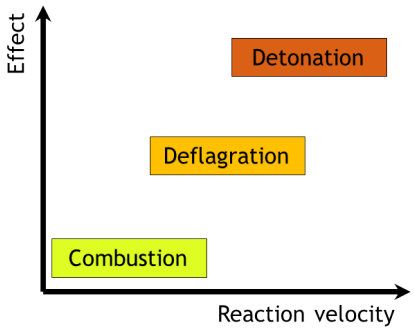

Figure 2.2: Explosion effects related to reaction velocity

Reaction velocity should be considered relative to the speed of sound of the medium the pressure waves are travelling in.

Low velocity combustion will only have negligible local effects which are mainly due to the heat release. The reaction does not alter surrounding conditions fast enough to create a pressure wave.

However, when combustion rates as high as tens of meters per second are reached, the effects to the surroundings become considerable. The combustion is now called a deflagration and it fits the definition of an explosion. A pressure front is indeed formed at some distance ahead of the reaction front. Away from the deflagration reaction, pressure waves with a rise time of some tenths of a second can be sensed.

At supersonic reaction velocity, the rise time of the pressure waves becomes so small that a sudden discontinuity front is observed. This is the leading shock front of compressed gases formed by a detonation. For ease of comparison, the pressure waves associated with a detonation are referred to as shock waves or blast waves.

Figure 2.3 on page 17 shows a standard pressure-distance profile some distance away from the explosion center for a deflagration and a detonation.

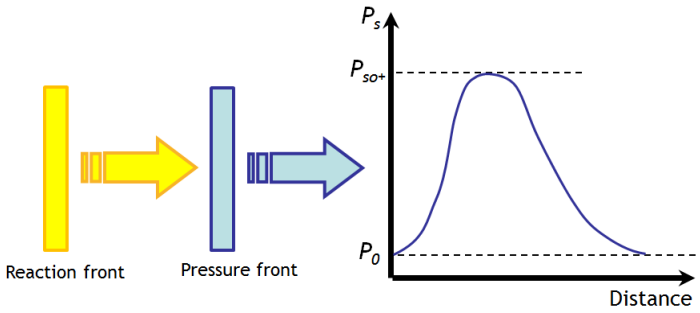

(a) Deflagration

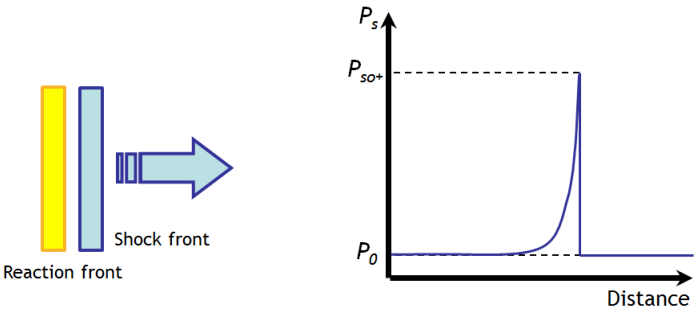

(b) Detonation

Figure 2.3: Pressure-distance shape following an explosion [77]

2.2.2 Pressure-time history of a blast wave

The focus of this master's thesis is further narrowed down to the effects from a blast wave related to a detonation. This choice is justified by the fact that consequence modelling is preferably applied to worst-case accident scenarios leading to the most stringent land use planning and development regulations related to the operation of the industrial activity at study.

Indeed, blast waves reach a significantly higher overpressure than pressure waves coming from a deflagration. They are further characterized by a subsequent zone of negative overpressure, due to the airy conditions at the center of the explosion.

The overall pressure evolution of the blast wave remains preserved over long distances from the burst point but vary in magnitude with distance. The maximum pressure in the blast wave decreases, and the length of time over which the blast pressure is above ambient, the positive phase duration, increases.

Consider a situation where a blast wave can travel in open air without surfaces nearby to interact with. For this simplistic detonation event known as a free-air burst, an idealized pressure-time profile at any incident location away from the explosion is predicted as shown in figure 2.4 on page 18. It is only observed under well-controlled experimental conditions.

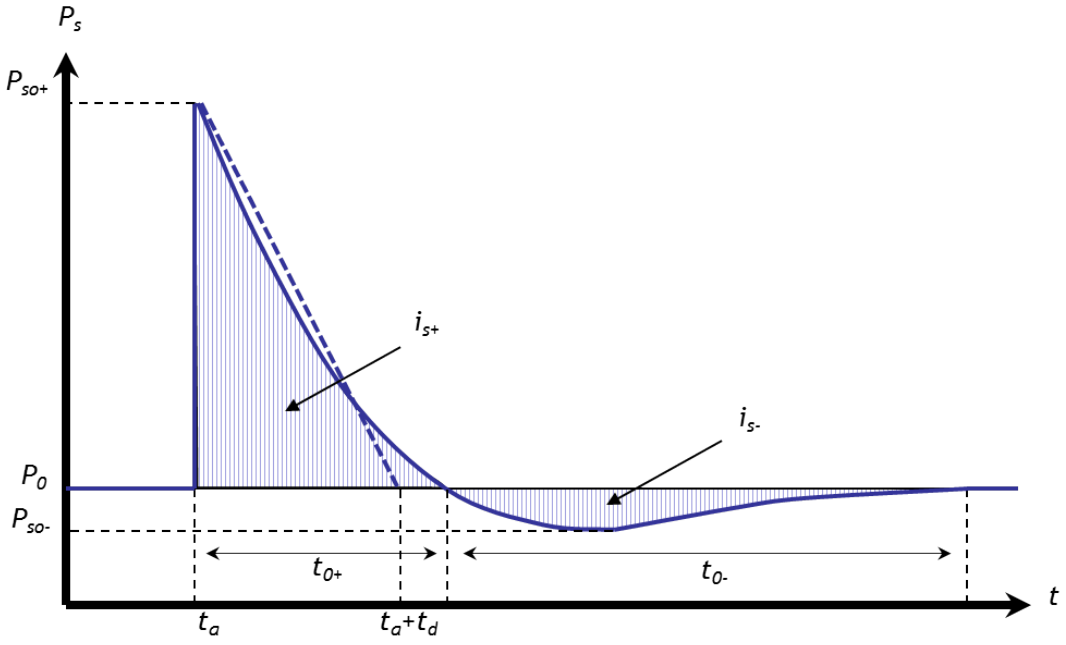

Figure 2.4: Ideal pressure-time history of a blast wave [11, 39]

In table 2.1 on page 19 the symbols associated with figure 2.4 are explained. These are fundamental characteristics, each playing a particular role in the analysis of blast wave interaction with structures or human beings.

Table 2.1: Pressure-time history parameters

Symbol	Description	Unit
P_0	ambient pressure	Pa
P_s	incident overpressure	Pa
P_{so^+}	peak (side-on) overpressure of positive phase	Pa
P_{so^-}	peak (side-on) overpressure of negative phase	Pa
t_a	arrival time	s
t_{0^+}	duration of positive phase	s
t_{0^-}	duration of negative phase	s
t_d	duration of linear decay	s
i_{s^+}	specific impulse of positive phase	Pa·s
i_{s^-}	specific impulse of negative phase	Pa·s

Different authors have aimed to fit the pressure profile of the positive phase of a free-air burst as a function of time (cf. Baker (1973) [6] pp. 5-6). To this end, the modified Friedlander equation 2.1 is commonly cited. It can be found in many technical manuals, including U.S. Defence documentation [69, 72] and E.C. Joint Research Centre documentation [64] related to explosion effects to predict pressure-time behaviour of energetic substances . The general use of the notion of Friedlander waveform as a synonym for an ideal blast wave confirms once more the importance of the Friedlander equation since its first introduction in 1946.

$$P_s(t) = P_{so^+}\left(1 - \frac{t}{t_{0^+}}\right)\mathrm{e}^{\left(-b\frac{t}{t_{0^+}}\right)} \tag{2.1}$$

The empirical decay coefficient or waveform parameter b must be considered as a property of the detonating substance. It is determined by use of experiments. In the modified Friedlander equation, the time variable t corresponds to a point in time relative to the arrival time t_a of the shock wave.

For reasons of simplification, assuming linear decay of pressure has become common of use in blast effect response calculations (cf. figure 2.4 on page 18). Analytically speaking, this means the exponential factor is withdrawn from equation 2.1 and the positive phase duration t_0 is adjusted to maintain true positive impulse i_{s^+}. The resulting triangularly shaped pressure-time history is then given by equation 2.2, where t_d corresponds to the duration of linear decay.

$$P_s(t) = P_{so^+}\left(1 - \frac{t}{t_d}\right) \tag{2.2}$$

2.2.3 Specific impulse

The impulse expresses both the magnitude and the duration of a blast wave, which explains its unusual units of (over)pressure and time. It corresponds to the surface area below the overpressure-time curve (cf. hatched zone in figure 2.4 on page 18) and can as such be determined using the integral function given in equation 2.3.

$$i_{s^+} = \int_{t_{0+}}^{t_a+t_{0+}} [P_s(t) - P_0]\,\mathrm{dt} \tag{2.3}$$

For the simplified case of a triangular load, the (positive) impulse is no more than the surface of the triangle with base equal to the duration of linear decay and height equal to the corresponding side-on overpressure as given in equation 2.4.

$$i_{s^+} = \frac{P_{so^+} \cdot t_d}{2} \tag{2.4}$$

2.2.4 Dynamic pressure

The destructive effects of a blast wave are frequently related to values of the peak overpressure. However, a subsequent pressure phenomenon called the dynamic wind pressure Q can be of importance as well. It is associated with the strong winds that accompany the passage of a blast wave, which exert forces on a structure that are quite analogous to those developed by natural winds. This drag effect can be thought of as a dynamic drag pressure Q_D acting on an object due to the velocity of the air moving past it. The dynamic pressure is therefore function of the drag coefficient C_D related to the object's shape, and of the kinetic energy of the air characterised by its density ρ and particle velocity v_p as expressed in equation 2.5.

$$Q_D = C_D \cdot Q = \frac{1}{2} \cdot C_D \cdot \rho \cdot v_p^2 \tag{2.5}$$

Blast wind forces however are transient in nature, and also may be of considerably greater magnitude than those developed by ordinary winds. For strong shocks (with $P_{so^+} > 500$ kPa, which is beyond the range of interest in this mater's thesis) the peak dynamic wind pressure Q_s is even larger than the peak (side-on) overpressure P_{so^+}. This can be demonstrated when solving equation 2.6 expressing peak dynamic wind pressure Q_s as a function of peak (side-on) overpressure P_{so^+}. This expression was first presented by Rankine & hugoniot in 1870 in a famous paper on theoretical shock front parameter prediction.

$$Q_s = \frac{5P_{so^+}^2}{2\,(P_{so^+} + 7P_0)} \tag{2.6}$$

2.2.5 Reflection with a surface

Different from the free-air burst which has already been introduced above as the idealized, unhindered semblance of a shock, the blast wave of an air burst undergoes reflections with a surface, usually the ground, before hitting a structure. The pressure which is felt by the surface is called the reflected pressure P_r and the resulting blast wave is then the reflected wave.

When the shock front impinges on a surface it does not bounce away directly, but rather is deflected so that it spurts along over the surface. This spurt effect takes the form of a shock approximately perpendicular to the surface and which is identified as a Mach stem. This is illustrated schematically in figure 2.5 on page 21 where the incident shock, the detached reflected shock, and the shock of the Mach stem are represented. Their intersection gives form to a so-called triple point.

From this simple drawing one can easily understand that a structure is subjected to a plane wave (uniform pressure) when the height of the triple point exceeds the height of the structure. For the Flemish 40 mbar requirement, applicable considerable distance away from the center of an explosion, it is reasonable to assume that the incident wave is a plane wave.

Mach stem arises at a given point in space away from the explosion, which is defined by the limiting angle of incidence β_{lim} between the incident shock and the reflecting surface. The incident shock is characterized by its Mach number M_i which is directly related to the limiting angle of incidence, as shown in figure 2.6 on page 22. The limiting angle of incidence in fact decreases with increasing incident blast wave velocity until a stabilisation of little under 40° is reached for $M_i = 1.47$.

Pressure-time histories of reflected shock waves are similar to the incident ones, but the peak reflected overpressure and specifc impulse are sensibly higher. Mathematical solutions for reflected wave properties in relation to the incident wave characteristics can for instance be found in Kinney & Graham (1985) [39].

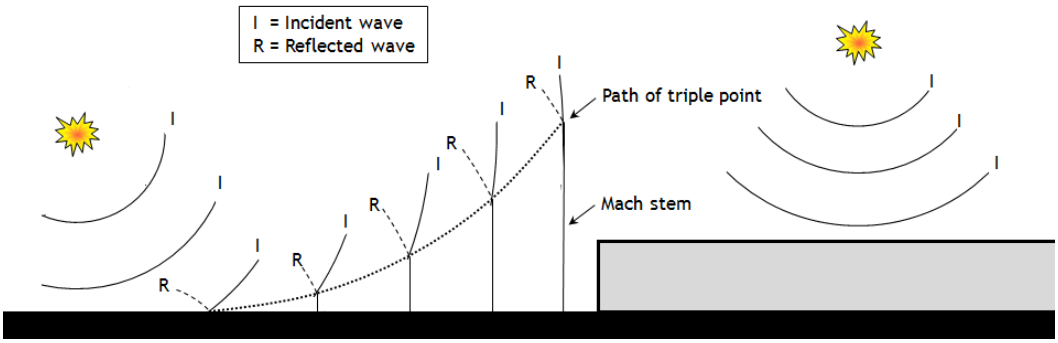

Figure 2.5: Air burst (left) versus free-air burst (right) [39]

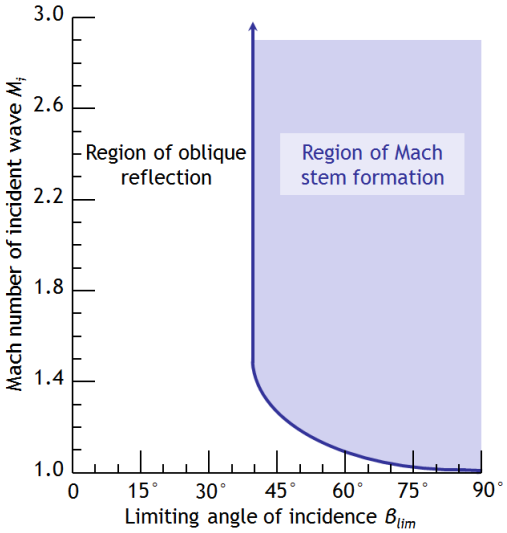

Figure 2.6: Limiting angle of incidence β_{lim} required to form a Mach stem front [39]

It is important to mention that properties of a reflected shock can be organised in terms of a reflection coefficient k_r. The reflection coefficient is defined as the ratio of reflected overpressure to the overpressure of the incident shock, given in equation 2.7.

$$k_r = \frac{P_r - P_0}{P_s - P_0} \tag{2.7}$$

The reflection coefficient for normal reflection can be expressed in terms of the Mach number for the incident shock M_i. Equation 2.8 by Rankine & Hugoniot pertains to ideal gases with isotropic coefficient $\gamma = 1.4$ as in air at overpressures of about ten bars or less.

$$k_r = \frac{8M_i^2 + 4}{M_i^2 + 5} \tag{2.8}$$

For very weak shocks, M_i approaches unity and by equation 2.8, the reflection coefficient approaches the value of 2. On the other hand, for very strong shocks, M_i is large and k_r approaches a theoretical upper value of 8.

It was later observed that this predicted upper value is clearly exceeded at higher values of P_{so^+}. Indeed, very high overpressures can create increased coefficients with values as high as 13[1] as can be seen from figure 2.7 on page 23. This is mainly due to the fact that the ideal gas law assumption is not considered to be 100 % valid for explosions, especially near the center of the explosion. Note that k_r is highest if the angle of incidence approaches 0° which indicates normal reflection.

[1]Sources for values as high as 20 are cited by Glasstone & Dolan (1977) [26].

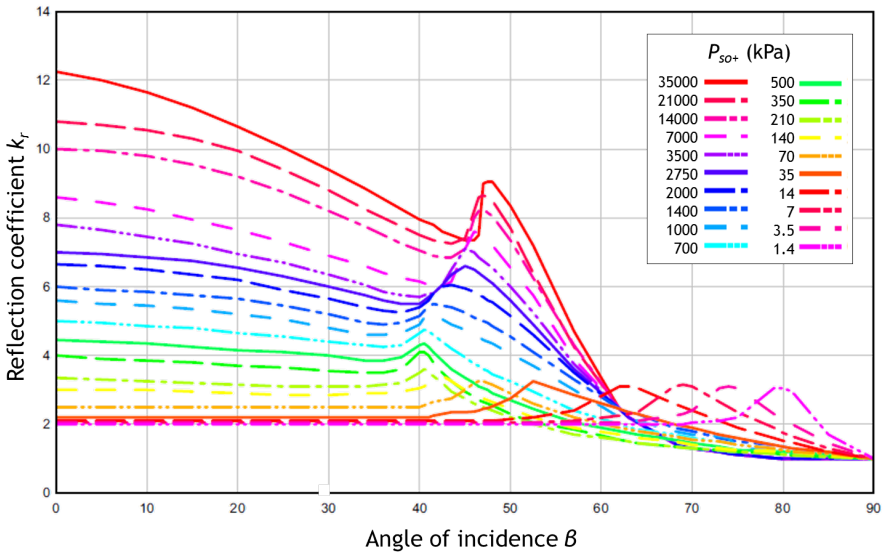

Figure 2.7: Reflection coefficient k_r in terms of peak incident overpressure P_{so+} [72]

2.3 Explosion energy

Recall from the classification strategy of explosions as presented in section 2.1 that sources of energy release associated with an explosion can differ significantly. This energy yield is formally known as explosion energy. In the case of a physical explosion, thermodynamic theory could be developed to estimate the expansion energy as a function of internal pressure and constant volume. For condensed phase high explosives however, the explosion energy is a mass specific thermodynamic property within the range of several MJ per kg. In some literature it is referred to as explosion heat analogously to the combustion heat of a flammable substance.

2.3.1 TNT equivalency in terms of explosion energy

Due to historical reasons, TNT was chosen as a reference to compare effects with when assessing any explosive phenomenon, a practice known as TNT equivalency. In terms of explosion energy, TNT equivalency is simply defined by comparing the heat of detonation of the explosive to that of TNT. A TNT equivalency that is greater than unity indicates an explosive with greater specific energy (explosive yield) than TNT. This value is then used as a conversion factor to calculate equivalent charge masses of different types of explosives as can be seen from equation 2.9. In the same way, the energy yield of a nuclear explosion is expressed in kilotons or megatons, referring to the energy yield of TNT having this particular weight.

$$W_{TNT} = \left(\frac{\Delta H_{EXP}}{\Delta H_{TNT}}\right) \cdot W_{EXP} \tag{2.9}$$

Table 2.2: TNT equivalency: conversion factors for explosives [43]

Explosive	**Explosion energy**	**TNT equivalency**
ANFO	3932 kJ/kg	0.870
TNT	4520 kJ/kg	1.000
Comp-B (RDX-TNT)	5190 kJ/kg	1.148
RDX	5360 kJ/kg	1.185
C-4 (RDX-plasticizer)	N/A	1.19 - 1.37
HMX	5680 kJ/kg	1.256

Most of the literature on blast contains tables with conversion factors for common high explosives, e.g. Baker et al. (1983) [5] pp. 110 or Mays et al. (2009) [43] pp. 39, of which some data is given in table 2.2 on page 24.

Although energy-based TNT equivalency has many practical conveniences, it is important to note that TNT is oxygen deficient and requires oxygen from the environment to complete the detonation, making the effects variable and bringing the universal status of TNT as the ideal explosive of reference into question [42].

For a fuel-air or vapour cloud explosion (VCE), TNT equivalency is hard to specify accurately for a number of reasons. Smith & Hetherington (1994) [63] suggest a factor between 0.4 and 0.6. Knowing that for typical hydrocarbons such as methane, propane and butane the heat of combustion is 10 times higher than the heat of detonation of TNT, it can be understood that the yield factor η for this type of explosions is considered as low as 4 to 6 % (equation 2.10).[2] Furthermore, important parameters influence the explosion yield, such as the stoichiometry of the flammable mixture and the location of the ignition.

$$W_{TNT} \approx 10 \cdot \eta \cdot W_{HC} \tag{2.10}$$

Because of these and other drawbacks of the TNT equivalency method, a more sophisticated method, called the multi-energy method by van den Berg (1985) [75] is often preferred to estimate the blast from gas explosions with variable strength. With this method, the degree of confinement is accounted for. It is based on numerically developed curves of a blast wave from a centrally ignited spherical cloud with constant velocity flames. Each curve corresponds to one out of ten well-defined explosion classes with respect to the initial strength of the blast, going from class 1 corresponding to a deflagration of insignificant strength to class 10 being the worst-case scenario of a gaseous detonation.

[2] See also HSE (1986) [31] for suggested values for efficiency and TNT equivalency of flammable gases and Lees (2005) [41] for a vast set of data on explosion hazards in the process industries.

2.3.2 TNT equivalency in terms of pressure and impulse

An alternative approach described by the U.S. Army Corps of Engineers [71] makes use of two conversion factors that allow the peak overpressure and the specifc impulse delivered to be matched separately for the particular explosive and the TNT equivalent. In some cases these conversion factors differ rather significantly, meaning pressure and impulse do not simply scale in the same way. Similar observations are reported by Janovsky et al. (2013) [37], where the same approach is chosen to compare the blast wave characteristics of a BLEVE to the effects of 1 g of TNT.

This approach is also selected by NATO's group of experts for the storage and transportation of ammunition. The data from table 2.3 on page 25 were taken from one of their publications, namely AASTP-4 [2], where the original table also includes a domain of validity in terms of pressure range. This comes forth from the fact that pressure and impulse are highly depending on the distance considered. Peugeot et al. (2006) [55] have edited a critical review on these and other issues regarding TNT equivalency for NATO's Munition Safety Information and Analysis Center (MSIAC). In conclusion, the concept of TNT equivalency must always be used with care. It is approximative and not absolute.

Table 2.3: TNT equivalency: conversion factors for pressure and impulse [2]

Explosive	**TNT equivalency Overpressure**	**TNT equivalency Impulse**
ANFO	0.83	0.81
TNT	1.00	1.00
Comp-B (RDX-TNT)	1.16	1.14
RDX	1.46	1.30
C-4 (RDX-plasticizer)	1.37	1.19
HMX	1.56	1.36

2.3.3 TNT equivalency in terms of damage criteria

In forensics finally, the exploitation of the notion of TNT equivalency is a little different. Damage phenomena such as the dimension of the crater at ground zero, or the farthest distance where window shattering is still observed, are examined in order to assess the weight of TNT presumably used. Quite often though, this methodology is performed using an intermediate step where a blast wave characteristic, usually peak (side-on) overpressure P_{so^+}, is related on the one hand to the damage observed and on the other hand to a quantity of standard explosive.

In table 2.4 on page 26 a non-exhaustive list of data on overpressure criteria in terms of window breakage is given. Apart from the observation that the values and

the associated descriptions are not always unambiguous, attention is drawn to the data taken from Mays et al. (2009) [43]. Clearly this demonstrates the importance of positive phase duration in addition to overpressure when damage is assessed. A larger charge can cause the same level of damage as a smaller charge, even though the associated overpressure is less, because the larger device generates a pulse of longer duration. Mays et al. thus conclude that impulse should be given equal consideration with overpressure when assessing the damage potential of a given threat. It is also understood from data out of PGS1 part 2B (2003) [57] that developments in building practice have led to the use of window panes with different composition and higher overall structural resistance. This is studied more deeply in chapter 3.

Table 2.4: Peak (side-on) overpressure related to observation of window breakage

Source	Description	P_{so^+}
[39]	Minimum damage to glass panels	1-3 mbar
[43]	5 % of window panes broken, $W_{TNT} = 10$ ton	7 mbar
[3]	Lower limit for breakage of glass	10 mbar
[17, 57]	Lower limit for breakage of glass (before 1975)	10 mbar
[43]	5 % of window panes broken, $W_{TNT} = 1$ ton	11 mbar
[11]	Lower limit for breakage of glass	20 mbar
[17, 57]	Lower limit for breakage of glass (after 1975)	20 mbar
[17, 57]	50 % of window panes broken (before 1975)	30 mbar
[26, 39]	Windows shattered	35-75 mbar
[3, 41]	Effective breakage of glass	40 mbar
[43]	90 % of window panes broken, $W_{TNT} = 10$ ton	42 mbar
[17, 57]	50 % of window panes broken (after 1975)	50 mbar
[43]	90 % of window panes broken, $W_{TNT} = 1$ ton	63 mbar
[81]	Danger from flying glass and debris	70 mbar

2.3.4 Scaling laws

Scaling of the properties of blast waves from explosive sources is a common practice to predict the characteristics of explosions at large scale based on tests on a much smaller scale (down to 1 gram of TNT [11]).

The most common form of blast scaling is the cube-root scaling. This law, first formulated by Hopkinson (1915) and independently by Cranz (1926), states that self-similar blast waves are produced at identical scaled distances $\bar{R}$ (or Z) when two explosive charges of similar geometry and of the same explosive, but of different sizes, are detonated in the same atmosphere [6]. For two points at identical scaled distances at identical scaled times, one thus registers identical (unscaled) overpressure (P_s, Q and P_r), identical velocities and identical scaled specific impulse.

The definition of the scaled parameters are given in equations 2.11a, 2.11b, and 2.11c. They all make use of the same cube-root-like scaling factor related to the total energy of the explosive charge. The choice of the symbol W points however to the common use of the total weight (assumed proportional to the total energy) of the explosive substance.

$$Z = \bar{R} = \frac{R}{W^{1/3}} \tag{2.11a}$$

$$\bar{t} = \frac{t}{W^{1/3}} \tag{2.11b}$$

$$\bar{i_s} = \frac{i_s}{W^{1/3}} \tag{2.11c}$$

Experimental validation has shown that the cube-root scaling applies over a remarkably large range of length and energy scale factors. In the limit of small scale, relevant for the experiments conducted in support of this master's thesis, one is restricted primarily by the practical considerations of the ability to detonate tiny explosive charges [6].

Several authors have plotted graphs containing scaled shock front parameters based on empirical relationships found by large-scale (often nuclear) experiments, such as Baker's abaci (1983) [5] for free-air burst and surface burst of spherically shaped charges of TNT.

However, the most widely used and accepted approach for the determination of blast parameters is the one proposed by Kingery & Bulmash (1984) where data from a 1 kg charge of TNT have been curve-fitted into polynomial functions of the logarithm of the scaled distance Z between 0.05 and 40 $\mathrm{m{\cdot}kg^{-1/3}}$. The resulting graphs are plotted in figure 2.8 on page 28. Their validity for small scaled distances has been confirmed, opposed to models based on data from nuclear blast where this is a concern. The polynomial functions of Kingery & Bulmash are programmed in the conventional weapons effects calculation programme `ConWep`, numerical aid to U.S. manual TM 5-855-1 (1997) [68] and used by the author to predict blast parameters associated with the experimental work performed for this master's thesis.

In an attempt to account for the effects of altitude or other changes in ambient conditions such as temperature on air blast waves, Sachs (1944) proposed a more general blast scaling law with dimensionless parameters which was later confirmed by a large set of experiments. Sachs's law is almost universally used to predict effects of change in the environmental condition on blast parameters. It includes Hopkinson-Cranz scaling as a special case, when there are no changes in ambient conditions. In Baker (1973) [6] the underlying dimension analysis is clearly developed and the use of the scaling law is documented more in detail.

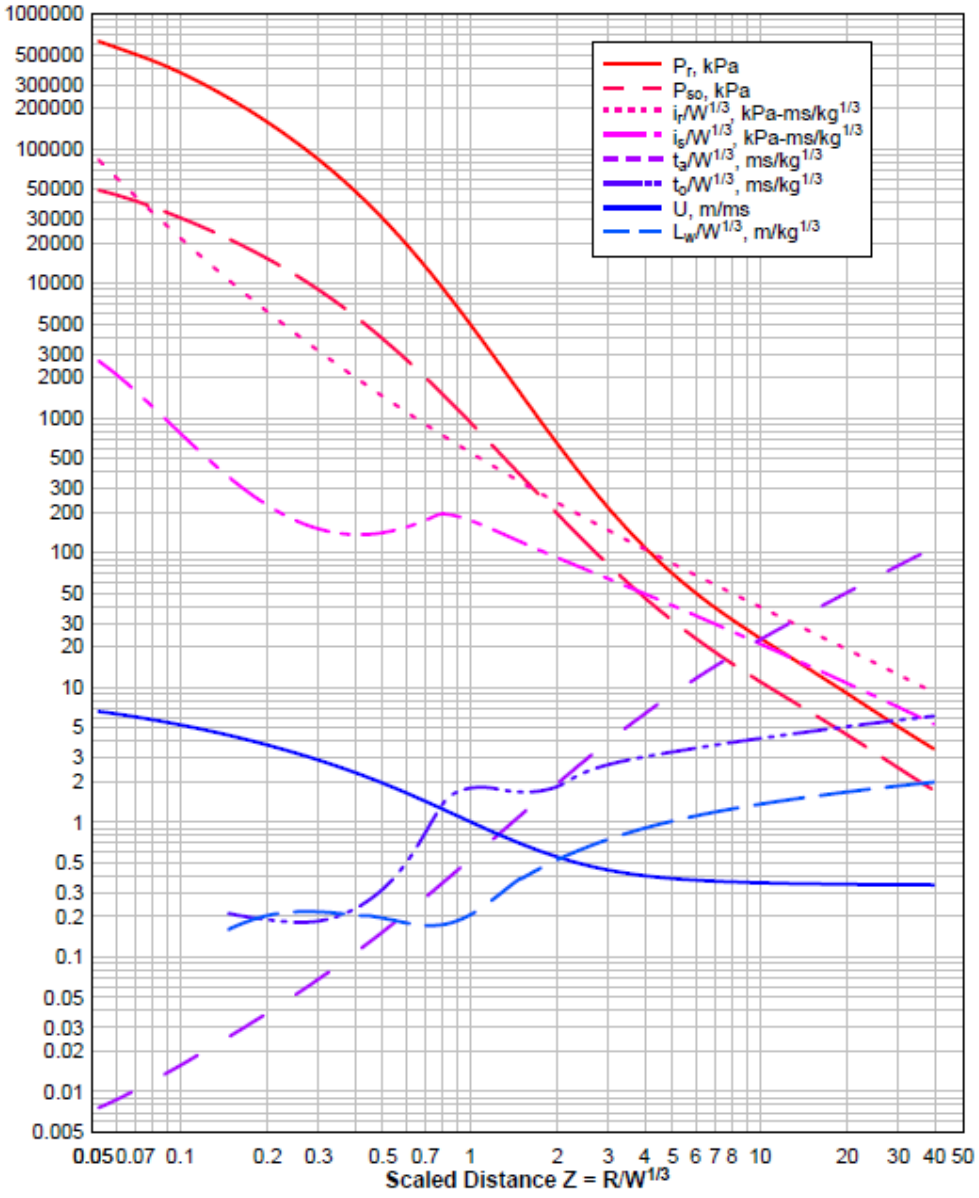

Figure 2.8: Positive phase blast parameters for spherical TNT explosions in air at sea level [64, 72]

2.4 Key point summary

This short introduction in explosion theory has aimed to convince the reader of the variety and complexity of the explosion phenomenon and to explain where lies its destructive potential.

Thorough understanding of the explosion characteristics is fundamental for the remainder of this master's thesis. They are the variables of interest in explosion modelling as part of the consequence modelling process that was presented in chapter 1. One should absolutely bear in mind the difficulties of pairing these characteristics when explosions with different energy source and reaction velocity are considered. This said, comparing the effects of different explosion phenomena with respect to a substance of reference such as TNT, a detonating high explosive which never guarantees a perfect match, still remains the most widely used method in academic and legal studies of effects of explosions.

Finally, it seems not more than fair to end this chapter on a positive note, by remarking that one does not only need to think of explosions in terms of calamities leading to structural, physical and environmental damage. In fact, there exist numerous useful applications of explosions as well, such as jet engines, propulsive rocket systems, critical fission reactors or well-controlled destruction activities as can be found in mining industries or in large building or bridge demolition projects, an example of which is shown in figure 2.9 on page 29.

Figure 2.9: Controlled explosive demolition of the main span of the Old Jamestown Bridge, Rhode Island, USA, 2006 (www.fhwa.dot.gov)

References

[2, 3, 6, 5, 7, 9, 10, 11, 14, 17, 19, 26, 31, 37, 38, 39, 40, 41, 42, 43, 55, 57, 63, 64, 68, 69, 71, 72, 75, 77, 78]

Chapter 3

Characteristics of glass subjected to a blast load

Recall the successive steps in the consequence modelling process, introduced in the first chapter and represented in figure 1.3 on page 4. Clearly, if the shock wave properties at a given location away from the burst center can be estimated, it will be possible to proceed to the damage modelling of the explosion event.

In this third chapter, the behaviour of window panes subjected to a blast load is discussed. Surely, before assessing the impact of glass fragments from a blast on near-by persons, which will be the subject of chapter 4, it is necessary to understand the vulnerable features of glass and the possible failure modes upon blast loading. The physicochemical properties are elaborated on firstly, because of the relation of the particular molecular nature of glass to its brittleness. Before discussing the dynamic (high strain rate) behaviour of glass panes, it fits to discourse the mechanical properties at normal conditions.[3] Additionally, manufacturing techniques such as thermal treatment and assembly are discussed, which turn glass as a construction material into windows with different levels of performance up to safety glazing or even explosion-resistant security glazing.

A TNO calculation procedure [57] is then presented, based on Biggs' quasi-static solution method, wich enables the researcher to estimate the blast strength of monolithic and double glass windows. The outcome is compared to chart-based results from the U.S. Department of Defence [72], founded on the same methodology. It is complemented with probit functions found in literature that predict the probability of window breakage for a given peak (side-on) overpressure P_{so^+}. The concept and use of iso-damage curves is also briefly touched. In the context of this chapter they can help predict if a glass element subjected to blast will break, accounting not only for the overpressure but also for the duration of the blast wave. In chapter 4 these so-called P-I diagrams will be useful to assess specific categories of harm to a person.

[3] Callister (2007) [15] is used as main reference for the sections on material properties. It is the handbook of choice in the RMA to teach Materials Science in the Engineering Faculty.

3.1 Physicochemical properties of glass

3.1.1 Chemical composition

Before diving into the molecular composition of window glass, it is necessary to introduce the material class of the silicates. Silicates are materials composed primarily of silicon and oxygen, two of the most abundant elements in the earth's crust. Indeed, the bulk of soils, rocks, clays and sand reside under the family of silicates. The crystal structure of these solids is characterised in terms of the various arrangements of a SiO_4^{4-} tetrahedron, presented in figure 3.1 on page 32.

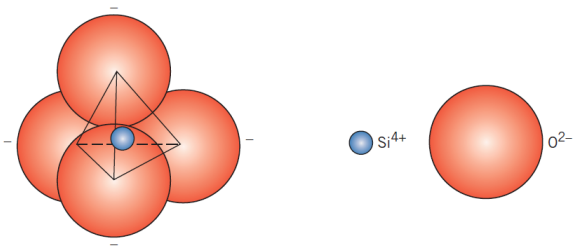

Figure 3.1: The silicon-oxygen (SiO_4^{4-}) tetrahedron [15]

Chemically, the most simple silicate material is silicon dioxide, or silica (SiO_2), which is a network forming oxide. Structurally, it consists of a three-dimensional network that is generated when every corner oxygen atom in each tetrahedron is shared by adjacent tetrahedra. Thus, the material is electrically neutral and all atoms have stable electronic structures. If these tetrahedra are arrayed in a regular and ordered manner, a crystalline structure is formed.

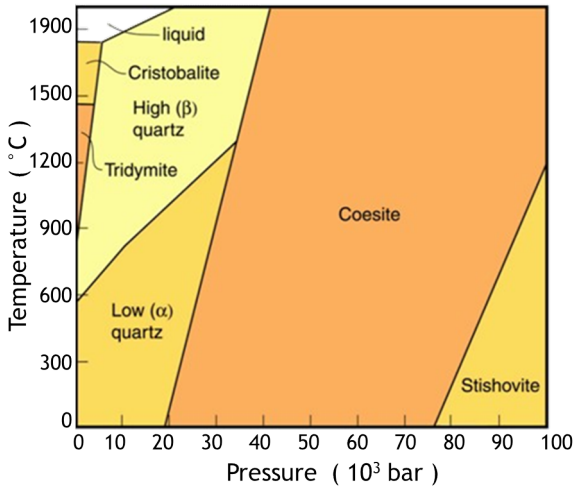

Figure 3.2: Phase diagram for the unary silica system (www.cefns.nau.edu)

Referring to the phase diagram of silica in figure 3.2 on page 32 one can conclude that three primary polymorphic crystalline forms of silica exist at atmospheric pressure. At room temperature the crystalline form of silica is called quartz. It has a relatively open structure, explaining its low density ρ of only 2.65 g/cm^3. The high strength of the Si−O interatomic bonds is reflected in a relatively high melting temperature T_m of 1710 °C.

Silica can also be made to exist as a non-crystalline or glassy material. It is then called fused silica and has a high degree of atomic randomness, which is characteristic of the liquid phase. Non-crystalline solids are also referred to as "amorphous" from the Greek words for "without form." As with crystalline silica, the SiO_4^{4-} tetrahedron is the basic unit for amorphous silica too. Beyond this structure, considerable disorder exists. The structures for crystalline and amorphous silica are compared schematically in figures 3.3 (a) and (b) on page 34.

The most common inorganic glasses are silica glasses to which have been added other oxides such as soda (Na_2O) and lime (CaO). These oxides do not form polyhedral networks. Rather their cations are incorporated within and modify the SiO_4^{4-} network. For this reason these oxide additives are termed network modifiers. The most prevalent type of glass used for window panes, bottles and jars is sodium-lime-silicate glass, or soda-lime glass (SLG). It normally consists of 60 − 75 wt% SiO_2, the balance being mainly Na_2O (12 − 18 wt%) and CaO (5 − 12 wt%). For SLG production the silica is usually supplied as common quartz sand, whereas Na_2O and CaO are added as soda ash (Na_2CO_3) and limestone ($CaCO_3$).

Still other oxides, such as titania (TiO_2) and alumina (Al_2O_3), physically substitute for silicon and become part of and stabilize the network. These are called intermediates.

Figures 3.3 (c) and (d) on page 34 show examples of the ion positions of network modifiers and intermediates. From a practical perspective, the addition of modifiers and intermediates lowers the melting point T_m and viscosity μ of a glass, and makes it easier to form at lower temperatures. This is discussed more deeply in the next paragraph.

3.1.2 Glass transition temperature

In molecular terms, glasses are materials that form amorphous rather than crystalline solids upon cooling, a phase transition known as vitrification. They become more and more viscous in a continuous manner with decreasing temperature but there is no definite temperature at which the liquid transforms to a solid as with crystalline materials. This can be understood from the dependence of specific volume ρ^{-1} on temperature, as illustrated in figure 3.4 on page 35.

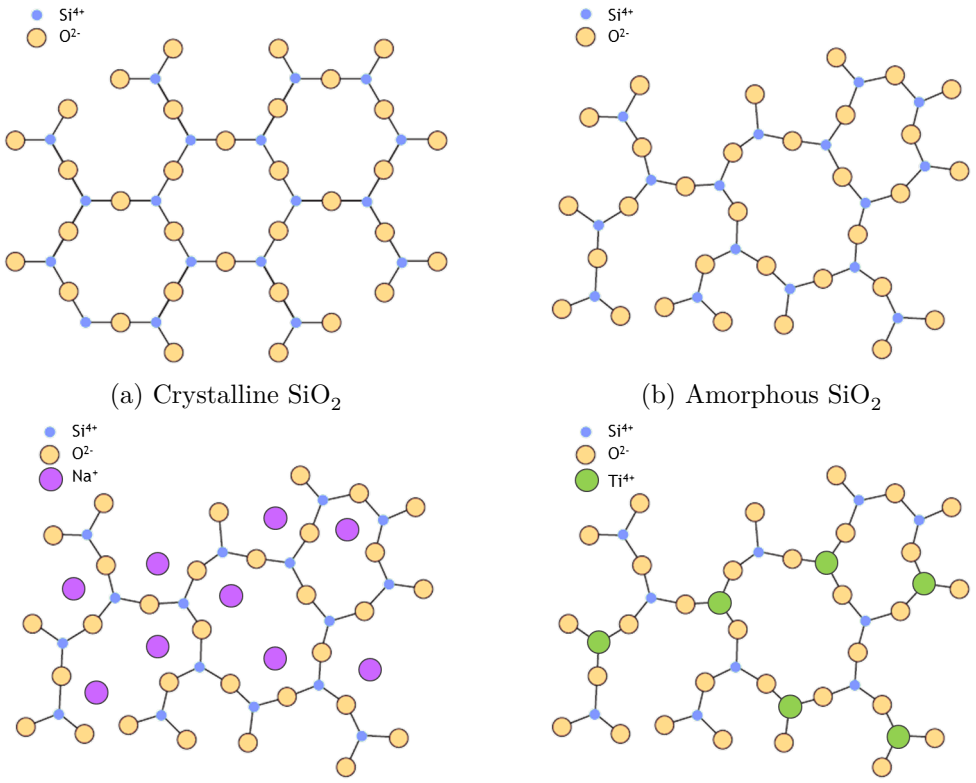

(a) Crystalline SiO_2

(b) Amorphous SiO_2

(c) Glass with added Na_2O as a modifier

(d) Glass with added TiO_2 as an intermediate

Figure 3.3: Silicon dioxide with added network modifiers and intermediates [15]

Crystalline materials solidify at the melting temperature T_m. Upon solidification, a discontinuous decrease in volume is observed. However, for glassy materials, specific volume decreases continuously with temperature reduction as the material gradually hardens. A slight decrease in slope of the curve occurs at what is called the glass transition temperature T_g. Below this temperature, the material is considered to be a glass. Above, it is first a supercooled liquid and finally a liquid when all matter has liquefied. It is further noted that upon warming and before melting, vitreous silica can easily transform into crystalline silica, a process known as devitrification.

There are many plausible explanations why materials vitrify rather than crystallize and the reason why vitrification occurs may be different for different materials. Influencing factors are, amongst others, viscosity, heat of fusion, colligative effects and of course the cooling rate. For most materials that vitrify, it is observed that if the cooling rate is slow enough, the probability of crystal growth and nucleation increases and the material will crystallize rather than vitrify. High viscosity on the other hand is a strong impediment to the formation and growth of crystal nuclei and will thus support a liquid's tendency to supercool and to vitrify. Silica is extremely viscous and is therefore particularly prone to vitrification.

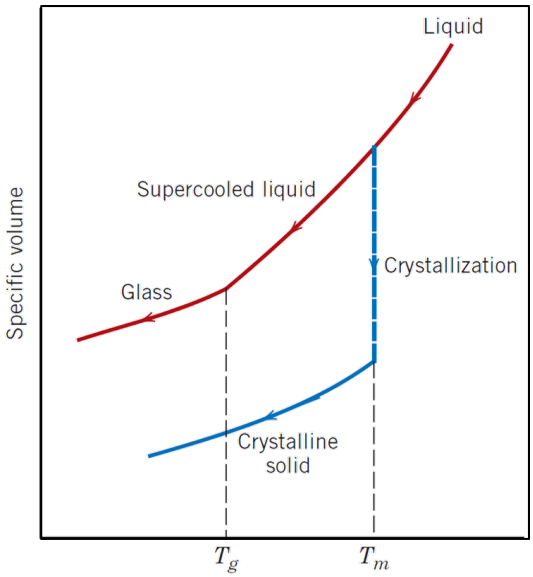

Figure 3.4: Glass transition temperature T_g of a vitrifying material versus melting temperature T_m of a crystallizing material [15]

Figure 3.5 on page 36 is important with respect to glass-forming operations. It shows the temperature dependence of liquid viscosity μ for fused silica and three silica glasses. It is used to determine the working range in terms of process temperature at which specific fabrication and processing operations of glasses are feasible. Looking at the softening point[4] which corresponds to the maximum temperature at which a glass piece may be handled without causing significant dimensional alterations, it is clearly seen that good engineering of the chemical composition can have a significant effect on the working range of a glassy material.

3.1.3 Optical transparency

Materials that are capable of transmitting light with relatively little absorption and reflection are transparent to a range of wavelengths known as visible light. On an atomic scale, a material would absorb (opposed to transmit) a light particle, called a photon, if the latter possesses enough energy to bridge the band gaps that exist between the discrete energy levels which can be occupied by electrons. The energy of a photon E_λ is inversely proportional to its wavelength λ as described by the Planck-Einstein relation given in equation 3.1. Here, h is Planck's constant and c corresponds to the speed of light in vacuum. Both are fundamental constants.

$$E_\lambda = \frac{hc}{\lambda} = \frac{1.986 \cdot 10^{-25}\ \mathrm{J \cdot m}}{\lambda} \tag{3.1}$$

[4] By definition, the softening point is reached at a viscosity equal to $4{\cdot}10^6$ Pa·s.

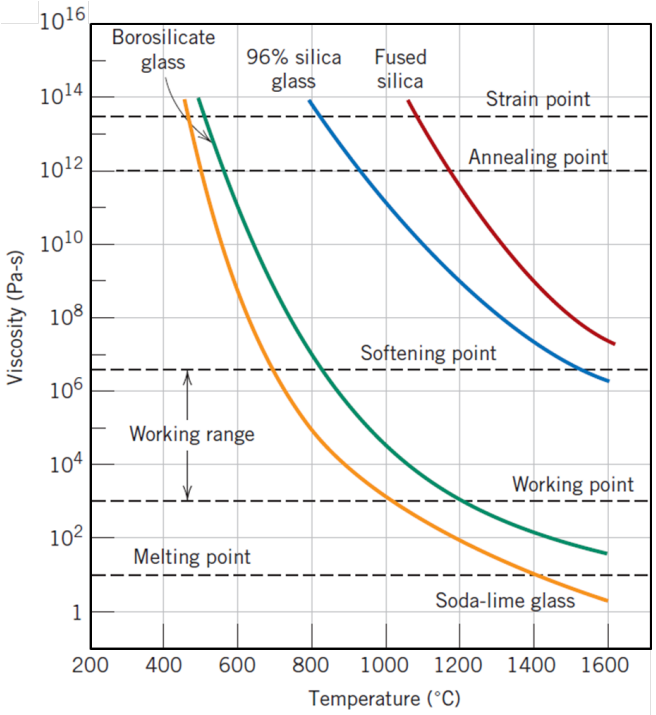

Figure 3.5: Influence of viscosity μ on vitrification [15]

Commercial silica-based window glass has large band gaps because of the strong interatomic Si−O bonds in silicates. The particle energy related to the wavelengths associated with visible light ($\approx 380 - 750$ nm) is not sufficient to excite a glass electron to a higher energy level. As a result, glass is transparent to visible light. Because of the possibility to easily rework silica into a transparent material, silica-based glass is the obvious material of choice in window pane industry. For higher energy levels ($\lambda < 380$ nm), associated with ultra-violet light, X-rays and γ-rays, radiation is absorbed.

Light that is transmitted into the interior of transparent materials experiences a decrease in velocity, and, as a result, is bent at the interface. This phenomenon is termed refraction and is characterised by a material property known as the refractive index n.

Glass produces isotropic, single refraction, which is exactly the kind of optical behaviour that is desired for window panes. For a typical SLG, n is approximately equal to 1.51. Glasses which contain heavy metal ions of larger size have higher indices of refraction. It is common to consider the refractive index as a material constant. It is however noted that its value is influenced by temperature.

3.1.4 Chemical durability

From the fact that numerous collections of very old glasses still exist today, one can assume that glass remains stable over a long period of time. Years of research on the influence of the state of the specimen, e.g. composition, homogeneity, thermal history, and surface conditions, and on external influences such as temperature, time, and pH have shown that glass performs extremely well in terms of chemical durability.

Glass is good at resisting most acids with short term exposure. For commercial window glass, no detectable attack is noticed for a pH upto 7, beyond which there is a detectable attack at a pH of 8 and 9, while with further increase in alkalinity the attack increases rapidly [32]. Alkaline products are found in cements. Contamination of the glass during the building phase is therefore a potential cause for chemical deterioration of the window surface.

3.2 Mechanical properties of glass

3.2.1 Strength

From its stress-strain curve associated with a static tensile test, such as the graph in figure 3.6 (a) on page 38, it is seen that glass behaves almost perfectly elastic until it exhibits brittle fracture. Indeed, due to the randomness of the molecular structure there are no slip systems present to allow plastic yielding. Therefore, the fracture strength σ_f of glass corresponds to the ultimate tensile strength σ_{UTS}. The slope of the linear elastic curve is the elasticity modulus or Young's modulus E. It is usually taken between 69 and 75 GPa for glass.

For ease of reference, the stress-strain history for a mild steel, exhibiting ductile behaviour is contrasted in figure 3.6 (b) on page 38. Ductility is a measure for the ability of a material to achieve large plastic deformations when elasticity is exhausted. Three subsequent deformation phenomena rule the plastic domain. At the yield stress σ_Y, local stress concentrations are reduced through stress redistribution, a process known as yielding. Next, the material will harden until the ultimate tensile strength σ_{UTS} is reached. This is the strain hardening phase. At the final stage of ductile failure a prominent decrease in the central cross-sectional area is observed, hence this phase is called the necking phase.

Before discussing numerical values for the tensile strength of glass, it is important to consider figure 3.7 on page 39. Bearing in mind the strong molecular forces present in silicates, the theoretical tensile strength of glass reaches somewhere above 10^4 MPa which is exceptionally high. However, it is of no practical relevance. Indeed, the actual tensile strength is many times lower. It is this contradictory fact that inspired Griffith (1920) to a new theoretical model of rupture, based on fracture surface energy, which led to the existence of the discipline of fracture mechanics.

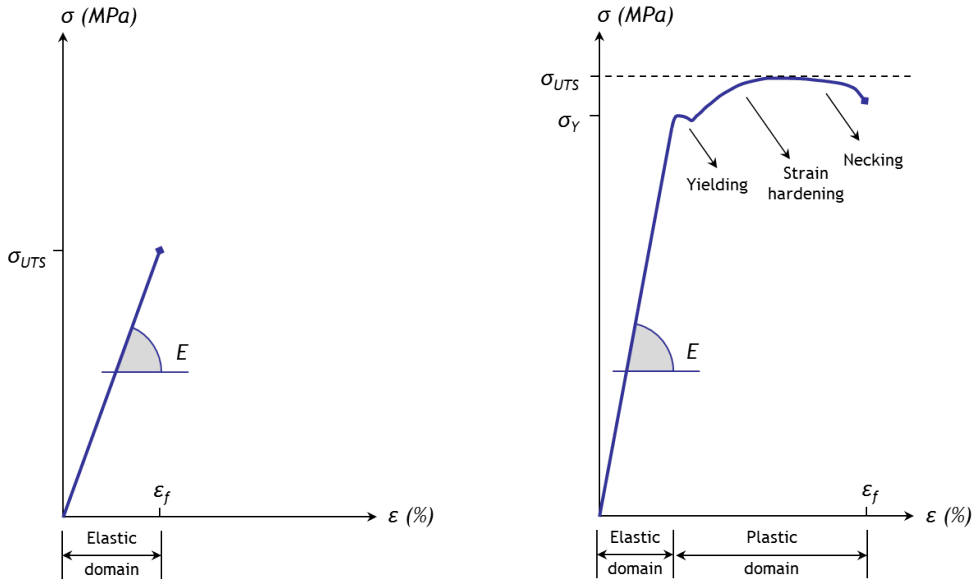

(a) Glass: brittle (b) Steel: ductile

Figure 3.6: Typical stress-strain behaviour to fracture [60]

Clearly the surface of window panes contains a large number of mechanical flaws of varying severity which are not necessarily visible to the naked eye. As with all brittle materials, the tensile strength of glass depends very much on these surface flaws. A glass element fails as soon as the stress intensity due to tensile stresses at the tip of one such flaw reaches its critical value. This explains the important loss of strength.

This also means that the tensile strength of glass is not a material constant. It is influenced by many parameters, such as the condition of the surface obviously, but also the size of the glass element which is proportional to the number of flaws present, and the action history which is related to the size of the cracks as they grow when subjected to the right load conditions. Hence an estimation of the tensile strength of a used window pane would be in the order of magnitude of $10^1 - 10^2$ MPa, which is rather low. Henceforth this property is termed static strength s.

In section 3.5 models are presented to estimate this so-called static strength S of window panes, and to translate this into a measure of dynamic (or quasi-static) resistance. Imperatively these are probabilistic approaches. The static strength will in a way remain uncertain and will as such be generally related to a 50 % failure probability p_f under specific loading conditions.

It is noted that, due to the fact that surface flaws do not grow or fail when in compression, the compressive strength σ_{UCS} of glass is much larger than the tensile strength σ_{UTS}. The latter is usually exceeded long before the critical compressive stresses are reached and is therefore determinant for fracture.

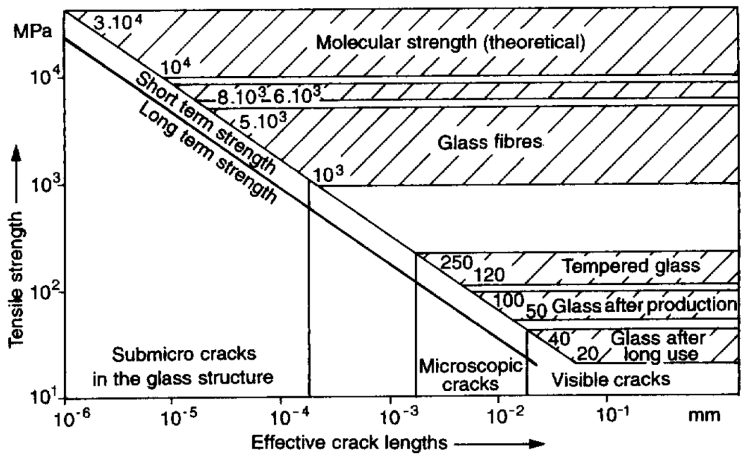

Figure 3.7: Influence of cracks on the tensile strength of glass [60]

3.2.2 Ductility

From equation 3.2 it can be seen how the ductility ratio Du compares the maximum elongation at break or fracture strain ϵ_f to the elastic strain ϵ_{el}. From the stress-strain history for brittle materials, presented above in figure 3.6 (a) on page 38, it follows that Du must be taken equal to 1 in the case of glass.

$$Du = \frac{\epsilon_f}{\epsilon_{el}} \tag{3.2}$$

3.2.3 Fracture toughness

Toughness of a material is a measure of its ability to absorb energy up to fracture.

For static (low strain rate) loading conditions, toughness may be ascertained from the results of a tensile stress-strain test presented earlier. It is the area under the $\sigma - \epsilon$ curve up to the point of fracture, expressing the energy absorption per unit volume of material (units: $\mathrm{J{\cdot}m^{-3}}$). Consequently, for a material to be tough, it must display both strength and ductility. For dynamic (high strain rate) loading conditions such as the blast loading following an explosion, and in the presence of a notch, the notch toughness is assessed by means of a Charpy or Izod impact test.

From the former it is clear that surface flaws are inherently present in window panes. Irwin (1957) understood their detrimental effect on the strength of brittle materials. He introduced the stress intensity factor SIF (or K) which expresses how an applied stress may be amplified or concentrated at the tip of a flaw. The critical stress intensity factor, better known as the fracture toughness K_c, is thus a more relevant energy absorption characteristic for brittle materials such as glass. It is a property indicative of a material's resistance to fracture when a crack is present.

In fracture mechanics a crack has a characteristic length a which is defined as half of the length of an internal crack. For specific loading conditions with give rise to a critical stress for crack propagation σ_c in the material, the crack can grow. From equation 3.3 it is seen that fracture toughness K_c can be expressed in terms of these two variables. Once the crack reaches a critical crack length a_c, the material fails.

$$K_c = Y \cdot \sigma_c \cdot \sqrt{\pi a} \tag{3.3}$$

Y is a dimensionless geometrical parameter related to the conditions of the crack. Its discussion leads beyond the scope of this master's thesis, although it is worth mentioning that for planar specimens containing cracks that are much shorter than the specimen width, it has a value of approximately unity.

When the specimen thickness is much greater than the crack dimensions, plane strain conditions are adopted and K_c becomes independent of the thickness. The K_c value for this thick-specimen situation is known as the plane strain fracture toughness K_{Ic} for mode I crack surface displacement (opening mode). It is a fundamental material property but it depends on several factors, as illustrated by the fact that it diminishes with increasing strain rate and decreasing temperature. Brittle materials, for which appreciable plastic deformation is not possible in front of an advancing crack, have low K_{Ic} values making them vulnerable to catastrophic failure. For SLG, a K_{Ic} value of $0.7 - 0.8$ MPa$\sqrt{\text{m}}$ is cited.

3.2.4 Values of selected properties

Table 3.1 on page 40 contains typical values for a list of mechanical properties of SLG, many of which have been discussed above. Callister (2007) [15] serves as primal source for the data enlisted. It is supported by a technical bulletin, released by one of the world's leading manufacturers of glass and glazing systems [53].

Table 3.1: Material properties of soda-lime glass (SLG) used for windows [15, 53]

Symbol	Mechanical property	Value	Unit
ρ	density @ 20 °C	2500	kg·m^{-3}
E	Young's modulus of elasticity	72	GPa
G	modulus of rigidity (shear)	28	GPa
ν	Poisson's ratio	0.23	-
ϵ_f	elongation at break	0.001	-
σ_{UTS}	tensile strength ($p_f = 50$ %)	41	MPa
σ_{UCS}	compressive strength	330	MPa
σ_{fl}	flexural strength	69	MPa
K_{Ic}	plain strain fracture toughness	0.75	MPa$\sqrt{\text{m}}$

3.3 Main types of glass

3.3.1 Monolithic glass

Annealed glass (ANG) is the most common form of glass available today. It is also known as plate, float or sheet glass. During manufacture it is cooled slowly. The process results in very little, if any, residual compressive surface stress. Consequently, ANG is of relatively low strength when compared to thermally tempered glass. It has large variations in strength and fractures into large, sharp shards such as seen in figure 3.9 (a) on page 42. Obviously these can cause serious injury.

Fully tempered glass (FTG) is manufactured from annealed glass by heating it to a high uniform temperature and then rapidly quenching it. As the internal temperature profile relaxes towards uniformity, internal stresses are created. The outer layers, which cool and contract first, are set in compression, while internal layers are set in tension. Figure 3.8 on page 41 shows the remaining stress gradient within the thickness of the glass after manufacture. From the foregoing section it is understood that failure originates from tensile stresses exciting surface flaws in the glass. The pre-compression equals around 90 to 170 MPa, which surely permits a larger load to be carried before the net tensile strength of the FTG pane is exceeded. As a rule of thumb, FTG is around four to five times stronger than ANG [72]. Furthermore, its fracture characteristics are superior to those of ANG as it will eventually fracture into small cubical-shaped fragments such as seen in figure 3.9 (b) on page 42.

Heat-strengthened glass (HSG) or semi-tempered glass is often marketed as safety glass. However, because of its lower surface pre-compression of approximately 40 to 80 MPa, it does not exhibit particular dicing characteristics upon breakage as can be understood from figure 3.9 (c) on page 42. It is about twice as strong as ANG enabling it to tolerate more rapid and uneven temperature swings during its service life. Hence it is mainly used for curtain walls which do not require safety glazing.

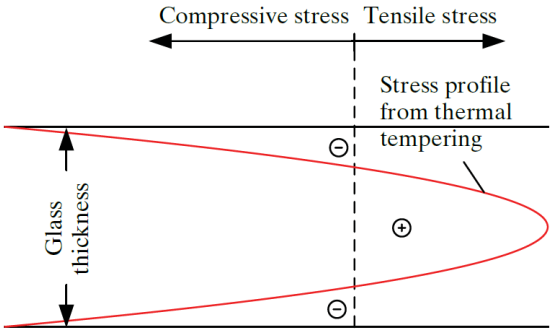

Figure 3.8: Residual stress profile produced by thermal tempering [54]

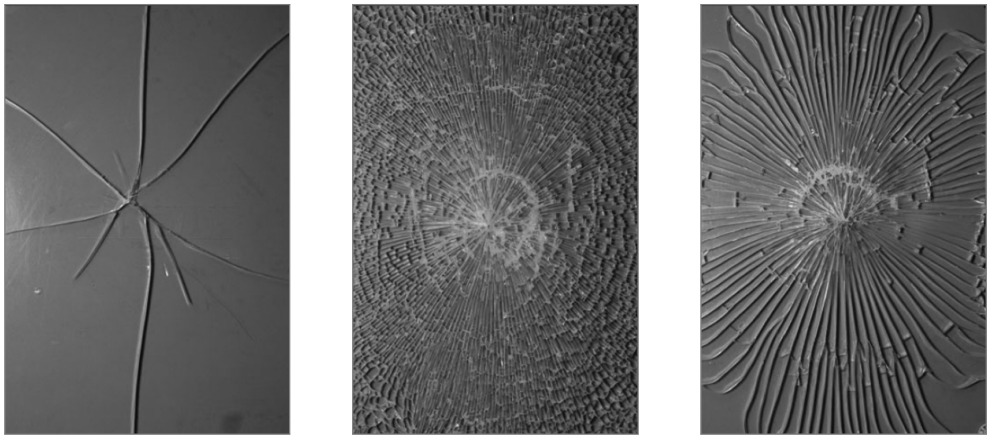

(a) Annealed glass (b) Fully tempered glass (c) Heat-strengthened glass

Figure 3.9: Images of glass fracture for different types of glass [54]

3.3.2 Laminated glass

Laminated glass is a type of safety glass[5] composed of two or more glass plies joined together by a visco-elastic interlayer. A schematic cross section is shown in figure 3.10 (a) on page 43. Any of the monolithic glass plies described above is fit for use as one of the glass laminates. The interlayering lamination material is a thermoplastic or thermosetting resin with good adhesion to glass, such as polyvinyl butyral (PVB) or ethylene-vinyl acetate (EVA). Laminated glass is assembled in an autoclaving process in order to optimise the bonding between the composing elements and to assure full transparency of the interlayer. Laminated glazing is denoted as $d_i d_o.d_l$, referring to an assembly of two plies with a respective thickness of d_i and d_o mm, joined together by an interlayer with a thickness of $d_l \times 0.38$ mm, the latter value being the standard thickness of one interlayering ply.

Laminated glass is predominantly used for automobile windshields where additional injuries from glass fragments after collision must be avoided. Surely, upon sudden impact or undue deflection, the interlayer will hold the entire glass pane together. Other applications include doors and windows to increase burglar resistance or glazing in climates where hurricane resistance codes apply that demand the use of safety glass. In Belgium, standard NBN S 23-002 (2007) [49] advises the use of safety glass in numerous situations where potential risks to people have been identified (e.g. tripping of a person or falling of glass fragments). Although this standard is essentially not mandatory, attention is drawn to the constructional purposes where the use of laminated glass is intended by the standard. These include glass used in ceilings, doors with a surface area larger than 0.5 m^2, hung sash windows and windows touching the ground surface.

[5] According to Belgian standard NBN S 23-002 (2007) [49], the only types of glazing which are considered as safety glass are fully tempered glass and laminated glass.

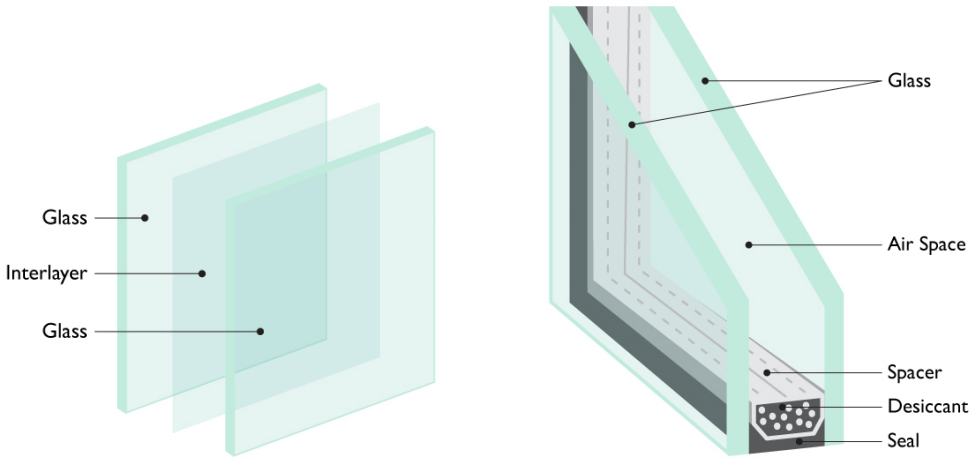

(a) Laminated glass (b) Insulated glass

Figure 3.10: Cross section of composed glazing systems (www.saand.ca)

3.3.3 Insulating glass

Insulating glass units (IGU) consist of two or more plies of glass enclosing a hermetically sealed, insulating air space filled with air or a noble gas, such as argon or krypton. The air space influences that heat transfer across the window opening in such a way that heat gain is controlled in summer opposed to wintertime when heat loss is reduced.

The most common IGU is constructed with two plies of glass and one sealed air space as seen in figure 3.10 (b) on page 43. In this configuration it is simply referred to as insulating glass, denoted as $d_o/d_a/d_i$ where d_o and d_i refer to the thickness of outer and inner ply respectively and d_a is a measure of the thickness of the air space (units: mm). The glass plies can be either monolithic or laminated, depending on the desired (safety) performance, and the laminated component can be placed either inboard, outboard or at both sides. The desiccant below the lower spacer of the IGU is present to absorb internal moisture.

Referring to figure 3.11 (a) on page 44, presented in a national energy consumption survey (ECS) conducted by Vito nv (2012) [79], it is concluded that the primary type of IGU found in Belgian households is standard double glazing, as expected. In figure 3.11 (b) on page 44 further distinction is made between standard double glazing and high efficiency (low emissivity or low-E) insulated glazing where specific coatings are added to improve the thermal properties and inboard surface temperature of the IGU even more. The latter has nowadays become the product of choice when new windows are installed in Belgian households, due to an increasing awareness on energy savings and the possibilities of premiums and tax deductions in Belgium. In this master's thesis, IGU will always refer to double glazing units, be it standard double glazing or high efficiency double glazing.

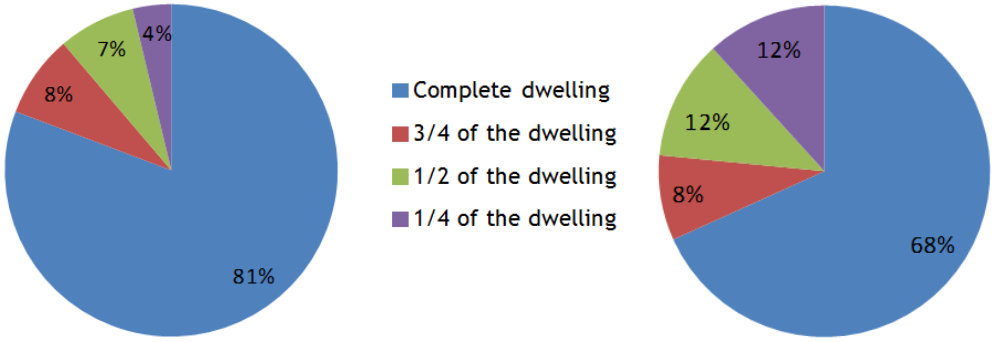

(a) Standard double glazing (b) High efficiency double glazing

Figure 3.11: Share of windows with insulated glazing in Belgian households [79]

For some specific purposes triple glazing is quietly gaining popularity because of its superior thermal properties. However, from figure 3.12 on page 44 it is seen that a 100 % share of the Belgian households reports having either single glass or insulated, double or high efficiency glass. Vito nv (2012) [79] compares own survey results (ECS) with a national socio-economical survey (SES) conducted in 2001. It is concluded that during the last decade an additional 12 % of the Belgian households has been (partly) equipped with double or high efficiency glass, raising the total share at 83 % at the time the survey was conducted. One can fairly assume that this share has continued to increase afterwards.

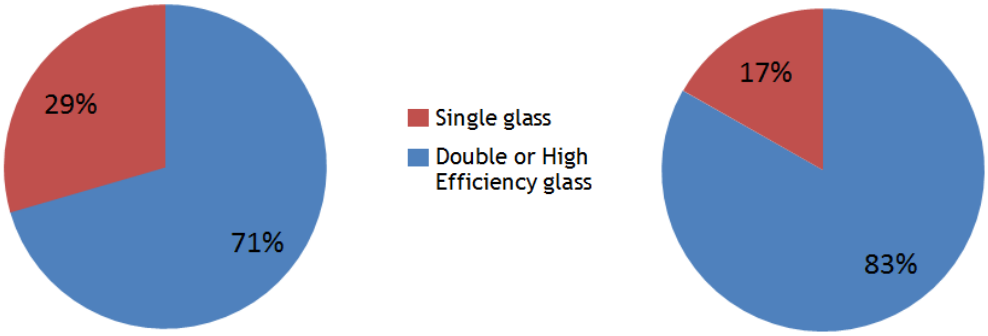

(a) SES (2001) (b) ECS (2012)

Figure 3.12: Evolution of use of insulated glazing in Belgian households [79]

Both 4 mm thick monolithic float glass and high efficiency 4/15/4 insulated glass (size 91 cm × 71 cm), mounted in commercial aluminium framing, have been subjected to short duration blast waves ($P_{so^+} \approx 20$ kPa and $i_{s+} \approx 16$ Pa·s) during the experimental work in support of this master's thesis.

3.4 Explosion-resistant glazing

Before elaborating on methods to estimate the blast resistance of some of the types of glazing which have been presented in the previous section, it seems appropriate to first introduce an additional, less common type of glazing, specifically designed for protection against explosions.

Explosion-resistant security glazing uses no extra features compared to the safety glazing previously discussed. However, by the nature of its assembly with thicker plies, multilayer laminates and robust framework and anchorages, it is able to resist blast waves resulting from an explosion. The degree of performance is tested with standardized conditions. Depending on the requirements which are met, a classification is accorded.

In the following paragraphs the European classification standards (by CEN) and the international classification standards (by ISO) are discussed. The classification codes they comprise are obviously amongst the most widely recognized codes around the world. The U.S. government standards for federal buildings (by GSA/ISC) and for Defence facilities (by DoD) are only briefly mentioned because of the significant overlap with the ISO-standards, which is explained by the fact that all of them refer to the same ASTM document as a basis for the classification criteria.

3.4.1 European standards

The European Committee for Standardization (CEN) has approved two European standards, each consisting of two parts, which encompass the prescribed test protocol and the performance requirements to be met for allocation of an explosion resistance classification, namely:

EN 13123-1 (2001) [45] Windows, doors and shutters - Explosion resistance - Requirements and classification - Part 1: Shock tube

EN 13123-2 (2004) [46] Windows, doors and shutters - Explosion resistance - Requirements and classification - Part 2: Range test

EN 13124-1 (2001) [47] Windows, doors and shutters - Explosion resistance - Test method - Part 1: Shock tube

EN 13124-2 (2004) [48] Windows, doors and shutters - Explosion resistance - Test method - Part 2: Range test

These European standards have been given the status of a Belgian standard after unaltered publication by the Belgian Institution for Normalisation (BIN) and are thus known as NBN EN 13123-1 (2001) [45], NBN EN 13123-2 (2004) [46], NBN EN 13124-1 (2001) [47] and NBN EN 13124-2 (2004) [48].

The 2001 standards concern a test method against blast waves generated using a shock tube facility to simulate a high explosive detonation in the order of 100 to 2500 kg TNT at distances of about 35 m to 50 m. The characteristics of the shock wave relate to the explosion pressure resistance (EPR) classification code which can be achieved, as seen in table 3.2 on page 46. Additionally, the duration of the positive phase t_{0+} must be no less than 20 ms. The standard adheres to the modified Friedlander equation 2.1, with a decay coefficient b between 0 and 4.

Table 3.2: Characteristics of the shock wave according to EN 13123-1 [45]

Class	P_{so+}	i_{s+}
EPR1	50 kPa	370 kPa·ms
EPR2	100 kPa	900 kPa·ms
EPR3	150 kPa	1500 kPa·ms
EPR4	200 kPa	2200 kPa·ms
Upper limit	250 kPa	3200 kPa·ms

The 2004 standards concern a test method against blast waves in open air resulting from high explosives that can be carried by hand and placed a few meters from a target. The characteristics of the attack in terms of charge mass W_{TNT}, radial stand-off distance R and height of burst HOB relate to the EXR classification code which can be achieved, as seen in table 3.3 on page 46.

Table 3.3: Characteristics of the attack according to EN 13123-2 [46]

Class	W_{TNT}	R	HOB
EXR1	3 kg	5.0 m	0.5 m
EXR2	3 kg	3.0 m	0.5 m
EXR3	12 kg	5.5 m	0.8 m
EXR4	12 kg	4.0 m	0.8 m
EXR5	20 kg	4.0 m	0.8 m

For both tests the window passes the test if neither perforation or opening through the test specimen nor opening between the test specimen frame and the test specimen support is evident through which a blunt 10 mm diameter rigid bar can pass.

The results of the test are further notated with an additional (S) or (NS) suffix with regard to the presence or absence of splinters originating from the rear (protected) face of the test specimen.

3.4.2 International standards

The International Organisation for Standardization (ISO) has approved two international standards, which encompass the prescribed test protocol and the performance requirements to be met for allocation of an explosion resistance classification, namely:

ISO 16933 (2007) [35] Glass in building - Explosion-resistant security glazing - Test and classification for arena air blast loading

ISO 16934 (2007) [36] Glass in building - Explosion-resistant security glazing - Test and classification by shock tube loading

These two international standards are in line with the two European standards in such a way that both accidental explosions and explosions from deliberate attacks have been addressed in two separate documents.

Different sets of scenarios are suggested for evaluation. ISO 16933 defines classification codes for seven standard scenarios involving vehicle bombs and seven standard scenarios involving hand-carried satchel bombs. ISO 16934 defines a more general explosion-resistant glazing classification comparable to the EPR classification out of EN 13123-1 but considering not four but six blast wave forms, summed up in table 3.4 on page 47.

Table 3.4: Classification of explosion-resistant glazing according to ISO 16934 [36]

Class	P_{so^+}	i_{s^+}
ER30(X)	30 kPa	170 kPa·ms
ER50(X)	50 kPa	370 kPa·ms
ER70(X)	70 kPa	550 kPa·ms
ER100(X)	100 kPa	900 kPa·ms
ER150(X)	150 kPa	1500 kPa·ms
ER200(X)	200 kPa	2200 kPa·ms

From this table can be seen that the classification code contains an extra parameter (X) which has not been identified yet. Indeed, there is an additional step to take in the classification method according to the ISO standards, namely the determination of a so-called hazard rating related to the specific load conditions.

The method to be followed to define the hazard rating is adopted from an older American Society for Testing and Materials (ASTM) standard, namely:

ASTM F1642-04 (1996) [4] Standard test method for glazing and glazing systems subject to air blast loadings

According to ASTM F1642-04 (1996) [4], the hazard rating achieved by the glazing is based upon the severity of fragments generated during the test. The fragment severity is based upon the number, size, effects and location of fragments.

Fragments are defined as any particle with a united dimension[6] of 25 mm or greater. A 3 m high witness panel is mounted at the very end of the 3 m long witness area. A cross-section of the witness area is represented in figure 3.13 on page 48.

For reasons of simplicity, the quantitative assessment is corresponding to a qualitative scale, coded A to F. Its meaning is given in table 3.5 on page 48.

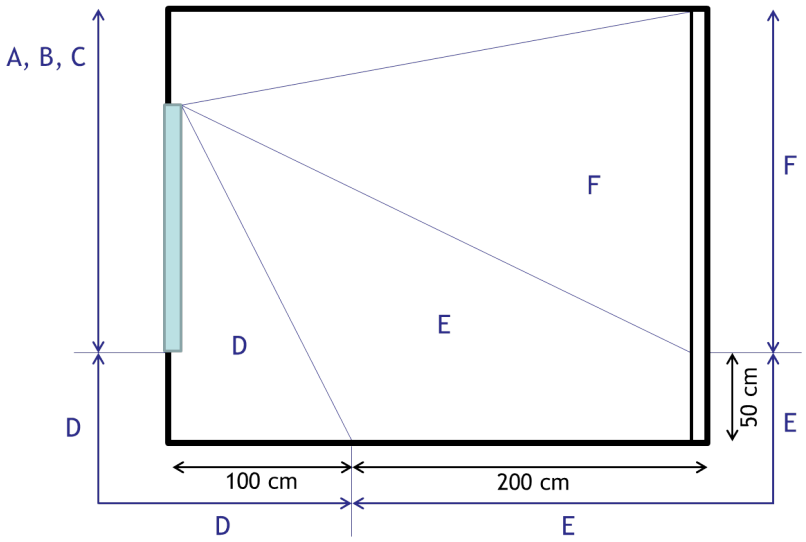

Figure 3.13: Cross-section through witness area for ISO tests [35, 36]

Table 3.5: Hazard ratings according to ISO 16933 and ISO 16934 [35, 36]

Class	Hazard rating
A	no break
B	no hazard
C	minimum hazard
D	very low hazard
E	low hazard
F	high hazard

[6]The united dimension of a glass particle is determined by adding its width, length and thickness.

3.4.3 U.S. government standards

In the wake of the 1995 terrorist bombing of the A.P. Murrah Federal Building in Oklahoma City, the U.S. government established the Interagency Security Committee (ISC), a permanent body that would continue to address government-wide security concerns. As such the ISC developed specific security design criteria to be met by the federal facilities of the U.S.

There is no information readily available as to the specific threat scenarios which should be addressed, as this is closely related to the so-called facility security level (FSL) of the building in question. However, a standard test method does exist for federal facilities (by GSA). As usual, the U.S. Department of Defence (DoD) buildings make use of their own technical procedures, the so-called Unified Facilities Criteria (UFC). The documents of interest are:

GSA-TS01-2003 [28] Standard test method for glazing and window systems subject to dynamic overpressure loadings

UFC 4-010-01 (2013) [73] Minimum antiterrorism standards for buildings[7]

The GSA criteria define five injury hazard performance conditions to indicate whether and how far glass shards penetrate into a room when the window and wall segment are subjected to a blast of calculated impact pressure.

The protection performance conditions are numerically defined from 1 (safe) through 5 (low protection) as indicated in table 3.6 on page 49. Mark from figure 3.14 on page 50 that the GSA conditions, which are characterized based on glass breakage within a ten-foot box, are very similar to the six hazard ratings included in the ISO standards.

Table 3.6: GSA/ISC protection levels [28]

Class	Protection level	Hazard level
1	Safe	None
2	Very High	None
3a	High	Very Low
3b	High	Low
4	Medium	Medium
5	Low	High

In UFC 4-010-01 a similar hazard rating is implemented to assess the level of protection of new and existing buildings.

[7] If it is evaluated that the minimum antiterrorism standards from UFC 4-010-01 are inadequate, additional protective measures per UFC 4-020-01 will be required.

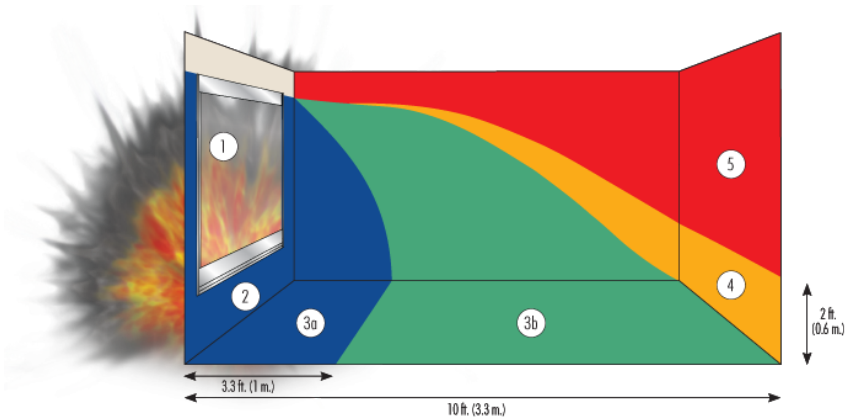

Figure 3.14: Hazard rating according to GSA-TS01-2003 (www.grahamwindows.com)

3.4.4 Mitigating elements

Protective glazing can only be effective when designed as a complete, unified assembly including glazing, frames, connection to other building envelope materials, and the structural frame. The connection between the glazing and the frame, as well as the bite, specifying how far the glazing is imbedded into the frame, are the main concern.

Depending on the window's or building's location, size of the glazed opening, occupant load, and criticality of functions and missions housed within the facility, additional elements could be installed to mitigate the glass fragment hazards. Some available features, discussed in a Whole Building Design Guide (WBDG) resource page by Smith & Renfroe (2010) [62], are briefly reviewed.

Anti-shatter films are tough, transparent films consisting of multiple, micro-thin polyester layers that work to hold shattered glazing together. The films are applied with adhesive to the interior-glazing surface. They are generally used in renovation or retrofit situations where entire window unit replacement with protective window systems is not practical or cost effective.

Curtain and shield systems may be added on the window interiors to serve as a catch system to further prevent the danger of flying glass fragments. These devices can range from heavy clear sheet plastic film hung from the window frame head to mechanical security window shades that have the appearance of commercial decorative shades.

Catch cable and catch bar systems are used to enhance protective glazing performance in buildings at risk of window blow-out in a blast attack. A blast wave causes the pane to flex at the center and pulls it away from the window framing system. Rigid cables or rods of steel are installed on the interior frame of windows and serve to back up the primary window framing system and dissipate air pressures more evenly over an entire window pane.

3.5 Empirical blast strength of glass

In the late 1980s the Dutch Committee for the Prevention of Disasters caused by Dangerous Substances issued several publications, formally known as the CPR-guidelines and often referred to as the *Coloured Books*.

Publication CPR 16E (1989) [17], known as the *Green Book*, discusses methods for the determination of possible damage to people and objects resulting from releases of hazardous materials. It is founded on research performed by TNO, The Netherlands Organisation of Applied Scientific Research.

In the early years of the 21st century a full revision process was accomplished, which transformed the CPR-guidelines into the actuated Publication Series on Dangerous Substances (PGS). The second chapter of the *Green Book* on the consequences of explosion effects on structures is since replaced by part 2B of PGS1 (2003) [57].

The newer version holds no differences as to the fundamental approach of study. The technique which was adopted by TNO departs from the concept that if the natural frequency, the static strength and the ductility ratio of the structure are known, the possible damage from a given blast can be determined. This is the so-called quasi-static solution method, introduced by Biggs in 1964 [8].

In this method the static strength of the structural component is first estimated, after which its dynamic response is determined by evaluating the phase duration t_d of the blast with respect to the natural period of vibration τ of the structural component. The ductility ratio Du has already been discussed above. Recall that from the brittle nature of glass, Du is taken equal to unity. The natural frequency f_n and the static strength S of window panes are introduced below.

There are however some differences between the old and new version as to the static strength calculation models presented. Firstly, PGS1 part 2B expanded the experimental data which have been reported in CPR 16E, improving the empirical formula of the dynamic strength D for windows. Secondly, PGS1 part 2B suggests an alternative approach for the iterative calculation of the static strength S as presented in CPR 16E with alternative equations which are easier to solve numerically.

Technical Manual TM 5-1300-1 (1990) [69] by the U.S. Department of Defence served for many years as guide of reference for the design of structures to resist the effects of accidental explosions in the U.S. It was superseded by UFC 3-340-02 (2008) [72] and is cited here because it contains a similar assessment approach for blast loading of fully tempered glass panes. The resulting strength predictions are therefore briefly compared with the results following the Dutch procedure.

3.5.1 The undamped SDOF system

Dynamic load problems can be studied approximatively by means of the single-degree-of-freedom (SDOF) approach. In this method the actual structural component is replaced by an equivalent system of one concentrated mass m and one weightless spring with spring constant K representing the resistance of the structure against deformation. This simplified system is under the effect of an external force $F(t)$ exerted by the dynamic load. The structural resistance of the system to this force is expressed in terms of the vertical displacement $z(t)$. For brittle materials such as glass, the resistance will be merely elastic, opposed to materials showing some ductility, where elasto-plastic behaviour is expected. The idealized SDOF system and its principal components are illustrated in figure 3.15 (a) on page 52.

For reasons of simplification the blast load $F(t)$ is also idealized as a triangular load with a peak force F_{max} and a duration of linear decay t_d. As can be seen from figure 3.15 (b) on page 52, the external force is derived from the given blast load by introducing the contact surface where the blast load hits the structure. For the scope of this master's thesis, the contact surface is expressed in terms of the dimensions of a window pane, so its width a and its height b. The blast load $F(t)$ is uniformly distributed normal to the contact surface thus due to the reflected (over)pressure P_r.

Equation 3.4 is Biggs' equation of motion for the undamped elastic SDOF system. Its general solution falls apart in expressions for displacement $z(t)$ and velocity $\dot{z}(t)$. From these expressions can be seen that the structural variables m and K of the SDOF system can be combined into one fundamental property of a structure, namely its natural angular frequency of vibration ω_n.

$$m\ddot{z}(t) + Kz(t) = F(t) = F_{max}\left(1 - \frac{t}{t_d}\right) \tag{3.4}$$

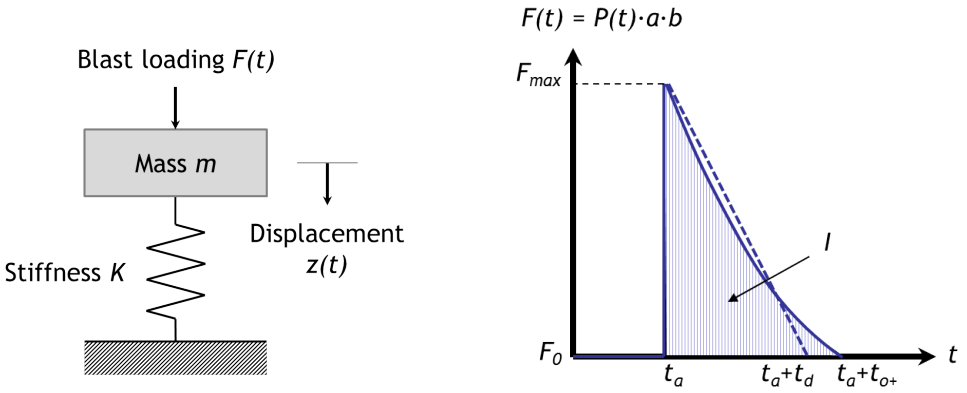

(a) The idealized SDOF system (b) Blast loading $F(t)$ on a surface $a \times b$

Figure 3.15: The idealized structural SDOF system with its triangular blast load [51]

3.5.2 Natural frequency

The natural angular frequency of vibration ω_n is related to the natural frequency f_n of the structure, which gives the number of vibrations per second of the structure if brought into simple harmonic motion. The inverse of f_n is of course the undamped natural period of free vibration τ. The relations are shown in equation 3.5.

$$\sqrt{\frac{K}{m}} = \omega_n = 2\pi f_n = \frac{2\pi}{\tau} \tag{3.5}$$

The undamped natural period of free vibration τ of a structure is crucial for the evaluation of its dynamic behaviour. It determines the time required for the vibration to go through one complete cycle during which the system twice reaches the maximum dynamic displacement $z_{max,dyn}$ from its state of equilibrium. Hence, the undamped natural period of free vibration τ is characteristic for the rate of response to a dynamic load. If the duration of the load t_d is long compared to the undamped natural period of free vibration τ of the structure, then $z_{max,dyn}$ will be reached. For loads of short duration the load will no longer be acting on the structure by the time the maximum deflection is reached, increasing the chances of survival for the same peak force F_{max} of the dynamic load.

In the latter situation ($\tau \ll t_d$), associated with high yield blast phenomena, the maximum response of the structure will take place during the first vibration, meaning the structure will vibrate with its lowest or first mode natural frequency f_1. Damping at that moment does not have any practical influence, which affirms the choice of an undamped SDOF system as the simplified structural model to study.

Equation 3.6 by Timoshenko (1959) [67] predicts the lowest natural frequency f_1 of a plate on the basis of its geometrical and mechanical properties.

$$f_1 = \frac{\pi}{2} \cdot \left(\frac{1}{a^2} + \frac{1}{b^2}\right) \cdot \sqrt{\frac{E \cdot d^2}{12 \cdot \rho \cdot (1 - \nu^2)}} \tag{3.6}$$

$a =$ width (or longest dimension) of the window pane;

$b =$ height (or shortest dimension) of the window pane;

$d =$ thickness of the window pane;

$\rho =$ density, approximately 2500 kg/m^3 for SLG;

$E =$ Young's modulus of elasticity, approximately 72 GPa for SLG;

$\nu =$ Poisson's coefficient, approximately 0.23 for SLG.

3.5.3 Dynamic load factor

To obtain the response of a linear elastic system, it is convenient to consider the concept of the dynamic load factor. The dynamic load factor DLF is defined as the ratio of the maximum dynamic displacement $z_{max,dyn}$ to the static displacement z_{st} which would have resulted from the static application of the peak force F_{max} of the dynamic load.

$$\text{DLF} = \frac{z_{max,dyn}}{z_{st}} \tag{3.7}$$

If the DLF is known, the maximum dynamic response $z_{max,dyn}$ is thus derived from a calculated static deformation z_{st} due to the peak force F_{max}. This expresses clearly why this calculation method is said to be quasi-static. The dynamic component is accounted for through the use of the dynamic load factor but the solution sequence is static of nature. From equation 3.7 can be understood that if the DLF is smaller than unity, the dynamic load which the structure is able to resist will be higher than the static one, and vice versa.

The dynamic response chart for the elastic SDOF system with triangular load is presented in figure 3.16 on page 55. It graphically shows the solutions of equation 3.4 in terms of the time at maximum dynamic displacement t_{max} for the maximum dynamic displacement $z_{max,dyn}$ of the structure. The latter can in turn be determined from the predicted value of the DLF using equation 3.7. In UFC 3-340-02 (2008) [72] more dynamic response charts are found, both for different types of loading and for different types of structural response (i.e. elastic as well as elasto-plastic). They originate from Biggs (1964) [8]. The solutions are explicitly written as a function of the ratio t_d/τ because the load duration t_d relative to the structure's natural frequency τ^{-1} significantly influences the structural response to blast loading (cf. supra). Hence, loading conditions are separated into three loading regimes:

a. impulsive loading regime for $t_d/\tau < 0.1$ [43] or $\omega_n \cdot t_d \leq 0.4$ [5],

b. quasi-static loading regime for $t_d/\tau > 10$ [43] or $\omega_n \cdot t_d \geq 40$ [5], and

c. dynamic loading regime for intermediate values of t_d/τ or $\omega_n \cdot t_d$.

From the chart it is seen that the quasi-static loading regime, where the load duration is the longest, must be associated with the highest values of the DLF and is thus considered as the more dangerous one for a structure. The green lines on the chart are related to the limit criteria put forward by Baker et al. (1983) [5]. According to Mays et al. (2009) [43] they should be slightly shifted to the right.

Unfortunately for windows with small dimensions the natural frequency f_n is large (cf. equation 3.6). This means that τ^{-1} is large as well, implying that window breakage is often a quasi-static load phenomenon ($t_d/\tau \gg$). The assumption that the Flemish 40 mbar criterion pertains to external human risk some distance away from the burst center, where t_d has become longer, supports this conclusion.

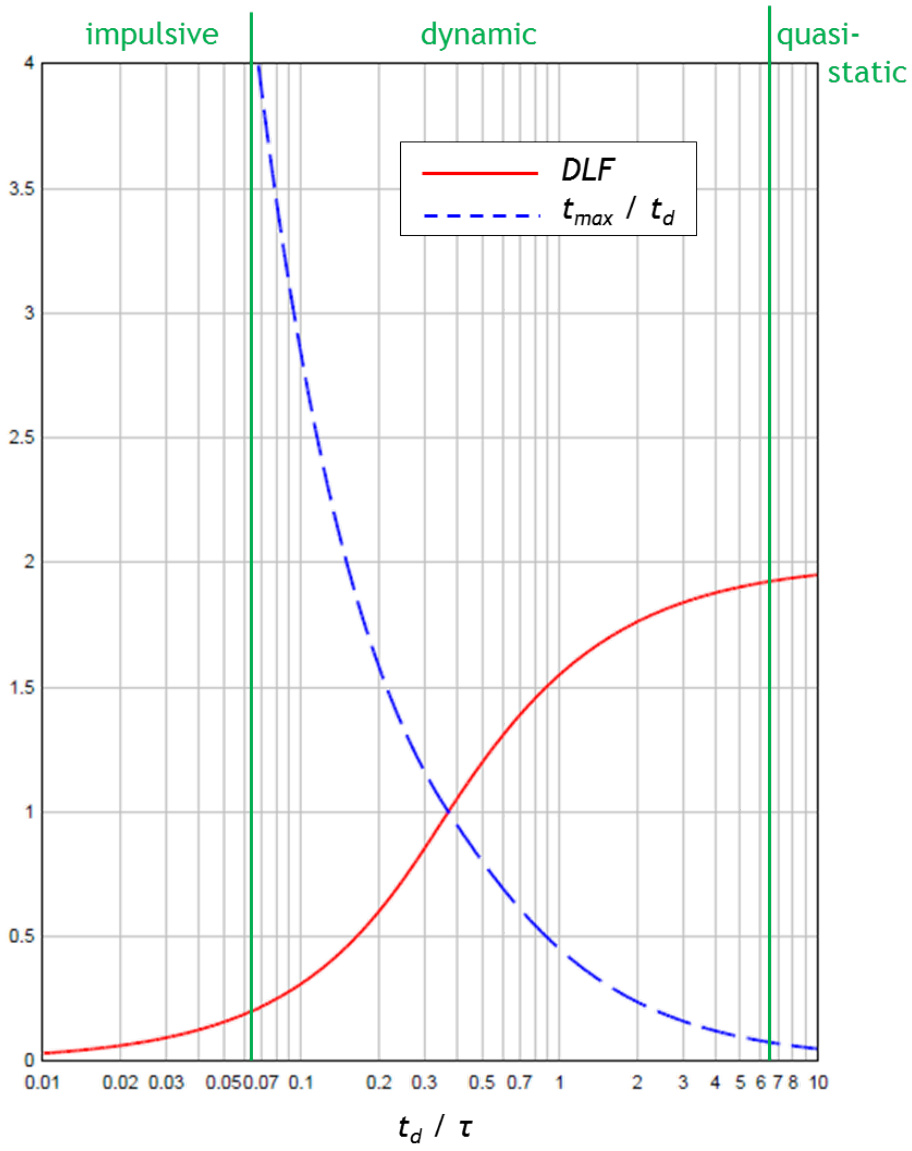

Figure 3.16: Maximum response of elastic SDOF system for triangular load [72]

3.5.4 Static strength

Recall from section 3.2 on the mechanical properties of glass that failure is dominated by the highest concentrations of tensile stress. These occur either in the center or in the corners of the ply. In his fundamental work on plates and shells Timoshenko (1959) [67] describes a theory allowing to estimate the principle stresses at these locations in relation to the deflection of the plate. The solutions for a simply supported ply, subjected to a uniformly distributed static force F_{st} which gives rise to a uniform static pressure P_{st} ($= F_{st}$ per unit surface area $a \times b$), are written here.

a. principle tensile stresses in the center of the plate:

$$\sigma_1 = 6\pi^2 \cdot \zeta \cdot P_{st} \cdot \left(\frac{b}{d}\right)^2 \left(1 + \nu \left(\frac{b}{a}\right)^2\right) \tag{3.8a}$$

$$\sigma_2 = 6\pi^2 \cdot \zeta \cdot P_{st} \cdot \left(\frac{b}{d}\right)^2 \left(\left(\frac{b}{a}\right)^2 + \nu\right) \tag{3.8b}$$

where it is seen that $\sigma_1 > \sigma_2$ when $a \geq b$

b. principle tensile stresses in the corners of the plate:

$$\sigma_1 = 6\pi^2 \cdot \zeta \cdot P_{st} \cdot \left(\frac{b}{d}\right)^2 \left(\frac{b}{a}\right) (1 - \nu) \tag{3.9a}$$

$$\sigma_2 = 6\pi^2 \cdot \zeta \cdot P_{st} \cdot \left(\frac{b}{d}\right)^2 \left(\frac{b}{a}\right) (\nu - 1) \tag{3.9b}$$

where it is seen that $\sigma_1 = -\sigma_2$

c. dimensionless factor ζ (from the Fourier series of the wave function):

$$\zeta = \frac{16}{\pi^6 \left(1 + \left(\frac{b}{a}\right)^2\right)^2} \tag{3.10}$$

If the maximum principle stress σ_1 in the plate exceeds the dynamic strength D, the plate will break. One could thus inverse the solutions from equations 3.8a and 3.9a in order to determine the uniform static pressure P_{st} for which this happens. P_{st} will then correspond to a (localised) static strength S of the plate (i.e. the exerted pressure at failure) which will be different in the center as in the corners.

a. static strength in the center of the plate:

$$S_{\text{center}} = \frac{D}{6\pi^2 \cdot \zeta \cdot \left(\frac{b}{d}\right)^2 \cdot \left(1 + \nu \left(\frac{b}{a}\right)^2\right)} \tag{3.11}$$

b. static strength in the corners of the plate:

$$S_{\text{corner}} = \frac{D}{6\pi^2 \cdot \zeta \cdot \left(\frac{b^3}{a \cdot d^2}\right) (1 - \nu)} \tag{3.12}$$

3.5.5 Critical deflection

The next question to be answered is where the plate will actually fail. Thick, stiff plates will show minor deflection. Here the stresses will be highest in the center of the plate, meaning S_{center} will dominate the static strength. Above a certain critical deflection δ_{cr} however, the stresses in the corners will become more important and S_{corner} will become determinant (equation 3.13). In PGS1 a linear interpolation for the static strength is suggested below the critical deflection (equation 3.14).

a. if $\delta(S_{\text{center}}) \geq \delta_{cr}$:

$$S = S_{\text{corner}} \tag{3.13}$$

b. if $\delta(S_{\text{center}}) < \delta_{cr}$:

$$S = S_{\text{center}} + \frac{\delta(S_{\text{center}})}{\delta_{cr}} \cdot (S_{\text{corner}} - S_{\text{center}}) \tag{3.14}$$

Harmanny experimentally determined that for square plates the deflection reaches its critical value after six times the thickness of the plate. The influence of the aspect ratio is accounted for with an exponential term. The resulting formula is given in equation 3.15.

$$\delta_{cr} = 6\ (\frac{a}{b})^{\frac{3}{2}} \cdot d \quad \text{for } a \geq b \tag{3.15}$$

The actual deflection δ caused by a uniform static pressure, here taken equal to the (localised) static strength S_{center} in the center of the plate, is calculated using equation 3.16 from the large deflection plate theory by Timoshenko (1959) [67].

$$\delta(S_{\text{center}}) = \frac{\zeta \cdot S_{\text{center}} \cdot b^4}{B} \tag{3.16}$$

The symbol B in the denominator refers to the bending stiffness of the plate, defined in equation 3.17.

$$B = \frac{E \cdot d^3}{12\ (1 - \nu^2)} \tag{3.17}$$

3.5.6 Dynamic strength

The only parameter which is currently still unknown, is the dynamic strength D. Therefore, the peak blast overpressure P_r needed for failure (at high strain rate) for a set of window panes was determined experimentally.[8] When this overpressure is multiplied by the dynamic load factor, the static pressure P_{st} is generated which

[8] For a window directly facing the source of the explosion, the reflection coefficient k_r is more or less equal to 2 (cf. chapter 2 page 22). For random orientation, Reed (1992) estimates an average k_r of 1.32 (from Lees (2005) [41] pp. 17/233).

would result in the equivalent failure event (at low strain rate). For this static pressure P_{st} the principal stress σ_1 in the window panes is calculated using either of equations 3.8a and 3.9a in accordance with the perceived location of failure. This stress eventually indicates the dynamic strength D of the window.

Note that the dynamics of the failure event are thus incorporated in a static calculation model. In other words, by combining a static (low strain rate) strength model with data from experimental testing with explosions, a dynamic (high strain rate) strength model was created.

From the collection of results an empirical formula with an average correlation difference of 10 % was edited to be able to calculate relatively easily the dynamic strength D of windows with only their geometrical characteristics as input variables. This important empirical result is expressed in equation 3.18.

$$D = 14.9\,\text{MPa} \cdot \left(\frac{d}{1\,\text{m}}\right)^{-0.32} \cdot \left(\frac{a}{b}\right)^{0.47} \tag{3.18}$$

It is admitted that the experiments related to the TNO models were conducted with new and intact window panes, excluding the influence of detrimental surface conditions in the empirical formula. This feature, although its importance has been clearly addressed, is by its very nature rather difficult if not impossible to study in practice. Therefore it usually remains unaccounted for in the damage predictions. However, it is sometimes assumed with some optimism that the detrimental effects are included in the standard deviation range of the empirical solutions.

For double glass with inner ply thickness d_i and outer ply thickness d_o, the loading distributes itself over both panes proportionally to their respective stiffness. The thickest pane governs the resistance behaviour. Therefore, the static strength S is calculated for the thickest pane and the result is multiplied with a factor, given in equation 3.19. If both panes have the same thickness, a factor of 1.4 should be adopted.[9]

$$\frac{d_i^3 + d_o^3}{[max(d_i, d_o)]^3} \leq 1.4 \tag{3.19}$$

Note that the *Green Book*, which is still considered an important work of reference nowadays (e.g. multiple citations in Lees' 2005 revision [41]), contains different (less operative) formulas for the (localised) static strength in the center and in the corners of the window and a different (older) empirical formula for the dynamic strength D of windows. In view of the own experimental work conducted for this master's thesis it was preferred to focus on the (newer) PGS1 method.

[9] The Belgian construction federation prescribes an uppervalue of around 1.2 for symmetrical double glass (from WTCB (1999) [80] pp 79-80).

3.5.7 PGS1 (2003) versus UFC 3-340-02 (2008)

It is interesting to compare the method to assess blast strength of windows from PGS1 part 2B, which is a research document that supports QRA calculations, with the approach of UFC 3-340-02, which is a U.S. government design code that is used for blast-resistant design.

Both present undamped SDOF-based solutions with a peak triangular-shaped pressure-time curve. However UFC 3-340-02 introduces a non-linear stiffness $K(z)$ in the SDOF system which results in a parabolic rather than linear elastic resistance function. The model calculates the peak blast pressures required to break fully thermally tempered glass (FTG, see section 3.3).

Different from the PGS1 report, UFC 3-340-02 clearly pertains to potentially blast-resistant windows. This is seen from the adopted design stress, or the maximum principal tensile stress σ_1 allowed for the glazing, which is set at 16 000 psi ($\approx$ 110 MPa). This value should correlate with a probability of failure p_f equal to or less than 0.001 which appears significantly different from the 0.5 probability of failure which is retained in PGS1. However, with a safety factor of no less than 8 involved, the latter is expected to produce comparable levels of resistance.

In UFC 3-340-02 the maximum deflection $z_{max,dyn}$ is defined as the center deflection where the maximum principle tensile stress σ_1 at any point in the glass first reaches the above mentioned limit value of the design stress. It is assumed that the point of maximum principle tensile stress will migrate from the center toward the corners of the plate as the central deflection exceeds a third of the thickness. The model further assumes that failure occurs when the maximum deflection exceeds ten times the glazing thickness. Finally, there are no solutions included for double glazing.

There are both tabular and chart-based solutions given in UFC 3-340-02, for combinations of the following design parameters:

a. a blast overpressure capacity up to 100 psi ($\approx$ 700 kPa);

b. an aspect ratio a/b between 1 and 4, where 4 remains applicable if $a/b > 4$;

c. a pane area $a \times b$ between 1.0 and 25 ft^2 ($\approx$ 0.1 to 2.5 m^2);

d. a nominal glass thickness d between 0.25 and 0.75 in ($\approx$ 6 to 18 mm).

Figure 3.17 on page 60 shows six of these charts. One can immediately observe how the peak blast pressure capacity P_r is asymptotically decreasing with blast pressure duration t_d, indicating that for large explosions the breaking pressure is essentially independent of duration. This is something which cannot explicitly be included in the PGS1 calculations. Recall however that the load duration is implicitly present in the empirical blast strength formula of PGS1 (equation 3.18) through the DLF of the quasi-static calculation model.

For ease of comparison, two equivalent PGS1 solutions have been plotted on each of the UFC-charts (green markings).

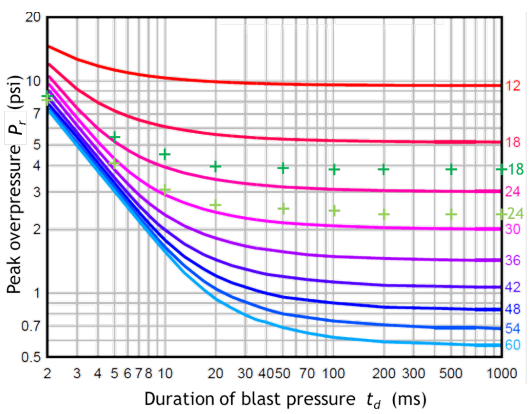

(a) $a/b = 1$; $d = 0.25$ in (≈ 6 mm)

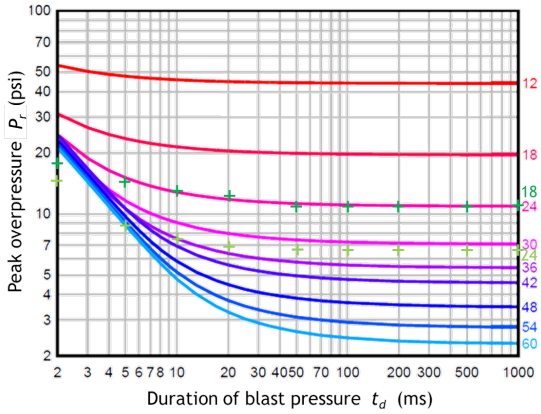

(b) $a/b = 1$; $d = 0.50$ in (≈ 12 mm)

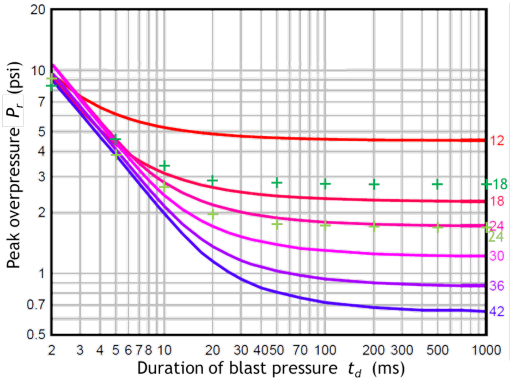

(c) $a/b = 2$; $d = 0.25$ in (≈ 6 mm)

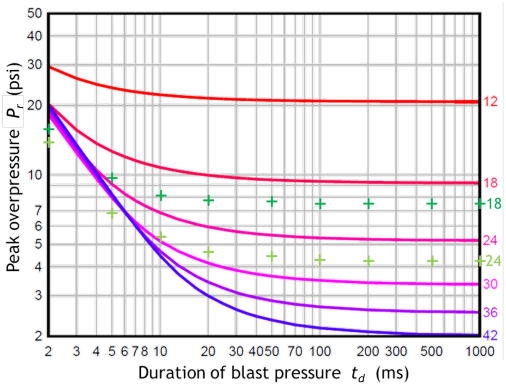

(d) $a/b = 2$; $d = 0.50$ in (≈ 12 mm)

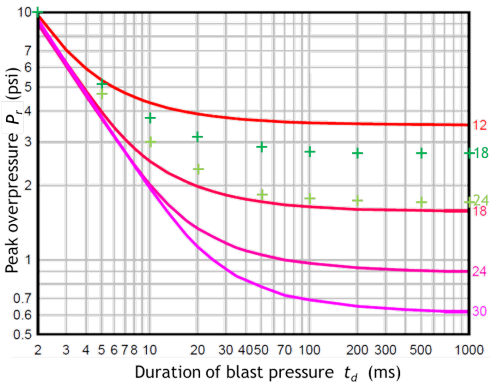

(e) $a/b = 4$; $d = 0.25$ in (≈ 6 mm)

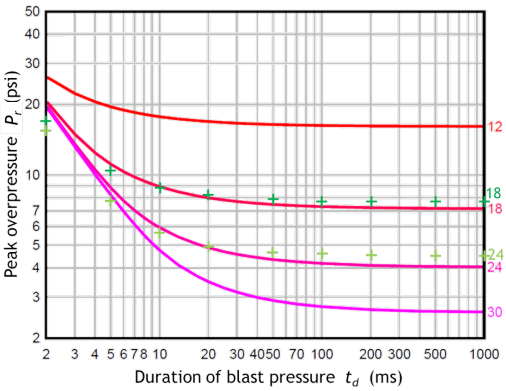

(f) $a/b = 4$; $d = 0.50$ in (≈ 12 mm)

Figure 3.17: UFC 3-340-02 design charts for FTG panes with aspect ratio a/b and thickness d; numbers next to the curves indicate pane dimension b (inches); green indicators refer to results of an equivalent window pane according to PGS1 [57, 72]

Making use of equation 3.20 as a rule of thumb for the lower limit of the quasi-static load domain (cf. figure 3.16 on page 55), it is found that the calculated results for 14 inch and 18 inch according to PGS1 enter the quasi-static loading domain for a duration of blast pressure t_d in a range between 21 ms and 141 ms. It could be argued whether the results lying below the lower limit of the quasi-static load domain have good validity. Anyway a rather good agreement is found between the two models for the entire range examined.

$$\frac{t_d}{\tau} \geq \frac{40}{2\pi} \approx 6.37 \tag{3.20}$$

Where UFC 3-340-02 clearly states that the windows which have been tested were made of FTG, PGS1 provides no information on the manufacturing technique used for the 137 glass plies with varying dimensions, which have been tested by TNO. However, referring to the level of agreement between the two methods which are discussed, it seems unlikely that TNO has made use of ANG, recalling that ANG should be typically considered four to five times less strong than FTG [72].[10]

Mutual comparing of the available charts leads to the ascertainment that:

a. thicker windows (parameter d) can cope with higher blast overpressures,

b. larger windows (parameter $a \times b$) are more prone to failure, and

c. windows with a larger aspect ratio (parameter a/b) fail more easily as well.

From the plotted PGS1 solutions it is seen that the first two observations are also valid when using the PGS1 model. They are generally confirmed by reports on similar experiments found in literature (e.g. Fletcher et al. (1980) [25]). However, some contradictory results occur with respect to the third observation, when considering an aspect ratio a/b equal to 4.

Harmanny's critical deflection formula (equation 3.15) originated from experiments with square specimens of glass and polycarbonate which resulted in the factor $6 \cdot d$ in the equation. In PGS1 there is no thorough explanation given for the reasoning behind the exponential term accounting for the aspect ratio $(a/b)^{1.5}$. The discrepancy between PGS1 and UFC 3-340-02 in figures 3.17 (c) and (e) or (d) and (f) could thus suggest validity issues for larger values of aspect ratio.[11] On the other hand it is noted that the UFC 3-340-02 solutions for an aspect ratio equal to 4 lie on the applicability limits of this calculation method. The fact that these solutions are accepted for all aspect ratios larger than 4 as well, might have been anticipated with more conservative results as a consequence.

[10] Oddly, TNO informed the author that regular float glass (i.e. ANG) was used.

[11] When inquiring TNO about this observation, the author was informed that due to significant deviations, TNO no longer uses the PGS1 method but has meanwhile adopted a new model.

For sake of completeness it is noted that the above-stated observations a. and b. have inspired some researchers to develop relations between pane thickness and window surface on the one hand and breaking pressure on the other hand.

Gilbert (1994) for instance analysed the results of the experimental study conducted by Marshall et al. (1977) on breaking of glass windows by internal gas explosions, to derive equation 3.21 (as reported in Lees (2005) [41] pp. 17/236).

$$P_r \text{ (kPa)} = 132 \cdot \left(\frac{d}{a \cdot b} \right) + 5.43 \tag{3.21}$$

Figures 3.18 (a) and (b) on page 62 show results from the work by Marshall et al. (1977) as reported in Lees (2005) [41], where the influence of thickness d and window area $a \times b$ are illustrated well. However, when comparing solutions from equation 3.21 to the solutions presented earlier, based on PGS1 and UFC 3-340-02 methodology, it is easily concluded that Gilbert's equation is highly conservative.

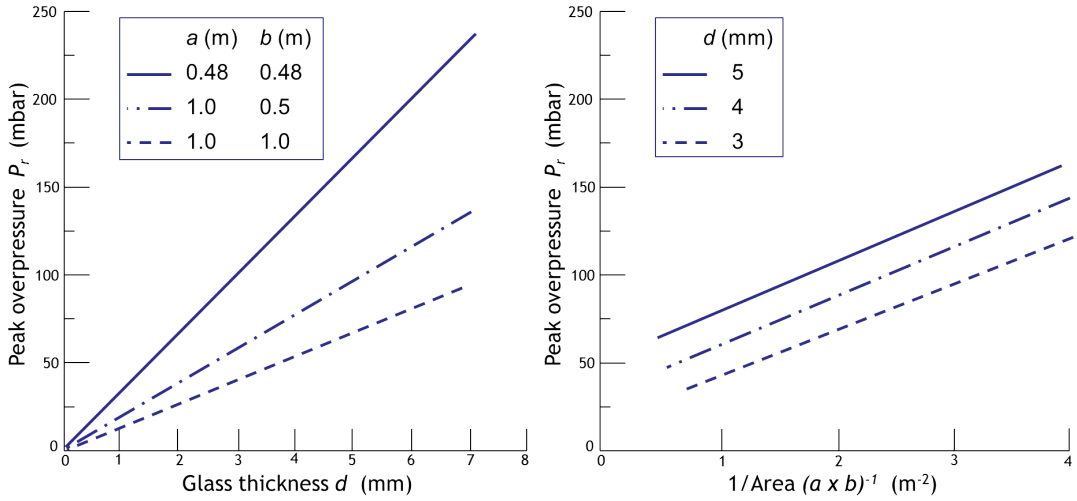

(a) Influence of glass thickness d

(b) Influence of window area $a \times b$

Figure 3.18: Reflected overpressure P_r at break
according to Marshall et al. (1977) as reported in Lees (2005) [41]

3.5.8 Probit relations for window breakage

Due to the uncertainty inherently linked to the strength (or failure) of glass, it can be reasonably expected that the probit function, as introduced in chapter 1, is a convenient concept to address the likelihood of glass breakage when subjected to a blast wave. This section is therefore concluded by a selection of probit functions available in literature (with values for P_{so+} needed in Pa).

Eisenberg et al. (1975) analysed data collected by Fugelso et al. (1972) on glass breakage of an internal gas explosion of 500l TNT equivalent, resulting in probit equation 3.22 as reported in Lees (2005) [41] pp. 17/236.

$$Pr = -18.1 + 2.79 \ln P_{so+} \tag{3.22}$$

CPR 16E (1989) [17] and PGS1 part 2B (2003) [57] both present the same pair of probit functions, developed by TNO, where distinction is made between windows in older buildings with lower strength (equation 3.23a) and windows in newer buildings with higher strength (equation 3.23b). The values for P_{so+} associated with a p_f of 1 % (lower limit) and 50 % have been included in table 2.4 on page 26.

$$Pr = -11.97 + 2.12 \ln P_{so+} \quad \text{(before 1975)} \tag{3.23a}$$
$$Pr = -16.58 + 2.53 \ln P_{so+} \quad \text{(after 1975)} \tag{3.23b}$$

Notice how the pressure for window breakage is generally quoted in terms of the peak side-on overpressure P_{so+}. In a range of values of P_{so+} up to 10 kPa, the solutions proposed by Eisenberg et al. (1975) and TNO have been compared to one another as can be seen from figure 3.19 on page 63. Attention is once again drawn to the fact that the force acting on the window is actually due to the reflected pressure P_r, as this could be misleading.

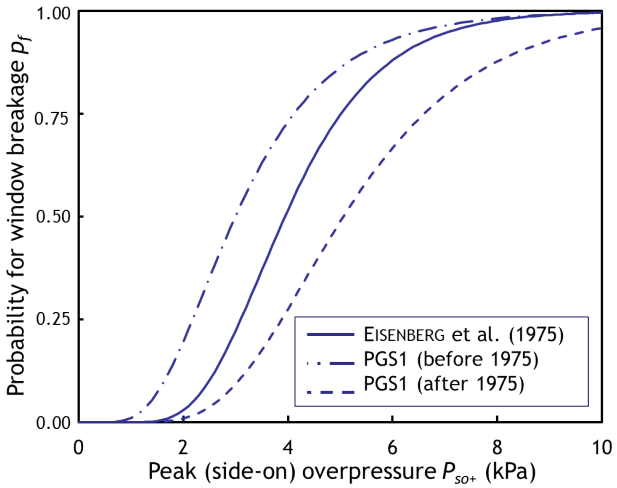

Figure 3.19: Solutions of selected probit functions for window breakage [41, 57]

From the observation that most of the models which have been discussed rely solely on peak overpressure information, the author concludes that the limit for window breakage which has been derived from historical accident data or large scale experiments was generally assessed at great distances away from the burst center

of a high yield blast event, characterized by a long phase duration. At first sight, this may seem in line with the concept of external human risk lying beyond the premises of a major risk installation. However from the substantially low efficiency factor related to industrial explosion scenarios compared to the high yield (military, nuclear) explosions, significant overestimation of the effects is to be expected [31].

Referring to the charted UFC solutions shown in figures 3.17 (a) to (f) on page 60 it is seen that the asymptotic values for window breakage can be thought of as lower limits. This makes them a conservative choice in risk management processes. Notice though how unthoughtful application of such models can lead to odd results where very low yield explosion events would theoretically still predict some injury or fatality probability even if there wouldn't be any structural damage at all. This can only be avoided if information on the duration of the shock wave is incorporated in the model as well. One way of doing so, is by adopting a so-called pressure-impulse diagram.

3.6 The pressure-impulse diagram

When altering F_{max} and i according to the transformation equations 3.24a and 3.24b, the response chart of the elastic SDOF system, plotted in figure 3.16 on page 55, can be transformed into a non-dimensionalised pressure-impulse or P-I diagram.

$$\bar{P} = \frac{2F_{max}}{S} = \frac{2F_{max}}{K \cdot z_{max,dyn}} \tag{3.24a}$$

$$\bar{I} = \frac{i \cdot \omega_n}{S} = \frac{i}{\sqrt{K \cdot m} \cdot z_{max,dyn}} \tag{3.24b}$$

This diagram enables the user to easily assess the response of a structural component to a specific load from the evaluation of the maximum dynamic displacement $z_{max,dyn}$ exhibited, opposed to the maximum allowable value. The curve thus indicates the combinations of pressure and impulse that will cause equal amount of damage, as seen in figure 3.20 on page 65. Load conditions that fall to the left of and below the curve will not induce failure while those to the right and above the graph will produce damage in excess of the allowable limit. For the impulsive load regime (left), it is seen that the expected damage depends on the value of the exerted impulse, independently of the shape of the load. Oppositely, for the quasi-static load regime (right), the peak load F_{max} and the structural behaviour, characterised by ω_n, dominate the effects on the structure. Brittle targets generally lie near the overpressure asymptote.

A determinant parameter in terms of structural response assessment is the allowable ductility Du related to the structural component which is studied. From section 3.2 it is understood that the ductility equals unity for glass elements. The iso-damage curve on a P-I diagram showing all load combinations that correspond to $Du = 1$, therefore marks a damage and a no damage region in this case.

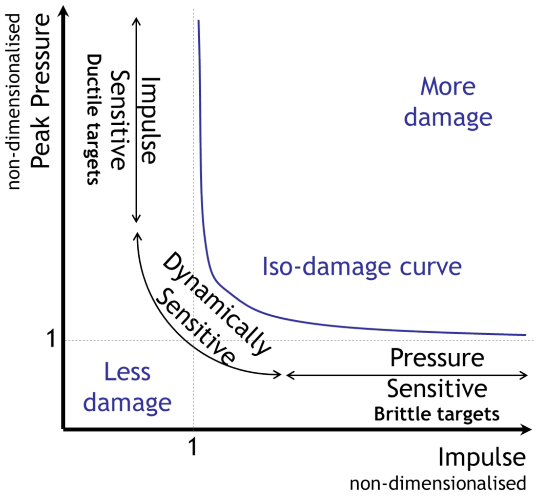

Figure 3.20: P-I diagram from a blast wave for an elastic SDOF system [31, 43]

Finally, whereas the foregoing relates to analytically derived pressure-impulse diagrams, it is also possible to derive iso-damage curves from experimental evidence or real-life events with conventional values of side-on peak overpressure P_{so+} and specific impulse i_{s+} on the axes. In figure 3.21 on page 65 a well-known curve fit by Jarrett (1968) is shown, involving blast damage to typical homes and factory buildings. It is based on bomb damage in Great Britain during World War II.

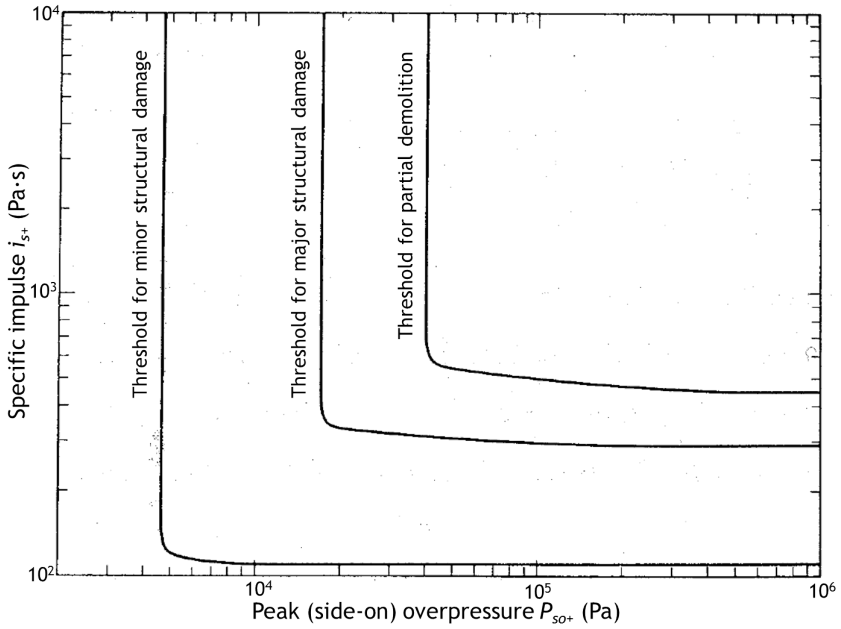

Figure 3.21: Jarrett's P-I diagram for constant levels of building damage [5]

3.7 Key point summary

This chapter has brought substantial information to the reader on the target material of this master's thesis, namely window glass.

From the discussion of the material properties of soda-lime glass (SLG), it should be understood that by its chemical composition, glass undergoes brittle fracture when the maximum allowable stress in the material is exceeded. The external loads causing glass to break, typically give rise to tensile stresses at the surface which are able to make surface cracks propagate until they reach a critical crack length, resulting in sudden failure in absence of plastic yielding. As the surface condition of a window depends on many factors that are hard to control or measure, its tensile strength is a probabilistic property, which is likely to deteriorate in time.

Some of the techniques have been reviewed that are available to counter the inconveniences of glass as a building material, related to the difficulty to estimate its tensile strength and to the inability of glass to deform plastically. It is particularly important to remember how thermal treatment of annealed glass (ANG) provokes residual compressive stresses at the pane surface, bringing surface flaws in a state of pre-compression, thus increasing the tensile strength of the finished product, so-called fully tempered glass (FTG). FTG not only exhibits greater strength, but also possesses superior fracture characteristics which significantly reduces the harmfulness of the projected glass fragments. Another type of glazing with safe performance is laminated glass. Here, glass plies are joined together by a visco-elastic interlayer which holds the entire glass pane together upon fracture.

In national standard NBN S 23-002 (2007) [49] FTG and laminated glass are the only types of glass referred to as safety glazing. In fact, this standard suggests a number of construction scenarios where such safety glazing is recommended. Today this is not enforced by national legislation. From a national energy consumption survey (ECS) conducted by Vito nv (2012) [79] can be concluded that 83 % of Belgian households is (partly) equipped with double glazing. No explicit data could be consulted on installation of safety glazing in Belgium. However, bearing in mind the scenarios where safety glazing is required, one must not expect a significant share as far as domestic houses and offices are concerned.

Finally, safety glazing, performing such that people are less severely harmed, is not to be confused with security glazing, such as explosion-resistant glazing, where performance is measured by the ability to prevent a breach. Both European and international test standards of explosion-resistant glazing have been discussed for two reasons. Firstly, in the context of the test campaign which was organised, test standards are a great source of inspiration for a test protocol where nothing is overlooked. Secondly, it seems interesting to be able to compare the blast load conditions of explosion-resistant glazing to the average blast resistance of normal glazing present in domestic houses.

In order to analytically estimate this blast resistance more generically, BIGGS' quasi-static calculation model has been adopted from PGS1 Part 2B (2003) [57]. An undamped elastic SDOF system was used to describe how a window ply behaves dynamically when subjected to a triangular blast load. It is expected that windows near the 40 mbar overpressure contour get loaded quasi-statically. From the corresponding dynamic load factor (DLF) it is understood that this situation is disadvantageous. The peak force P_{so+} of the triangular blast load which the window is able to resist, is in fact merely half its static strength S. For double glazing, the thickest pane governs the resistance behaviour. Its static strength is multiplied with a factor (cf. equation 3.19) to account for the complete assembly.

The results from a comparable solution method, developed by the U.S. Department of Defence and described in UFC 3-340-2 (2008) [72], have been compared to some self-calculated PGS1 solutions. From both models can be concluded that thicker windows can cope with higher blast overpressures and that larger windows are more prone to failure. Because the models adopt a different approach to account for the membrane effect of a deforming plate, there is no unity between the models regarding the influence of the aspect ratio on the blast resistance.

The involvement of probit functions in the confrontation of solutions has finally led to the conclusion that the data at hand to assess the likelihood of window breakage under dynamic load conditions is generally based on explosion events which are characterised by large phase durations. The author suspects that the reasons to use such events to stipulate limit conditions for window breakage, or any structural damage really, are threefold as itemized hereunder.

a. QRA activities are usually performed in favour of high risk installations where a LOC scenario could potentially lead to a large yield explosion.

b. In order to be granted a permit for start-up, high risk installations must assess the external human risk related to their desired operation. This risk is found beyond the installation's fence, where peak pressures will surely have decreased but the overall loading might have entered the quasi-static loading realm.

c. SDOF calculations have shown that the breaking pressure is essentially independent of duration for large yield explosions, characterised by significantly large durations. The breaking pressure then reaches a lower limit value. While adopting this rather conservative value, one remains on the safe side for any imaginable scenario.

References

[4, 5, 8, 15, 17, 28, 29, 31, 32, 35, 36, 25, 41, 43, 45, 46, 47, 48, 49, 51, 52, 54, 57, 59, 60, 62, 69, 72, 73, 74, 79, 80]

Chapter 4

Blast effects on human beings

If the explosion event is determined in terms of blast wave characteristics and the destructive interaction between the blast wave and the target object is assessed, one is able to address the last step of the consequence modelling process described schematically in figure 1.3 on page 4, namely the resulting impact on an exposed human being in terms of injury or lethality.

In chapter 1 the concept of external human risk was introduced. It was explained how *Seveso-III* [61] imposes upper-tier establishments to issue a safety report to which purpose location-based risk and societal risk are calculated quantitatively. Figure 1.2 on page 3 illustrated how this is achieved. On the one hand the accident frequency is estimated in terms of a number of events per annum. On the other hand the severity of the same event is estimated in terms of the likelihood of a certain consequence or effect. In the context of lethal response to flying glass, this likelihood p_{tot} must be derived as a combination of three probabilities as can be seen in equation 4.1.

$$p_{tot} = p_f \times p_i \times p_h \quad \text{where} \tag{4.1}$$

p_f = the probability of failure of a typical glass window,

p_i = the probability of injury due to flying window shards, and

p_h = the probability of being hit, i.e. the likelihood of a person standing in the danger zone behind a failing window.

There are several ways in which injury may be correlated. One is in terms of single values of the injurious physical effect, of which the threshold value and the value for 50 % probability of injury are particularly important. Another option is a probit equation, which also generally correlates the probability of injury with a single physical effect, typically overpressure. A third way is in the form of a P-I diagram. Because the author has no medical background, the evaluation of the severity of injuries from an explosion, as assumed by the models found in literature and presented hereunder, is never put into question.

In the first section of this chapter the different types of blast injuries are presented in order to narrow down the topic to the types of injury associated with the QRA guidelines related to external human risk. For these injuries, which are due to flying glass and complete building demolition, the best-known models are explored in the subsequent section. Both the experimental origin and the practical relevance are discussed. Next, a review of the translation of some of these injury models into probit functions is given. It is important to distinct between relations predicting a probability of injury p_i "as such" and relations for a "combined" probability of injury $p_f \times p_i$ assessing both failure mechanisms and the associated personal harm. Strengths and weaknesses are identified and a tentative modification is proposed.

Returning to equation 4.1, the attentive reader understands that one last factor should be discussed in order to retrieve the total probability p_{tot} that a person indoors would die from a blast event. This remaining factor is p_h or the probability of being hit by fragments, be it cutting or crushing, capable of wounding a person fatally.

A thorough comprehension of location in time and space of glass sheds from a window pane subjected to a blast load is subject-matter for specialists in the domain of external ballistics. One can imagine that point-mass or true-shape trajectory modelling, accounting for brittle fracture, aerodynamic drag, rotative movement, mutual collision of fragments and the negative phase of the blast wave, could indeed predict fragment spreading and due potential hitting of a target. As such a study lies beyond the objectives of this master's thesis, it is only briefly addressed in this introduction for sake of completeness.

To keep things simple, p_h is considered to depend on the location and the presented area of the victim with respect to the windows of the building. In this way the analyst can use information on the characteristics of the danger zone behind the window to assess the likelihood of a person being present near this zone. PGS1 part 2A (2003) [56] for instance suggests a hit probability value p_h of 5 % (no source given) but leaves possible increase of this factor during working hours open for interpretation. In PGS1 part 2B (2003) [57] this is elaborated more mathematically.

If the total probability p_{tot} that a person indoors would die from a blast event is multiplied by the frequency of the associated accident scenario, the location-based risk is determined. For location-based risk p_h will always equal unity since location-based risk is assessed in terms of a person being continuously present at the location under study without any protection.

If the total probability p_{tot} that a person indoors would die from a blast event is multiplied by the number of people present in the building, the total number of casualties is found. In this way an $F - N$ curve can be constructed for multiple pairs of accident frequency f_i and associated number of fatalities n_i. Clearly this requires an additional evaluation of the number of people exposed, based on time-dependent population data as can be found in chapter 7 of the *Green Book* (1989) [17].

Finally, mitigating effects (e.g. protective clothing) are not explicitly included in equation 4.1. Note though that this can be accounted for in terms of p_i when lethal response is assessed for a human being wearing clothes, opposed to bare skin evaluation which is obviously more conservative. Alternatively, an additional reduction factor p_p can be used to express the risk reducing effect of a protection feature present. It is however difficult to assume such a feature to generally exist for all locations outside the company's premises.

4.1 Blast injury categories

Blast injuries are traditionally divided into four categories, namely primary, secondary, tertiary, and quaternary (or miscellaneous) injuries. For ease of reference, a summary of the possible injuries is given in figure 4.1 on page 71. Logically, a victim may be injured by more than one of these mechanisms.

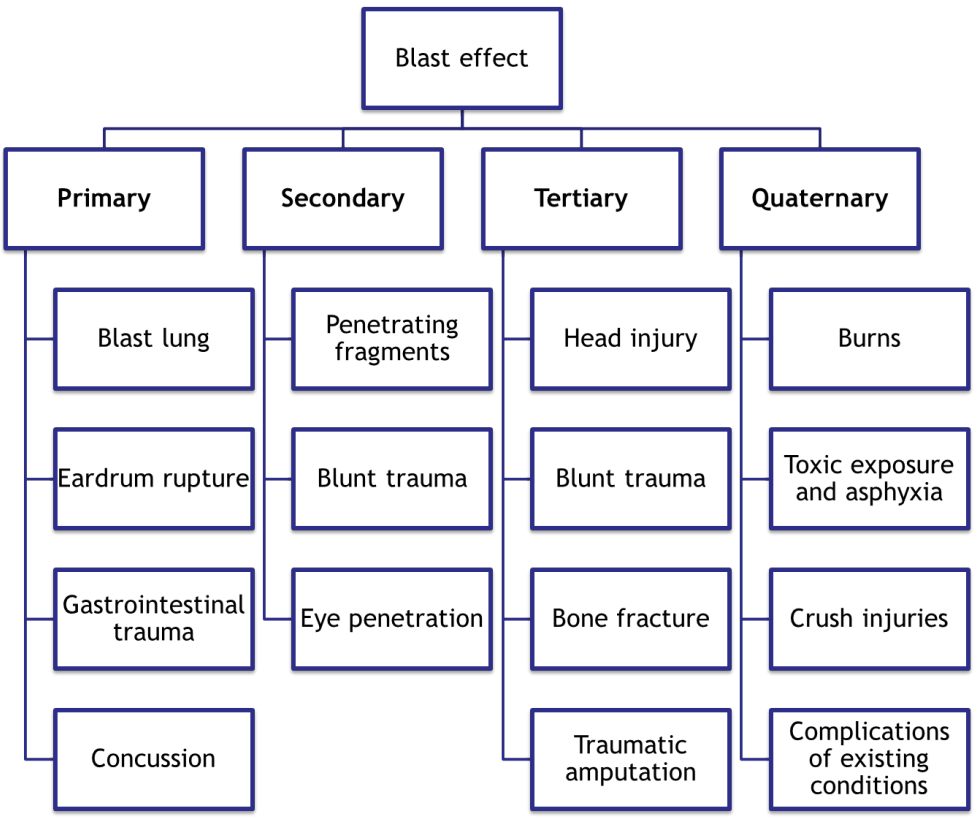

Figure 4.1: Blast injury categories [66]

Primary blast injuries are caused when the blast wave compresses the tissues of the internal organs containing air, such as the lung, ear and gastrointestinal tract. Of these three organ systems, the ear is the most easily damaged. Primary injuries are also commonly referred to as the direct effects of the blast on a human being, opposed to the indirect effects where not the blast wave itself but another phenomenon related to the explosion causes harm.

Secondary blast injuries are much more common than primary blast injuries. They are caused by flying objects that strike people. These can produce both penetrating and blunt trauma, depending on their size and travelling speed. The penetrating injuries occur most often in the exposed areas, such as the head, neck, and extremities, but thoracic and abdominal injuries may occur as well. As distance from the blast center increases, the effect of the blast itself is reduced, and the effect of fragments and debris propelled by the explosion becomes more important. As glass fragments cause many of the secondary blast injuries, this category will be elaborated in detail further in this chapter.

Tertiary blast injuries are caused when the victim's body is propelled into another object by the blast winds. This effect is formally known as whole body displacement. If vulnerable body parts such as the skull, the torso or extremities hit a rigid structure, this can obviously cause considerable trauma.

Quaternary blast injuries encompass all other injuries caused by the explosion, including burns from fire or radiation, poisoning from carbon monoxide or other toxic products and inhalation of dust.[12] Crush injuries associated with structural collapse also fall under the quaternary or miscellaneous injuries. Although the loss of structural integrity is observed at rather low overpressure, it is often fatal for the occupants. It thus requires a brief discussion as well.

For sake of completeness it is noted that post traumatic stress disorder (PTSD) as a psychological trauma typically occurs in explosive blast survivors. Its prevalence extends to victims showing complete absence of physical injuries.

There exist some data on the overall distribution of the different injury modes from military and industrial explosions. During World War II, Bell (1944) for instance reported on the casualties admitted to individual hospitals after V-1 flying bomb raids on Great Britain. In table 4.1 on page 73 the breakdown of injuries related to his descriptions is shown. Notice the high injury rate related to glass fragments and the high fatality rate associated with structural debris. Out of the 211 surgical cases reported, nearly 75 % was caused by these two blast effects.

[12] E.g. in the aftermath of the 9/11 attacks (2001) on the World Trade Center, New York, USA, thousands of first responders and New York City residents are suffering "Ground Zero illnesses" from the exposure to dispersed substances such as asbestos, crystalline silica, lead, cadmium, dioxins and polycyclic aromatic hydrocarbons.

Table 4.1: Distribution of injuries in casualties requiring surgery admitted to a London hospital during the V-1 flying bomb raids after Bell (1944) as reported in Lees (2005) [41]

	Cases		Deaths	
Injury cause	**No.**	**%**	**No.**	**%**
Glass	100	47.4	1	6.3
Bomb splinters	24	11.4	3	18.7
Masonry	52	24.6	9	56.2
Blast	26	12.3	2	12.5
Burns	9	4.3	1	6.3
Total surgical	211			

4.2 Blast injury from fragments

Both primary and tertiary injuries are encountered close to the burst center at overpressures above 100 mbar, opposed to the region of external human risk outside the fence of the industrial installation which is the subject of study in this master's thesis. As such, they will not be further developed. The interested reader is encouraged to consult Lees (2005) [41] chapter 17.38 on explosion injuries to persons outdoors, where numerous probit function relations and P-I diagrams related to lung injury, eardrum rupture and whole body displacement are bundled. Nevertheless, for secondary injuries from debris with a mass comparable to the mass of the skull ($\approx$ 4.54 kg), the tertiary injury model for skull fracture is widely adopted and must therefore be included hereunder.

For the remainder of this chapter, emphasis is put on explosion injuries to persons indoors, which mainly rely on the correlation of injury with damage to structures. Clearly, the secondary injuries from window breakage or structural debris will represent most of the associated injuries. Their evaluation is particularly delicate for no less than four reasons, namely:

a. structural response calculations rely on simplifying assumptions which makes them hardly ever 100 % comparative to the actual structure,

b. the possibility of a residing person actually being hit by fragments or debris is probabilistic of nature, depending on his/her position with respect to the failing structural element,

c. the potential of a fragment to penetrate the human skin depends on numerous characteristics of the fragment, such as mass, slenderness, sharpness and velocity, which are rather difficult to predict, and

d. the protection offered by the victim's clothes can have a non-negligible positive impact on the extent of the injuries compared to a theoretical vulnerability model based on bare human skin.

Injury to people due to fragment impact is usually divided into two subcategories. One injury subcategory involves penetration and wounding by small fragments and the other involves blunt trauma by large, non-penetrating pieces of debris. The former is extensively elaborated, since glass fragments usually belong to this subcategory. However, the latter must be sufficiently explored as well, in order to cover events where larger glass fragments ($m > 0.1$ kg) are projected or entire windows are thrown out from their frame.

In order to cover all the mechanisms, a comprehensive set of models will be explored and compared throughout this chapter. Overlap between models, applicable ranges and lethality criteria might confuse the reader. However, broadly speaking, the scheme in figure 4.2 on page 74 should help to situate the presented theories.

Further, because of the possibly large extent of harm associated with full collapse of a building, this type of quaternary injury deserves some consideration as well during a quantitative risk assessment process evaluating external human risk. This is briefly addressed in the subsequent section when the Flemish structural damage criterion is reviewed.

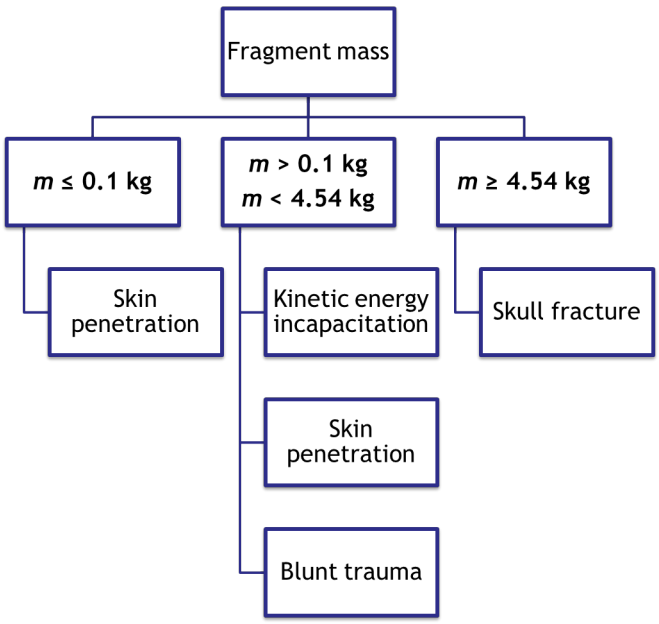

Figure 4.2: Secondary blast injury mechanisms explored in this section

4.2.1 Penetrating fragments with $m \leq 0.1$ kg

The study of fragments penetrating the human skin belongs to the research domain of terminal (wound) ballistics. In Baker et al. (1983) [5], a review of related test results by several investigators is given. The empirical model by Sperrazza & Kokinakis (1967), which is put forward to assess whether fragments with specific characteristics cause body penetration through the skin, is later adopted by CPR 16E (1989) [17] and by its improved revision, part 2A of PGS1 (2003) [56].

Sperrazza & Kokinakis (1967) explored the ballistic limit velocity v_{50} for animal targets. The v_{50} velocity is the striking velocity at which one expects half the impacting missiles to perforate an object. They found that this velocity depended on the fragment presented area to mass ratio A_f/m. They fired steel cubes, spheres and cylinders of various masses up to 0.015 kg into 3 mm thick isolated skin from humans and goats to establish a ballistic limit. One of their assumptions was that, if the projectile penetrates the skin, its residual velocity will be sufficient enough to cause severe damage. This cautious assumption is appropriate for establishing a certain margin of safety in the calculation. Their conclusions were that, in the range of their data for steel cubes, spheres and cylinders, v_{50} depended linearly on the projectile's A_f/m ratio. Specifically,

$$v_{50} = 1247.1 \ \frac{\text{kg}}{\text{m} \cdot \text{s}} \cdot \left(\frac{A_f}{m} \right) + 22.03 \ \frac{\text{m}}{\text{s}} \tag{4.2}$$

$$\text{where } A_f/m \ \leq \ 0.09 \ \text{m}^2/\text{kg} \text{ and } m \ \leq 0.015 \ \text{kg}.$$

Equation 4.2 pertains to the least-squares fit to the average values of the experiments. In figure 4.3 on page 76, edited by Baker et al. (1983) [5], the linear relation of v_{50} versus A_f/m formulated by Sperraza & Kokinakis (1967) is plotted.

During a subsequent study, Kokinakis (1974) fired plastic sabots end-on into 20 % gelatin that was 1 cm thick, simulating isolated human skin. The average values for these experiments also lie near the line drawn for the prior study, thus adding a degree of confidence in the analysis.

Unfortunately, other authors did not present their penetration data in the same form as Sperrazza & Kokinakis. Hereunder, Baker's argumentation is reproduced, which allowed him to expand the Sperraza & Kokinakis data on figure 4.3 on page 76 with other data on steel fragments by White et al. (1961) as well as with data on glass fragments by Glasstone (1962) and Custard & Thayer (1970).

Glasstone (1962) expressed the probability of glass fragments penetrating the abdominal cavity in terms of the mass of the glass fragments without further notice of the cross-sectional area, thickness or density. To compare his conclusions with the linear model of Sperrazza & Kokinakis (1967), Baker et al. had to make a few assumptions, itemized hereunder.

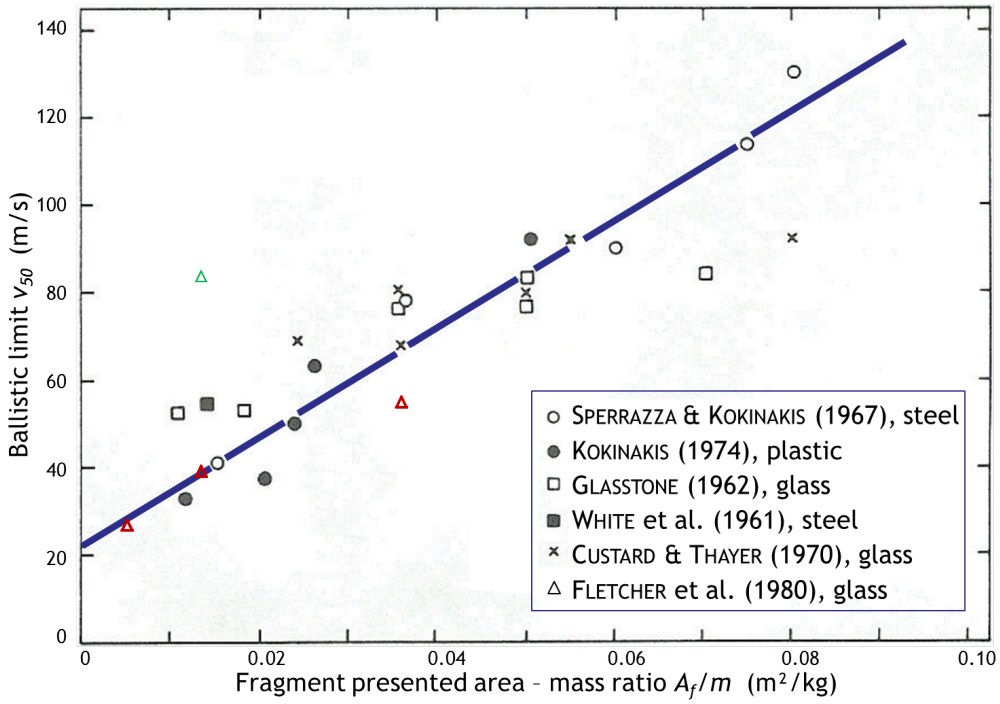

Figure 4.3: Ballistic limit v_{50} versus fragment presented area to mass ratio A_f/m for isolated human and animal skin [5, 25, 56]

Above all, the glass fragment velocity for 50 % probability of penetration of the abdominal cavity must be considered as biologically equivalent to the ballistic limit velocity v_{50} for penetrating isolated human skin.

Furthermore, the following assumptions about the characteristics of the glass fragments are needed:

a. The fragments are propelled edge-on, which is supposedly the worst case.[13]

b. They have a square shape with thicknesses d of 3.175 to 6.350 mm (1/8 to 1/4 inch).

c. They have an average density ρ of 2.47 g/cm^3.

With these suppositions, the fragment surface area to mass ratio A_f/m can be computed according to equation 4.3:

$$\frac{A_f}{m} = \sqrt{\frac{d}{\rho \cdot m}} \tag{4.3}$$

[13]The symbol θ is used to describe the angle subtended by the fragment. If θ approaches 180°, the contact surface approaches the total surface of the edge. This reduces the cutting potential of the fragment, making it less hazardous. Baker et al. seem to have overlooked this issue (cf. supra).

Table 4.2: 50 % probability of glass fragments penetrating the abdominal cavity according to Glasstone (1962) as reported in Baker et al. (1983) [5]

m	v_{50}	$\left(\frac{A_f}{m}\right)_{3.175\ \text{mm}}$	$\left(\frac{A_f}{m}\right)_{6.35\ \text{mm}}$
$1.0{\cdot}10^{-4}$ kg	125 m/s	0.1136 m^2/kg	0.1603 m^2/kg
$5.0{\cdot}10^{-4}$ kg	84 m/s	0.0507 m^2/kg	0.0717 m^2/kg
$1.0{\cdot}10^{-3}$ kg	75 m/s	0.0358 m^2/kg	0.0507 m^2/kg
$1.0{\cdot}10^{-2}$ kg	55 m/s	0.0113 m^2/kg	0.0160 m^2/kg

Glasstone's criteria for 50 % probability of glass fragments penetrating the abdominal cavity are shown in table 4.2 on page 77. This table also contains the estimates for A_f/m for glass thicknesses of 3.175 and 6.35 mm. The velocity values and calculated values for A_f/m which fall in the range of values used by Sperrazza & Kokinakis are plotted on figure 4.3 on page 76 (squares). Even with the crude assumptions mentioned above, the calculated points fall very near the v_{50} line.

Custard & Thayer (1970) specify velocity in the same way as Glasstone, namely as a function of mass only for 50 % penetration of glass fragments. Making the same assumptions as above, A_f/m was again calculated by means of equation 4.3, allowing for the results to be plotted on figure 4.3 on page 76 (crosses).

White et al. (1961) also related skin penetration velocity to the masses of impacting fragments. They concluded that skin laceration occurred when spherical steel bullets with a mass of 8.7 g were propelled into the body at 57.9 m/s. Assuming that the density ρ of steel equals 7925 kg/m^3, the A_f/m ratio is calculated as 0.0148 m^2/kg, leading to the black squared datum point in figure 4.3 on page 76. This point appears to be a little higher than expected, especially since only slight skin laceration is expected at these velocities instead of 50 % penetration.

Anyway, the data generally correspond well. Baker et al. thus conclude that for values of A_f/m up to 0.09 m^2/kg and values of m up to 0.015 kg, the functional relationship expressed in equation 4.2 is an adequate representation of 50 % probability of skin penetration by a projectile that can result in serious wounds.

Finally, the work by Fletcher et al. (1980) [25] is discussed. It elaborates on the biological effects of individual glass fragments and shattering window panes on sheep and dogs. Different animal body parts in both covered and uncovered condition were impacted in order to assess different types of injury as well as the protective influence of casual clothing.

As a first approach of study the author transformed Fletcher's data according to Baker's assumptions itemized above, and added them to the data for the linear model of Sperrazza & Kokinakis (1967), shown on figure 4.3 on page 76. The red

markings pertain to v_{50} values for impact on bare skin abdomen. They are clearly in line with the other results. The green marking shows the effect of protection offered by two layers of clothing on the v_{50} value.

The tests that have been selected to incorporate here were all executed on regularly shaped specimens with an angle θ subtended by the glass fragments of 180°. It is of the utmost importance to acknowledge that this does not represent the worst possible event. On the contrary, it minimises the cutting potential of the fragments. The author believes this is precisely why data from glass fragments are able to match well with data from high density projectiles. In fact, for lower values of θ down to 45° as well as for significantly lighter fragments Fletcher et al. predict significantly lower v_{50} values needed for skin penetration.

The same data set is now approached differently, without adaptations towards Sperrazza & Kokinakis' model. The previously selected data points are complemented with data for small glass fragments (0.0543 to 1.90 g) with irregular shapes, for which the orientation upon impact could not be recorded. The complete set of data which is studied is enlisted in table 4.3 on page 79.

From the proceedings in Fletcher et al. (1980) [25] it is known that a rather close linear behaviour arises. This is illustrated well in figure 4.4 on page 79. The original regression equation is rather weighty from the fact that it is able to account for the orientation θ. The author thus presents a more elegant power law, given in equation 4.4a, which specifically pertains to the selection of data studied (red dash-dotted line).

From the single datum point with θ equal to 180° available for the clothed target, a protection factor of 2.1 is found compared to bare skin conditions. This factor can be used to shift the v_{50} line according to equation 4.4b (green dash-dotted line). This approach seems to be adhered to in PGS1 part 2A (2003) [56]. However, it is noted that Fletcher's data for other values of θ clearly show that below an angle of about 100°, the protection factor steadily drops down to unity for a value of 0°, expressing that clothing would offer minimal resistance to a needle-like fragment.

Mind that it is not the intention to minimise the protective nature of clothing. In fact, Fletcher et al. do report an increase of the maximum wound depth with increasing fragment impact velocity for clothed subjects similar to bare subjects, but areas of multiple, serious, incised wounds or denudation are not observed. Instead, large areas of welting under the clothing at higher overpressures are reported.

$$v_{50}(\text{bare skin}) = 16 \cdot m^{-0.192} \tag{4.4a}$$

$$v_{50}(\text{clothed}) = 2.1 \cdot v_{50}(\text{bare skin}) \tag{4.4b}$$

Table 4.3: 50 % probability of glass fragments penetrating the abdominal cavity according to Fletcher et al. (1980) [25]

m	v_{50}	θ
$5.43{\cdot}10^{-5}$ kg	139.0 m/s	randomly
$1.31{\cdot}10^{-4}$ kg	85.7 m/s	randomly
$3.18{\cdot}10^{-4}$ kg	62.8 m/s	randomly
$7.69{\cdot}10^{-4}$ kg	55.4 m/s	randomly
$1.9{\cdot}10^{-3}$ kg	56.9 m/s	180°
$1.0{\cdot}10^{-3}$ kg	55.2 m/s	180°
$1.0{\cdot}10^{-2}$ kg	39.3 m/s	180°
$1.0{\cdot}10^{-1}$ kg	27.0 m/s	180°

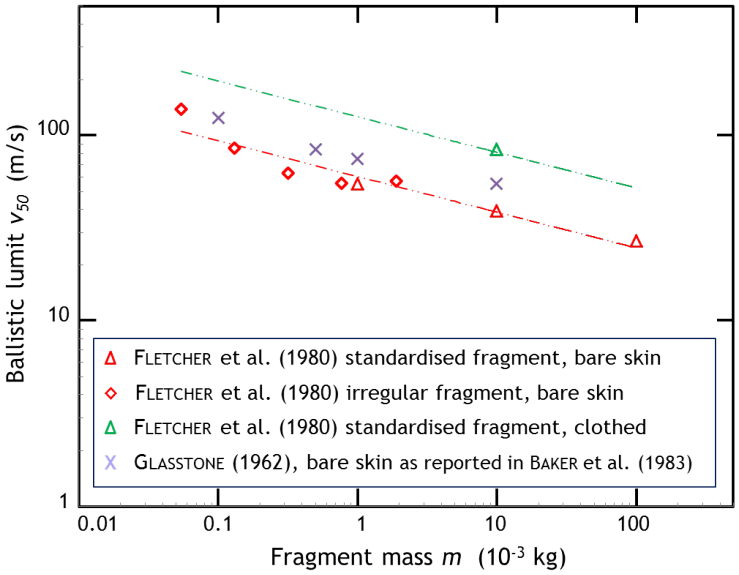

Figure 4.4: v_{50} line for bare skin and clothed abdominal penetration of glass fragments (point-on impact; $\theta = 180°$) by Fletcher et al. (1980) [25]

Interestingly, when Glasstone's previously used experimental data points on glass fragments are added (cf. table 4.2 on page 77), a rather similarly shaped linear trend is observed, be it with an overall estimated factor of increase of 1.4.

The foregoing results are assumed to apply directly to man. However, the surface area exposed to a window should be about 40 % greater for a face- or back-on man than the corresponding area for a side-on animal [25]. Therefore, the number of injuries registered in Fletcher's study might be low for the extreme case of a man broad-side-on and centred behind a window larger than himself.

4.2.2 Non-penetrating debris with $m \geq 4.54$ kg

If non-penetrating debris collides with a human being, it causes internal stresses in the body, capable to bruise or break bones and to damage the organs. Because of the delicate nature of the head, it is widely accepted that translation damage criteria for whole body displacement, put in relation with this type of fragment injury, should be based on head injuries such as skull fracture or concussion.

After whole body displacement, bodily damage can occur during the accelerating phase or during decelerative impact. According to Glasstone (1962) the extent of injury due to decelerative impact is the more significant. In Baker et al. (1983) [5], experimental data by Clemedson et al. (1968) and White (1968, 1971) for skull fracture tolerance are given. From their studies it was concluded that a drag velocity v_D of 13 ft/s (3.96 m/s) should be taken as a threshold for skull fracture. Assuming that the impact of a relatively large piece of debris with the head is equivalent to the event of the skull colliding with a rigid object, these data can be used to assess lethality. The lower limit for the mass characterizing large debris equals 10 lb (4.54 kg), which happens to coincide with the average mass of the human head.

Clearly, objects that are heavier than 4.54 kg will provoke an increased injury probability. However, this cannot be assessed with the experimental data which are presently existing. Furthermore, since body impact position is likely to be randomly oriented after translation, this factor could be taken into account in determining expected amounts of impact damage. White (1971) formulated criteria for tertiary damage due to whole body impact. Considering that the likelihood, that upon collision of the whole body only the skull will be involved, is smaller than one, he determined a lethality threshold for whole body impact of 21 ft/s (6.40 m/s). He also found that the mostly safe velocity criterion is identical to the skull fracture criterion, namely 10 ft/s (3.05 m/s).

Table 4.4 on page 81 summarizes the drag velocity thresholds and upper, lower, and average values causing fatal skull fracture and whole body impact as presented by Clemedson et al. (1968) and White (1968, 1971). In Baker et al. (1983) [5] two corresponding pressure versus scaled impulse diagrams are plotted. Here the impulse is scaled with respect to the victim's mass as this clearly influences the translation velocity v_D attainable by the victim. In PGS1 part 2A (2003) [56], two corresponding P-I diagrams are plotted for a human being with a length-to-width ratio of 7 and a body mass of 70 kg. They have been combined on figure 4.5 on page 81. The drag velocity criteria for skull fracture are drawn in blue. The grey curves refer to whole body displacement criteria. The black curve is the mostly safe line corresponding to a v_D of 3.05 m/s for both injuries. Attention is drawn to a statement from PGS1 part 2A (2003) [56], that the drag velocity v_D of the victim is overestimated in reality because of the rotational movement of the body during translation.

Table 4.4: Criteria for tertiary damage (decelerative impact) to the head according to Clemedson et al. (1968) and White (1968, 1971) and criteria involving whole body impact according to White (1971) as reported in Baker et al. (1983) [5]

Injury	**Extent**	**Drag velocity v_D**	
Skull fracture	mostly safe	10 ft/s	3.05 m/s
	threshold	13 ft/s	3.96 m/s
	50 % lethality	18 ft/s	5.49 m/s
	near 100 %	23 ft/s	7.01 m/s
Whole body impact	mostly safe	10 ft/s	3.05 m/s
	threshold	21 ft/s	6.40 m/s
	50 % lethality	54 ft/s	16.46 m/s
	near 100 %	138 ft/s	42.06 m/s

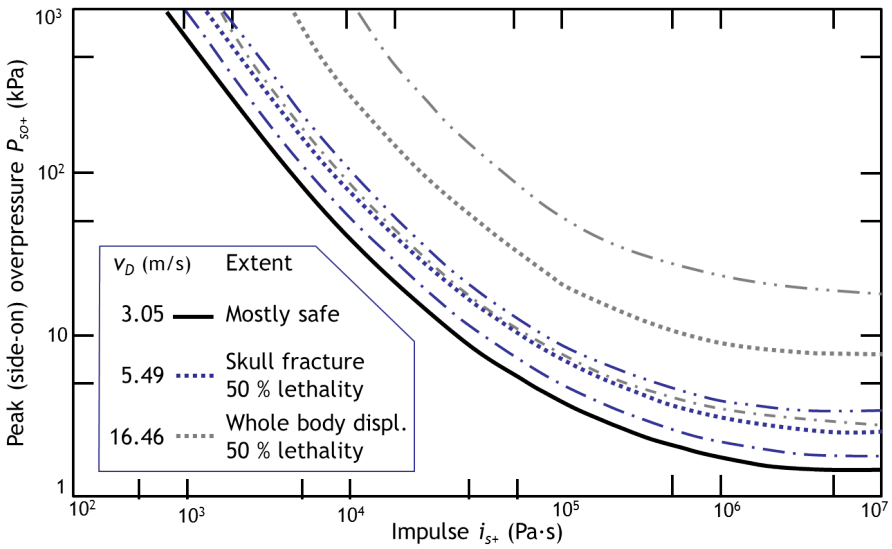

Figure 4.5: P-I diagram showing lethality criteria for skull fracture and whole body displacement for a human being weighing 70 kg [5, 56]

The author concludes that the use of the skull fracture criterion for tertiary injuries to assess secondary (quaternary) injuries caused by large pieces of debris results in conservative threshold impact velocities for a fragment mass of 4.54 kg but could possibly lead to underestimation of injuries caused by heavier pieces of debris.

As it is clear that the fragment mass of interest for this master's thesis is significantly lower than 4.54 kg, the latter issue is left alone. For the first observation, attention is drawn to table 4.5 on page 82 from Baker et al. (1983) [5] where tentative criteria for indirect blast effects from non-penetrating fragments with a mass of 4.54 kg are given.

Table 4.5: Tentative criteria for indirect blast effects from non-penetrating fragments with a mass of 10 lb (≈ 4.54 kg) according to Clemedson et al. (1968) and White (1968, 1971) as reported in Baker et al. (1983) [5]

Injury	**Extent**	**Impact velocity v_0**	
Skull fracture	mostly safe	10 ft/s	3.05 m/s
	threshold	15 ft/s	4.57 m/s
	near 100 %	23 ft/s	7.01 m/s

Note how the threshold impact velocity has been increased from 3.96 to 4.57 m/s, whereas lower and upper limits have not been altered with respect to the skull fracture criteria by Clemedson et al. (1968) and White (1968, 1971). The author hypothesises that this threshold relaxation entered Baker's 1983 publication after evaluation of the differences in the extent of injury between fragmentation impact and bodily damage during decelerative impact, which somewhat jeopardizes the validity of the above mentioned assumption that the impact of debris with the head and skull collision with a rigid object are equivalent.

4.2.3 Fragments with 0.1 kg $< m <$ 4.54 kg

A gap still remains between the upper limit of the skin penetration model (0.1 kg) and the lower limit for skull fracture (4.54 kg). In this range, the most often cited personnel injury criterion is the 58 ft-lbf incapacitation criterion. According to this criterion, a fragment is considered hazardous, i.e. able to incapacitate a human being, when its kinetic energy equals 58 ft-lbf (≈ 79 J) or more.

It is important to note that a clear definition of incapacitation involving wounding criteria is not given. More specifically, the question still remains whether incapacitation is explicitly linked to any kind of penetration, blunt trauma, the loss of arm and leg function, or yet another definition.

The kinetic energy criterion has been in vogue since the early 1900s and literature abounds with references to it. It is adopted by the NATO working group AC 258 responsible for the safe storage of ammunition [1, 10] and it is cited in the original *Green Book*, formally known as CPR 16E (1989) [17] as well as in its latest revision, part 2A of PGS1 (2003) [56]. According to Lees (2005) [41], 58 ft-lbf is also the value which is traditionally used in Great Britain and the U.S.

von Rohne (1906), a German General of the Artillery during World War I, is usually given credit for establishing this criterion, which was probably intended as nothing more than a rough rule of thumb, which did not seem to rely on experimental data [44]. Clearly, without giving additional consideration to other parameters such as shape, size, mass and impact location, energy-based hazard assessments can be misleading.

In figure 4.6 on page 84, taken out of a critical review by Neades (1983) [50], the 58 ft-lbf incapacitation criterion is compared to experimental data for both penetrating and non-penetrating trauma. Important discrepancy is thus visualised between impact velocities predicted by the kinetic energy model and impact velocities predicted by the other models, presented hereunder.

The previously cited study by Sperrazza & Kokinakis (1967) as well as comparable data from a study by Lewis et al. (1978) are credited for their skin penetration models, based on experiments with high density fragments. The resulting graphs show the lack of penetrating injury data for projectiles with a mass $m > 0.015$ kg.

Neades considers the fact that the studied fragment mass does not correspond with the interval of interest a first important shortcoming in the review of the 58 ft-lbf incapacitation criterion. Nevertheless, with his approach to compare the kinetic energy criterion to skin penetration models, Neades gives away his belief that penetration is the primary damage mechanism of interest. This implies it could be argued whether the 58 ft-lbf law should be applied for non-penetrating blunt trauma estimations as is the case in CPR 16E (1989) [17] and AASTP-1 (2015) [1], where lethal p_i values for head, chest, abdomen, and limbs blunt impact injuries are associated with discriminating limits of kinetic energy. The inability to determine von Rohne's original definition of incapacitation thus becomes apparent.

Neades also draws experimental data from non-penetrating traumas into his discussion. The four-parameter model[14] by Clare et al. (1976) is mentioned as the state of the art in blunt trauma modelling. The curves which are plotted give a threshold for liver fracture, based on data with low density projectiles (average 1.31 g/cm^3) for a test animal (target weight: 11.3 kg) extrapolated to a man's body weight (70 kg). The mass test data interval was from 0.003 to 0.381 kg, which includes partly the interval of interest. However, Neades considers the lack of non-penetrating injury data for projectiles with densities greater than about 1.31 g/cm^3 as a second important shortcoming in the review of the 58 ft-lbf rule.

Finally, a blunt trauma relationship by Shank et al. (1974) is also shown. It is based on tests with non-lethal ammunition, where superficial or slight damage is observed. The relationship is not directly applicable to humans, but for non-lethal ammunition it can be of interest from an injury threshold point of view.

McCleskey (1990) [44] readdresses these two shortcomings, further criticising the fact that the 58 ft-lbf incapacitation criterion lacks any from of transition between the assessment of a fragment being either hazardous or not. In order to deal with this problem, he presents a transitional criterion which he calls the continuous probability of injury criterion (CPIC). It is based on the work by Lewis et al. (1978) mentioned above, which involves bare skin penetration as the injury criterion.

[14] The four parameters are projectile mass, diameter and velocity, and target (body) mass.

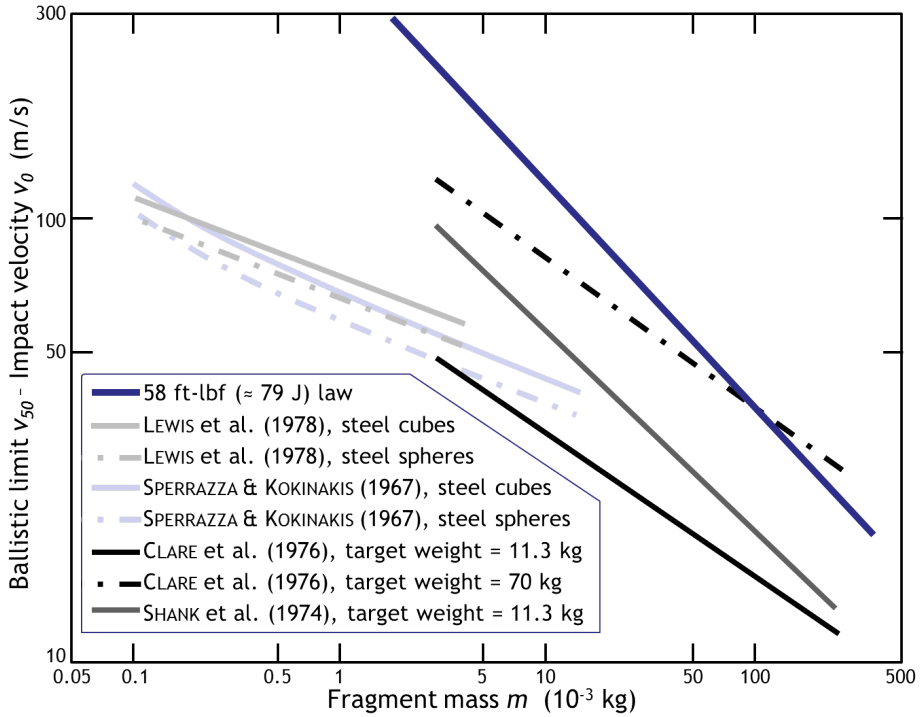

Figure 4.6: 58 ft-lbf rule compared with experimental incapacitation energy data [50]

During their research on the hazards related to the environmental debris associated with the manipulation of small rocket-motor launched weapons and the like, Lewis et al. (1978) applied the logistic relation given in equation 4.5 for estimating the probability of skin penetration by various projectiles, including low density fragments.

$$p_i = \frac{1}{1 + \mathrm{e}^{-\left[C_1 + C_2 \cdot \ln\left(\frac{m v_0^2}{10 A_f}\right)\right]}} \tag{4.5}$$

The striking fragment is characterised by its mass m, its impact velocity v_0, and its average presented area A_f. The latter parameter is certainly a consideration for skin penetration which is ignored in the 58 ft-lbf incapacitation criterion. The causative factor that combines the parameters of the striking fragment is given the symbol χ as seen in equation 4.6. Notice how χ is divided by 10 in equation 4.5 which was necessary to allow for the use of consistent SI-units.

$$\chi\,[\frac{\mathrm{J}}{\mathrm{m}^2}] = \frac{m v_0^2}{A_f} \tag{4.6}$$

C_1 and C_2 are constants related to the linear curve fit. They are presented in table 4.6 on page 85 for bare skin penetration as well as for conditions where the effect of skin protection was investigated. It goes without saying that improvements in skin protection represent a significant reduction in skin penetration probability.

Table 4.6: Constants for linear curve fits of the skin penetration model by Lewis et al. (1978) as reported by Neades (1983) [50] and McCleskey (1990) [44]

Model	**Target**	C_1	C_2
Lewis et al. (1978) [50]	Bare skin	-28.42	2.94
	Two-layer uniform	-48.47	4.62
	Six-layer uniform	-50.63	4.51
McCleskey (1990) [44]	Bare skin	-27.35	2.81

McCleskey's continuous probability of injury criterion (CPIC) relies on the same logistic equation 4.5 but uses different constants. In table 4.6 on page 85, these constants are also included. They come forth from data on fragmentation of four conventional weapons which were produced numerically using `FRAGHAZ`, a computer programme for fragment hazards from stored munitions.

Verification by the author for the same causative factor χ has demonstrated that the assessment of fragment velocities using either model leads to comparable results. For a 1 % probability of injury p_i, McCleskey's predictions are merely 0.3 % lower than the results based on the model from Lewis et al. (1978). For higher values of p_i, McCleskey's results are situated little above Lewis' estimations. For a p_i of 50 %, McCleskey predicts fragment velocities that are some 3.4 % higher. At 99 % probability of injury, the difference reaches 7.2 %. Generally speaking, McCleskey's results are thus slightly less stringent compared to Lewis' findings, but the predictions are clearly within a permissible range of agreement.[15]

The outcome of the CPIC is shown graphically in figure 4.7 on page 86 for different probabilities of injury p_i. Note how this criterion theoretically covers a much larger range of fragment masses, ever assuming human skin penetration.

For sake of comparison, the kinetic energy criterion is also plotted in figure 4.7 on page 86. Notice its appearance as a continuous line starting at a fragment mass as low as 0.065 mg,[16] contrary to the available experimental data for the kinetic energy criterion. As the slopes for the two criteria are quite different, they could result in large differences, especially for small fragment masses, where McCleskey believes significant underestimation of the probability of injury is made when using the 58 ft-lbf criterion. Bearing in mind the era of creation of the 58 ft-lbf incapacitation criterion and the armature in use at that time, the author concludes that the kinetic energy criterion was never intended for small fragment masses in the first place, and therefore requires a selected lowest mass, delimiting its range of validity.

[15] The author respectfully vouches that §17.42.4 from Lees (2005) [41] on perforation of skin as presented by Lewis et al. (1978) contains quite a few errors; in this master's thesis the correct formulations can be found (after [1, 44, 50]).

[16] 0.065 mg corresponds to a mass of 1 grain, which was the lowest mass McCleskey explored.

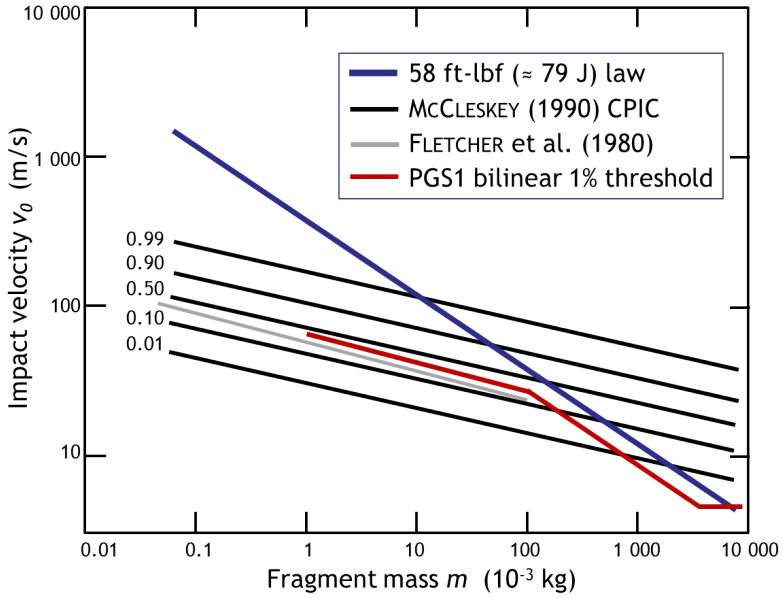

Figure 4.7: Personnel injury criteria thresholds compared to the CPIC [44]

The continuous 1 % threshold of the Dutch PGS1 injury criterion has also been added to figure 4.7 on page 86 as well as the v_{50} bare skin penetration line by Fletcher et al. (1980) [25] from which the former was developed. The slight upward shift of the PGS1 curve, towards the experimental data on skin penetration by Glasstone (1962), which was plotted in figure 4.4 on page 79, can be defended bearing in mind the protective effect of clothing.

The author considers the PGS1 model as the best available injury criterion for fragments, and underlines that the lack of transition of the 58 ft-lbf incapacitation criterion, addressed by McCleskey, is coped with using additional kinetic energy data which adds a probabilistic dimension to it. The chosen models in the Dutch approach as well as the corresponding probit relations are summarised hereunder.

a. For fragments with a mass m above 4.54 kg, the skull fracture criterion by Baker et al. (1983) [5] after Clemedson et al. (1968) and White (1968, 1971) is adopted. Equation 4.7 expresses the relationship between the impact velocity v_0 and the probit value P. Note how a possible deteriorating effect of increasing mass remains unaccounted for.

$$Pr = -13.19 + 10.54 \ln v_0 \tag{4.7}$$

b. For fragments with a mass m between 0.1 and 4.54 kg, the 58 ft-lbf kinetic energy criterion by von Rohne (1906) is adopted. Use is made of the known intersecting points at 4.54 kg to derive equation 4.8.

$$Pr = -17.56 + 5.30 \ln \left(\frac{1}{2} m v_0^2 \right) \tag{4.8}$$

c. For fragments with a mass m below 0.1 kg, the skin penetration model by Fletcher et al. (1980) [25] is adopted. In the same way as above, known intersecting points at 0.1 kg are considered to establish equation 4.9, thus achieving a continuous injury criterion for any probability value of interest.

$$Pr = -29.15 + 2.1 \ln\left(m v_0^{5.115}\right) \tag{4.9}$$

4.3 Probit relations for glass fragments

Where the former models, pertaining to fragments and debris, already seem to build quite a bit on experimental data of possible harm from glass fragments, still additional models or adaptations exist which are particularly meant for indoor risk evaluation of window breakage.

The probit function that is associated with the Flemish 40 mbar overpressure criterion is one of those models. It is reviewed in this section. It provides a straight link between one of the explosion characteristics associated with a source model, namely the peak (side-on) overpressure P_{so^+}, and the possible harm that can be caused to a person inside a building. The latter implicitly relates to the structural damage that is observed for the given overpressure level. In its explicit form, this type of probit relation is the most practicable approach in QRA to undertake a damage modelling calculation. However, it is noted that the inability to account for the load duration t_{0+} of the explosion has an important impact on the conservativeness of the results obtained.

Further, from the discussion on the blast strength of glass in section 3.5, it follows that a second approach could combine the dynamic peak pressure from the blast on the window with the characteristics of the window in order to derive the possible injury potential. This was originally suggested in the *Green Book* but was later slightly adapted and complemented in PGS1 part 2A (2003) [56] as will be explained below. In these models, developed by TNO for the Dutch authorities, use is made of the dynamic load factor DLF. Via the DLF the load duration aspect of the explosion event is brought into the evaluation. As the modified PGS1 model makes use of the same causative parameter P_{so^+} as the Flemish probit function, both models can be readily compared to one another.

Referring to some of the other models presented above, it should be clear that a third approach could be adhered to, where the characteristics of the fragments are associated with lethality. Therefore the work by Gilbert et al. (1994), as reported in Lees (2005) [41], is briefly mentioned. It elaborates upon equation 4.5 from the skin penetration model by Lewis et al. (1978) to establish a predictive model where mass m, impact velocity v_0 and fragment presented area A_f are related to a lethality probability. For sake of comparison experimental data relating overpressure to these fragment characteristics is selected from the work by Fletcher et al. (1980) [25].

4.3.1 Structural damage criterion, Dept LNE (2011)

AMINAL (1993) [3] is the oldest document where the author found references for the Flemish probit function on overpressure written in the guidelines of the Safety Reporting Division (2011) [22]. Indeed, the graphical solution of the overpressure criterion, which is plotted in the annexes to AMINAL (1993) [3], coincides with the probit relation suggested by the Flemish Environmental Department (Dept LNE), as illustrated in figure 4.8 on page 88 where the mathematical expression, given in equation 4.10, is plotted as an overlay on the graphical AMINAL solution.

$$Pr = -8.23 + 1.31 \ \ln P_{so+} \tag{4.10}$$

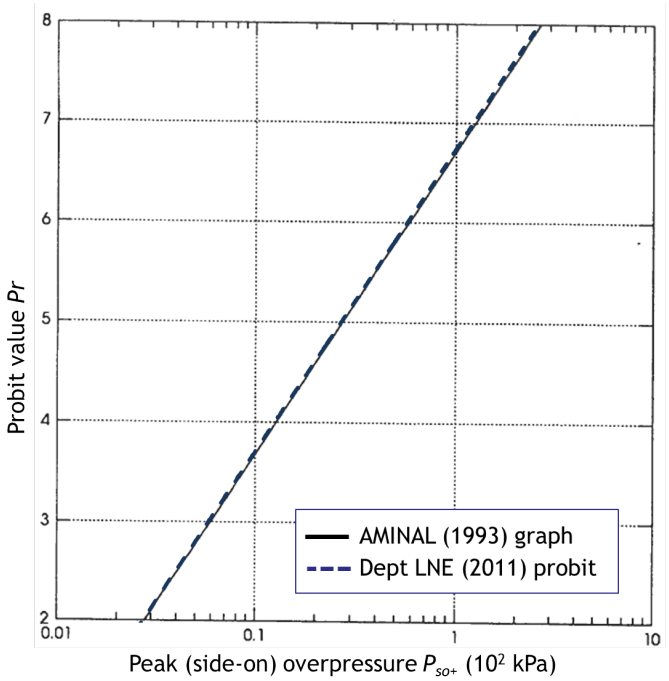

Figure 4.8: The Flemish probit relation for overpressure [3, 22]

Equation 4.10 may be considered as the mathematical expression of the 40 mbar scenario selection criterion introduced in the introducing chapter 1 on QRA in Flanders. It encompasses lethality from overpressure based on secondary glass shard injuries and crushing injuries due to structural collapse.

According to a technical report on injury prediction of industrial accidents by Protec Engineering nv (2001) [58] it were Protec engineers who developed equation 4.10 with data from Lees (1983) and HSE (1986) [31]. However, in the documentation available to the author no information is given on the choices that were made when the probit function was established.

Hereunder are given two possible sets of data points that lead to similar probit relations. Both of them rely on data on structural damage caused by blast waves. This is in line with the generally accepted theory that people inside are protected from the direct blast effect of an explosion event and the tertiary effects related to whole body displacement due to blast winds. The resulting expressions, similar to the better-known probit equation 4.10, are given in equations 4.11a and 4.11b.

$$Pr = -8.22 + 1.32 \ln P_{so+} \tag{4.11a}$$

$$Pr = -8.18 + 1.30 \ln P_{so+} \tag{4.11b}$$

The first set of data points, used to develop probit equation 4.11a, is selected from similar damage tables found in AMINAL's originally cited references HSE (1986) [31] and Lees (2005) [41]. Two thresholds with respect to window breakage are combined with an overpressure level associated with almost complete demolition of housing. These three points of choice are commented below.

1a. A mostly safe value $p_f \times p_i$ of 10^{-4} is related to the lower threshold for overpressure where one out of two windows is damaged (1.4 kPa).

1b. According to PGS1 part 2A (2003) [56] the hit probability p_h for people indoors equals 0.05. Assuming that these hits will cause injury, a 5 % lethality probability is associated with an overpressure of 6 kPa, for which the probability for window breakage p_f is higher than 0.90.

1c. A 95 % overall lethality is taken for the lower limit for overpressure where almost complete demolition of housing could be observed, which is 80 kPa.

The second set of data points, discussed below, is selected from the damage table presented in AMINAL (1993) [3]. The same methodology is followed. This time one of the selected overpressure levels has already been given a lethality probability, namely the 40 mbar (or 4 kPa) overpressure criterion, referring to a 1 % lethality limit. The probit relation that is thus computed is given in equation 4.11b.

2a. A mostly safe value $p_f \times p_i$ of 10^{-5} is related to the lower overpressure threshold for damage to windows, which equals 1 kPa.

2b. In AMINAL (1993) [3], the 1 % lethality limit is literally linked with an overpressure value (40 mbar), making it very likely that this link was used as a data point for the original probit relation.

2c. The highest overpressure given in AMINAL (1993) [3] is 70 kPa, which is an average value for whole building destruction. It is given a 90 % overall lethality indicating that most of the occupants would not survive.

Table 4.7: Overpressure versus casualty probability selection based on the structural damage observed (compiled from war data and accidental explosions) [3, 31, 41]

Source	**Structural failure**	P_{so^+}	$p_f \times p_i$
HSE (1986) [31]	50 % window panes broken	1.4 kPa	10^{-4}
pp. 39 table 5.1	> 90 % window panes broken	6.0 kPa	0.05
	housing almost completely demolished	80.0 kPa	0.95
AMINAL (1993) [3]	lower threshold for window breakage	1.0 kPa	10^{-5}
pp. 88 table 3.3.2	overpressure criterion for 1 % lethality	4.0 kPa	0.01
	all buildings totally destroyed	70.0 kPa	0.90

Table 4.7 on page 90 summarizes the specific criteria that were chosen for both argumentations discussed above. These findings were presented to Em. Prof. dr. ir. Berghmans who was involved in the original development process of the probit relation in question. In his reply, Prof. Berghmans confirmed the adherence of data points 2b. and 2c.

The true origin of the 40 mbar datum point (2b.) is as such left unexplained. However, attention is drawn to § 167 of the *Second report* of the British Advisory Committee on Major Hazards (ACMH) by Harvey et al. (1979) [30]. Based on a brief review of experimental findings, the ACMH concluded that ample justification was available for regarding the risk from an overpressure of 0.04 bar as tolerable. Given the influential status of the ACMH towards safety in the process industries, the author hypothesizes that their tolerable threshold was adopted when the probit function of study was developed. It is also noted that the ACMH even opened the door for a possible increase of permissible overpressure in their above mentioned report but recognised the need for further investigation.

Furthermore, the actual validity could be argued of the supposition that an incident overpressure of 700 mbar, capable of bringing down structures, will eventually cause harm to 9 out of 10 people present inside. Since these figures are primarily based on historical war data and military, very high yield (nuclear) experiments (e.g. Glasstone & Dolan (1977) [26]), they surely represent an overestimation of the breaking potential of an explosion from an industrial accident.

In this view, PGS1 part 2A (2003) [56] enumerates different case studies where housing damage and associated fatalities are investigated. Both earthquake and domestic explosion data are compared. Because of the correspondence in figures between the two types of calamities, PGS1 assumes that they are capable of causing equivalent personal harm. Ultimately, PGS1 concludes that a fatality rate of merely 20 to 50 % is to be associated with structural collapse due to an explosion event. With this in mind the author concludes that a fatality rate of 90 % at a peak pressure of 700 mbar (2c.) is probably on the pessimistic side and should be revised.

Additionally, the well-known Bowen curves for lung damage due to blast for an average man (target mass: 70 kg) are represented in figure 4.9 on page 91. They originate from scaled P-I curves, determined from experiments with animals by Bowen et al. (1968) [12]. They are added to underline that the threshold for lung damage due to an unobstructed blast is situated around 1000 mbar. Even though it must be noted that confinement of the blast wave indoors will influence the response disadvantageously, it may be fairly assumed that primary injury can never explain the high fatality rates originally put forward for datum point 2c.

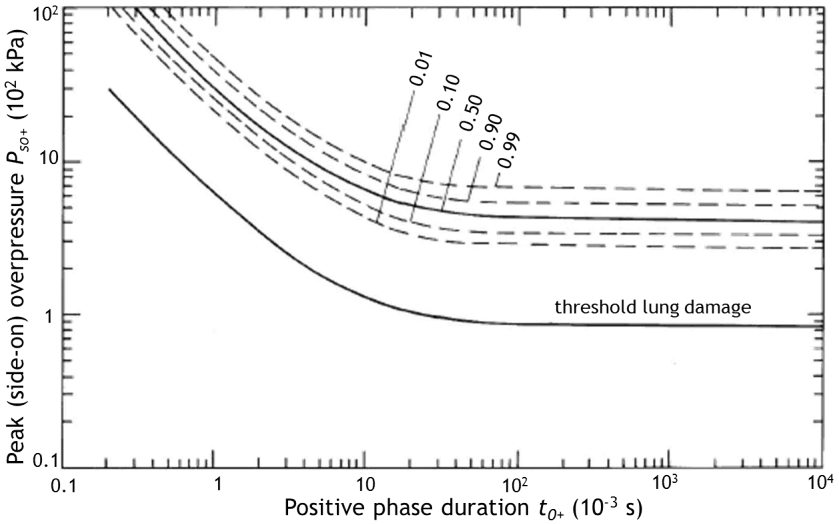

Figure 4.9: Bowen curves related to lung damage for a person weighing 70 kg [12]

4.3.2 Skull fracture from glass fragments criterion, PGS1 (2003)

CPR 16E (1989) [17] and PGS1 part 2A (2003) [56] report on the evaluation of experiments by Nowee (1985) on window panes of 1.68 × 1.13 m^2 in order to assess the probability of survival for a person located 1.75 m behind the pane. Remarkably it is assumed that the victim will consequently suffer skull fracture injury. A probability of injury p_i of 94 % is determined for a dynamic load P_r that equals twice the static strength S. The resulting probit relations, reported in CPR 16E (1989) [17] and PGS1 part 2A (2003) [56] respectively, slightly differ in the prelogarithmic fitting constant as can be seen from equations 4.12a and 4.12b.

$$Pr = 2.67 + 5.62 \ \ln\left(\frac{\mathrm{DLF} \cdot P_r}{S}\right) \tag{4.12a}$$

$$Pr = 2.67 + 3.38 \ \ln\left(\frac{\mathrm{DLF} \cdot P_r}{S}\right) \tag{4.12b}$$

PGS1 part 2A (2003) [56] complements equation 4.12b with a reasoning that leads to the additional probit equation 4.13 which is more practicable to use and does not rely on information on the dimensions and static strength of the window pane. Similar to the Dept LNE relation, this additional equation depends only on the peak (side-on) overpressure P_{so^+}.

$$Pr = -15.7 + 2.20 \ln P_{so^+} \tag{4.13}$$

Argumentation from PGS1 part 2B (2003) [57], elaborated in chapter 3, is needed to elucidate how equation 4.13 was established. Basically, the probit function for window breakage in buildings built after 1975, given in equation 3.23b, is correlated with a probability of skull fracture injury as observed from tests by Nowee. It builds on the principle presented in section 3.5 on the empirical blast strength of glass that a window fails when the dynamic peak load P_r equals the static strength S of the window times the DLF. The correlating probabilities, as well as the combined probability $p_f \times p_i$ are given in table 4.8 on page 92.

Table 4.8: Probability of window breakage and skull fracture as well as the combined effect due to impact of glass fragments [56]

P_{so^+}	$\left(\frac{P_r}{S \cdot \mathrm{DLF}}\right)$	p_f	p_i	$p_f \times p_i$
2 kPa	1	0.01	0.01	0.0001
5 kPa	1	0.50	0.01	0.0050
4 kPa	2	0.01	0.94	0.0094
10 kPa	2	0.50	0.94	0.4700

Notice how the combined probability $p_f \times p_i$ is lower for a peak (side-on) overpressure of 5 kPa than for 4 kPa, although it is generally assumed that more dangerous fragments are formed with increasing dynamic load [56]. The linear curve fit which was applied to be able to derive a continuously increasing probit relation between overpressure and lethality, as given in equation 4.13, is thus somewhat arbitrary in the range of the 40 mbar versus 1% lethality threshold. Moreover it extrapolates low overpressure data towards a higher overpressure region which makes it rather stringent above 10 kPa overpressure.

4.3.3 Bare skin penetration criterion, Gilbert et al. (1994)

Gilbert et al. (1994) formulated a probit relation with respect to Lewis' logistic equation 4.5. Their expression for bare skin penetration is given in equation 4.14a. From subsequent analysis of in situ observations, Gilbert et al. concluded later that the threshold for skin penetration and skin perforation should correspond with

a causative factor χ of $3{\cdot}10^5$ J/m^2 and $3.6{\cdot}10^5$ J/m^2 respectively. Consequently, the intercept of equation 4.14a needed adjustment to impose a probability p_i of 1 % for the threshold value thus assumed. This ultimately led to equation 4.14b.

$$Pr = -20.5 + 1.54 \ln\left(\frac{mv_0^2}{A_f}\right) \tag{4.14a}$$

$$Pr = -17.0 + 1.54 \ln\left(\frac{mv_0^2}{A_f}\right) \tag{4.14b}$$

It might be of some importance to comprehend that this transformation is far from evident. In fact, Lewis' formulation is a so-called Walker-Duncan estimation, proposed by Walker & Duncan (1967) to estimate the probability of an event as a function of several independent variables. However, during the short introduction of the stochastic probit function in chapter 1 it was explained that a probit function best describes a one-on-one stimulus-response relationship. In other words, one must be able to consider the stimulus χ as a single variable defined by some function of independent variables. Whether the three test variables are all truly independent could be argued.

4.3.4 Dept LNE (2011) versus PGS1 (2003)

The Flemish probit equation 4.11 is easily compared to the modified PGS1 probit equation 4.12 since they both depend on the same causative parameter P_{so^+}. Their outcomes are plotted in figure 4.10 (a) on page 94 for a range of overpressure between 1 and 100 kPa (i.e. from 10 mbar to 1 bar). In this range the secondary injuries related to fragmentation hazards are more likely to cause harm than the primary blast injuries, which are known to be potentially lethal if the striking overpressure rises above 1 bar (cf. super).

In figure 4.10 (b) on page 94 a detail is given around the value of interest. It shows the combined probability of injury $p_f \times p_i$ for a peak (side-on) overpressure of 40 mbar ± 30 mbar, indicating the 1 % threshold by means of a red dotted line. Both the Flemish and the Dutch model are predicting a comparable 1 % lethality threshold of 4.12 kPa and 4.24 kPa respectively.

Although everything below the 40 mbar threshold has no significant importance from a risk assessment point of view, it can be noted that the predicted risk reduces more rapidly with overpressure when adhering to the PGS1 model. Above 4.42 kPa, where the models meet, the opposite effect occurs and the resulting probabilities become firmly divergent. At 6.54 kPa overpressure the predicted lethality is already twice as high according to the PGS1 model (8.5 %) compared to Dept LNE (4.25 %). The highest discrepancy is registered around 11.27 kPa with a ratio of 2.75 between the resulting lethality probabilities (43.1 % for PGS1 versus 15.7 % for Dept LNE).

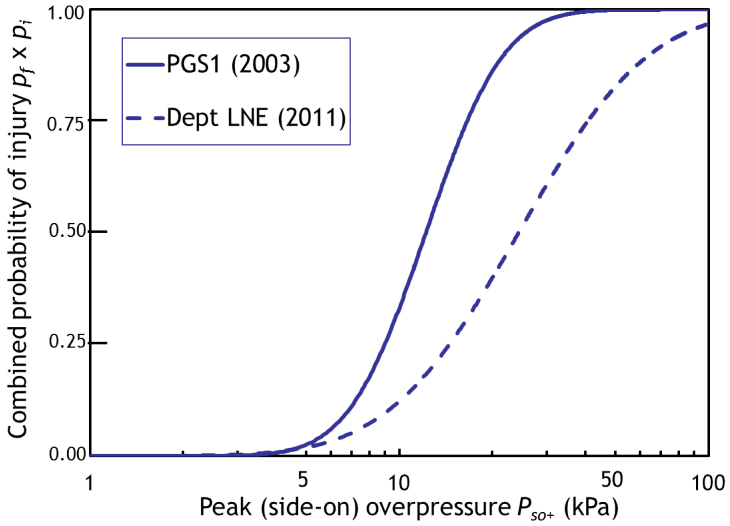

(a) Wide range of solutions: 1 kPa $\leq$ P_{so+} $\leq$ 100 kPa (logarithmic scale)

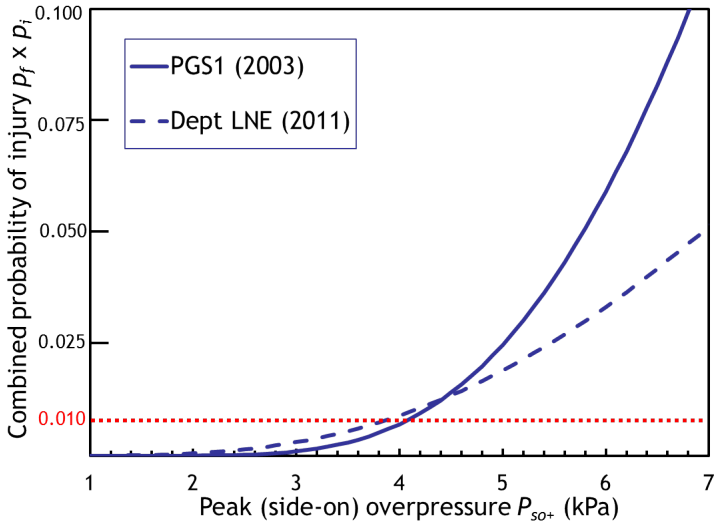

(b) Detail range for 1 % threshold: 1 kPa $\leq$ P_{so+} $\leq$ 7 kPa (arithmetic scale)

Figure 4.10: Solutions of selected probit funtions for glass injury [22, 56]

The author is convinced that the important deviations between these models originate from their dissimilar methodology of construction.

a. The Dutch model on the one hand only uses low overpressure data correlating window breakage and consequent potential skull fracture, including a theoretical extrapolation to 10 kPa if $\left(\frac{P_r}{S \cdot \mathrm{DLF}}\right)$ is equal to 2. The significance of the resulting probabilities above a certain value of P_{so^+} is thus uncertain.

b. The Flemish model on the other hand adopts historical data of structural damage to include both low and high overpressure data. Because here the higher probabilities of lethality are associated with building collapse, occurring around 70 to 80 kPa, the probit equation becomes less steep and therefore less stringent in the region of higher overpressures. However, the number of fatalities due to building collapse considered earlier to match the Flemish probit equation to the overpressure levels for structural damage can only fall back on casuistic data referring to high yield explosions.[17]

4.3.5 Dept LNE (2011) versus Gilbert et al. (1994)

The involvement of Gilbert's bare skin penetration criterion in the comparison requires experimental data such as recorded by Fletcher et al. (1980) [25] which relates overpressure to the different inputs needed to construct the causative factor χ, namely fragment mass m, impact velocity v_0 and fragment presented area A_f.

The threshold value for χ related to skin perforation was said to be equal to $3.6{\cdot}10^5$ J/m^2. Gilbert et al. (1994) seem to have associated this extent of injury with a 1 % lethality. Indeed, according to equation 4.14b a 1 % lethality ($Pr = 2.67$) is found for a value of χ equal to $3.53{\cdot}10^5$ J/m^2. The small derivation from the theoretical value can be assumed to be the result of the linear curve fitting applied during development of the probit relation.

In an attempt to give proof of this concept of comparison, Fletcher's data for 40 mbar of incident overpressure were looked up. More specifically, velocities and masses of fragments trapped in a witness plate 2.1 m behind two 107 × 51 × 0.317 cm^3 glass panes exposed face-on to a 175 ton HE detonation at an incident overpressure P_{so^+} of 4 kPa were interpreted in order to determine geometric mean values[18] for fragment mass m (1.06 g), impact velocity v_0 (22.6 m/s) and fragment presented area A_f (2.01 cm^2) based on Fletcher's least-squares linear regression equations. It is seen that the resulting causative factor found is much lower than the predicted threshold value.

[17] E.g. Gilbert et al. (1994) report a 96 % probability of lethal injury in case of complete building demolition (from Lees (2005) [41] Table 17.55).

[18] The geometric mean is defined as the n^{th} root of the product of n numbers: $\left(\prod_{i=1}^{n} x_i\right)^{1/n}$.

Only in the event where the heaviest fragments (22 g) travel at the highest recorded velocity (56 m/s) the threshold value is approached. Given the low density of glass, this kind of fragments would be rather large, thus significantly less aerodynamic. According to this argumentation such particular combination of mass and velocity seems highly unlikely. More so it can be reasonably assumed that it is difficult to accept that mass and velocity are independent from each other.

It is shortly noted that, although the overpressure P_r required to break a window face-on is approximately inversely proportional to pane area (cf. chapter 3), the geometric mean fragment velocity v_0 seems reasonably independent of pane area.[19]

Further it is interesting to acknowledge that the geometric mean presented area A_f decreases with increasing overpressure P_r (down to 0.2 cm^2 at 80 kPa reflected overpressure). Given the fact that the causative factor χ is by definition inversely proportional to A_f, the author hypothesises (for now) that Lewis' bare skin penetration criterion as adapted by Gilbert et al. (1994) might show better validity at higher overpressures but should not be adhered to in the range of overpressure of interest in this master's thesis. One can indeed expect that smaller glass shards will have higher cutting potential and will thus more likely penetrate the human skin.

In search of confirmation of this hypothesis, high density fragment data are explored. Referring to figure 4.6 on page 84 it is seen that research data for steel cubes and spheres by Sperrazza & Kokinakis can easily serve as an alternative of Lewis' data in lack thereof. With data from one of the earlier articles by Sperrazza & Kokinakis (1965) [65] on criteria to incapacitate soldiers with fragments and flechettes, the causative factor χ is calculated for a number of steel fragments of different shape. From the resulting table 4.9 on page 96 it is seen that only the flechettes compare with Gilbert's criterion for skin penetration.

Table 4.9: Data on steel fragments tested by Sperrazza & Kokinakis (1965) completed with the corresponding causative factor χ [65]

Shape	m	v_{50}	A_f	χ
Sphere	0.055 g	85.6 m/s	0.044 cm^2	$9.16{\cdot}10^4$ J/m^2
Cube	0.136 g	94.5 m/s	0.101 cm^2	$1.20{\cdot}10^5$ J/m^2
Cube	1.037 g	62.8 m/s	0.393 cm^2	$1.04{\cdot}10^5$ J/m^2
Cube	14.580 g	47.2 m/s	2.300 cm^2	$1.41{\cdot}10^5$ J/m^2
Flechette	0.111 g	61.6 m/s	0.016 cm^2	$2.63{\cdot}10^5$ J/m^2
Flechette	0.467 g	52.4 m/s	0.042 cm^2	$3.05{\cdot}10^5$ J/m^2
Flechette	0.985 g	55.2 m/s	0.075 cm^2	$4.03{\cdot}10^5$ J/m^2

[19] In his master's thesis (2008) [19], the author presented a simple argumentation showing that the fragment velocity is impulse-driven and is only depending on density ρ and thickness d.

Upon this observation it is finally concluded that Lewis' skin penetration model in its adapted form by Gilbert et al. (1994) seems to reflect hazardous effects of penetrating fragments from conventional weapons developed to this cause. However, in order to be able to predict the lethal response from window breakage, adaptation of the causative factor χ is required. Most likely the criterion must shift towards the range of 10^3 to 10^4 J/m^2. Obviously, validation will be needed. With the different tests and models for glass fragments mentioned above, there is already quite some data available to investigate this further.

4.3.6 PGS1 (2003) versus Gilbert et al. (1994)

The same strategy as above can be followed, using comparable experimental data to construct χ, in order to evaluate the likelihood of skull fracture adhered to in the Dutch PGS1 model. By means of point-on impact tests of regular shaped glass fragments on anesthesized and sheared sheep, Fletcher et al. (1980) [25] recorded a ballistic limit v_{50} for skull fracture as given in table 4.10 on page 97. Assuming that for the test event characterized by an angle θ equal to 180°, the fragment presented area A_f equals d^2, a lethality of around 12 % is found with the model of Gilbert et al. (1994).[20]

In order for the models to agree, the PGS1 probit equation 4.13 thus requires a peak (side-on) overpressure P_{so^+} of around 7 kPa. The ballistic limit v_{50} is selected as the most suited parameter to connect a point-on impact test of a glass fragment to an overpressure shattering a window. Clearly, this can be argued from the fact that the positive incident impulse i_{s^+} plays a predominant role during fragment acceleration (cf. Debroey (2008) [19]).

Table 4.10: 50 % probability of glass fragments causing skull fracture according to Fletcher et al. (1980) [25]

d	m	v_{50}	θ
0.312 cm	1 g	39.9 m/s	45°
0.312 cm	10 g	36.3 m/s	180°
0.312 cm	10 g	14.7 m/s	90°
0.421 cm*	10 g	10.8 m/s	45°
0.569 cm	100 g	4.69 m/s	90°
0.569 cm	100 g	2.74 m/s	45°

* geometrical mean of 0.312 cm and 0.569 cm

[20] Given the regular shape of the studied fragment, one could also assume A_f to be equal to 0.25 times the surface area as suggested by Sperrazza & Kokinakis (1965) [65] for cubes. The resulting lethality would then drop to around 3.5 %.

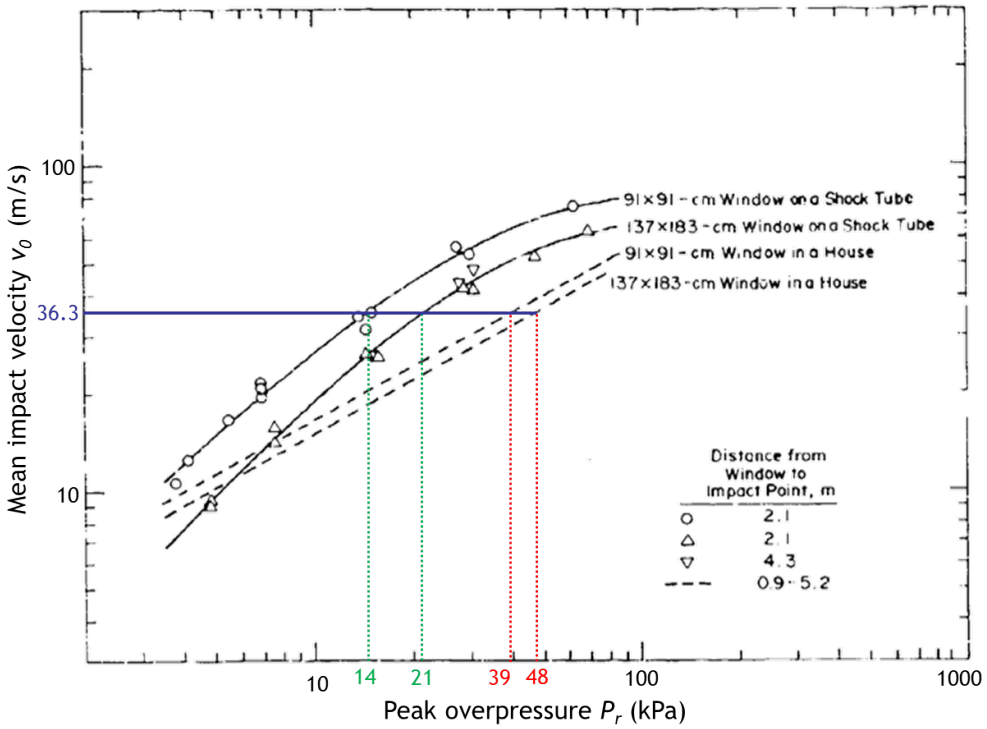

Figure 4.11: Mean impact velocity v_0 of the fragments as a function of peak overpressure P_r [25]

From Fletcher's reporting on mean impact velocity of fragments due to a given peak overpressure P_r on windows tested with a shock tube, it is found that an impact velocity of 36.3 m/s could be associated with an overpressure P_r of around 14 to 21 kPa (cf. green markings on figure 4.11 on page 98). This is two to three times the predicted peak (side-on) overpressure. From figure 2.7 on page 23 it is known that a reflection coefficient k_r equal to 2 can indeed be expected as an upper value for very low overpressure, long duration blast waves. However a k_r value of 3 in theory already requires a peak incident overpressure of 150 kPa or more.

Moreover, when repeating the exercise for data by Fletcher et al. on windows which were tested in a more realistic environment opposed to the shock tube set-up, peak reflected overpressures in the range of 39 to 48 kPa appear necessary to provoke the same mean impact velocity (cf. red markings on figure 4.11 on page 98). The same inconsistencies previously discovered seem thus once again revealed.

4.3.7 Spatial density of (trapped) fragments

Still there is one other aspect from the study by Fletcher et al. (1980) [25] which deserves some discussion, namely the spatial density of (trapped)[21] fragments ρ_D.

Two interesting observations from the experiments are summarized hereunder:

a. From a qualitative point of view, it is important to note that the region of maximum density is situated directly behind the window. At an angle of 25°, the density of glass fragments has dropped to approximately one-tenth of the density measured directly behind the window. The danger zone is thus roughly limited to the space up to some two meters directly facing the window.

b. Quantitatively speaking, thinner glazing and higher levels of overpressure yield higher spatial densities. These observations have inspired Fletcher et al. to regression equation 4.15 which can be used to predict spatial densities for window shattering due to long-duration blast waves.

$$\ln\left(\frac{\rho_D}{4.910 \cdot \mathrm{e}^{-5.012 \cdot d}} + 22.28\right) = 3.1037 + 0.05857 \cdot P_r \tag{4.15}$$

The predicted spatial density ρ_D as a function of reflected overpressure for a number of window thicknesses d according to equation 4.15 is plotted in figure 4.12 on page 99. Consider for example for a 4 kPa peak (side-on) overpressure that the effective, reflected overpressure P_r equals 8 kPa. Fletcher's equation then predicts a spatial density ρ_D of 9 fragments per m^2 in the case of a 4 mm thick window.

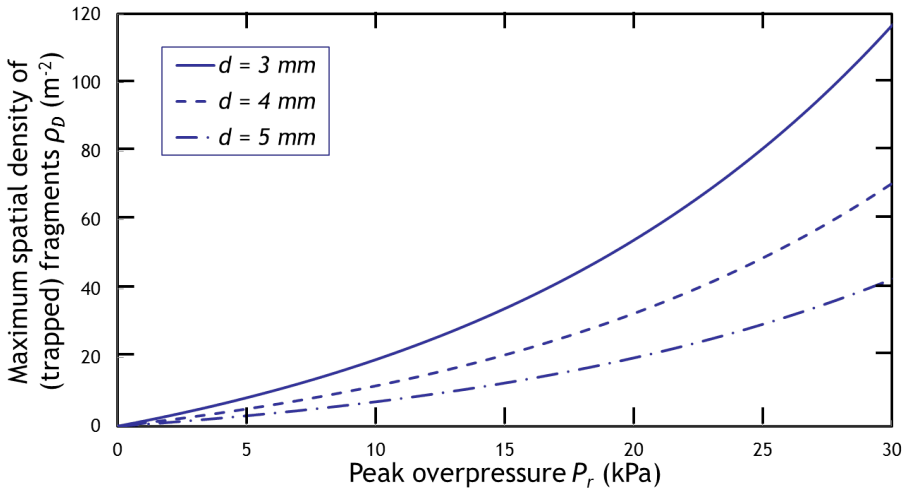

Figure 4.12: Maximum spatial density ρ_D of (trapped) fragments as a function of peak overpressure P_r according to the model by fletcher et al. (1980) [25]

[21] Other, presumably less hazardous, fragments struck the witness plate leaving impressions but were not retained and as such excluded from the analysis.

It is interesting to examine how double glazing affects the spatial density. From his own experimental work the author can attest that the effect of the subsequent shattering of two 4 mm windows increases the spatial density with a factor of 1.5 to 1.6 in a region up to two meters behind the window. To demonstrate this, six frames related to the fragment projection of a 4/15/4 IGU are shown in figure 4.13 on page 101.

Sheds coming from the outer ply generally travel less far than the sheds from the inner ply. Beyond two meters away from the window, fragments from the outer ply are rare and the factor of increase becomes less than 1.25. This can also be confirmed by the fact that a larger portion of the outer ply will remain framed if the incident overpressure is lower. This is easily demonstrated qualitatively when picture (b) and (c) in figure 1.6 on page 12 are compared to one another.

From chapter 3 on the characteristics of glass subjected to a blast load it is understood that double glazing will resist dynamic loading better. However, once double glazing is shattered, the potential harm to exposed personnel will be significantly higher due to the increased amount of mass projected.

If one would try to translate these observations to a probit relation expressing the likelihood of injury upon window breakage $p_f \times p_i$ such as the one given by Dept LNE (2011) [22], the author hypothesises that the resulting linear curve:

a. would shift to the right, adjudging a higher incident overpressure to the 1 % lethal response threshold, and

b. would have a stronger slope, accounting for the fact that upon failure, and particularly if the blast wave becomes more powerful, more sheds are projected inwards, resulting in a higher probability of multiple penetrations and lacerations.

Finally attention is drawn to the fact that the previous observations do not affect the hit probability p_h in any way. Indeed, the cloud of projected fragments is more or less characterised by the same distance envelope and impact velocity. Only there are more fragments for the same hitting surface involved. The value of p_h will just depend on the location and the presented area of the victim with respect to the windows of the building, irrespective of the presence of single or double glazing.

When safety glazing is present in the building, the situation is completely different. In section 3.3 was explained how manufacturing of fully tempered glazing results in windows with higher static strength, provoking less hazardous fragments upon failure. This means that both p_f and p_i will be significantly reduced. Even better is the use of laminated glass, where fragments are retained by the visco-elastic interlayer. Only at larger overpressure, risk of projection of the complete window pane (in one piece) might be given some consideration within a reduced danger zone. However at limited overpressure it is plausible to assume that p_h will be zero and no risk to the personnel indoors is to be expected.

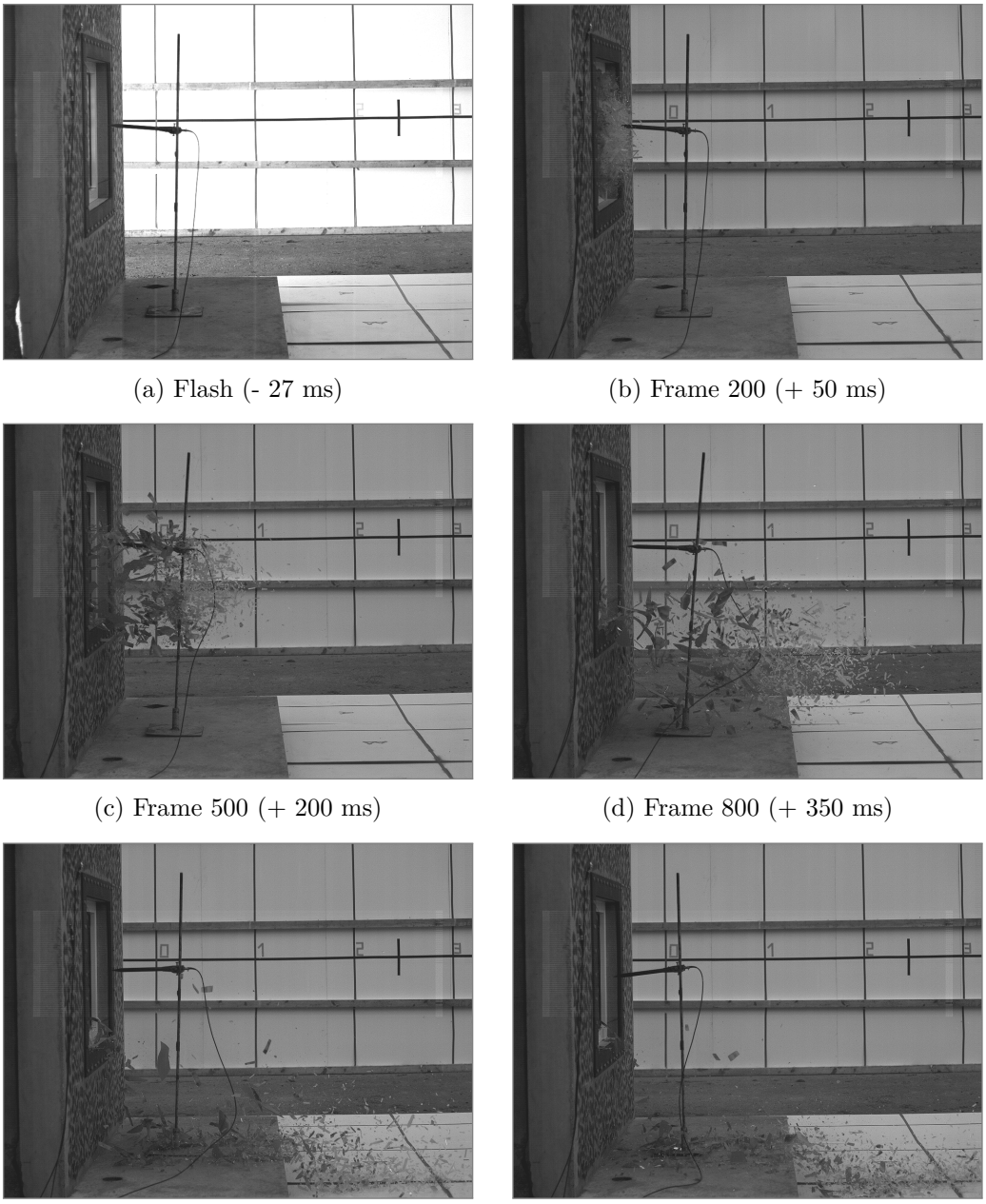

(a) Flash (- 27 ms)

(b) Frame 200 (+ 50 ms)

(c) Frame 500 (+ 200 ms)

(d) Frame 800 (+ 350 ms)

(e) Frame 1100 (+ 500 ms)

(f) Frame 1400 (+ 650 ms)

Figure 4.13: 4/15/4 IGU subjected to a 20 kPa − 16 Pa·s blast load produced by an air burst of 0.100 kg C-4 at 3.33 m.
Frames taken from HighSpeed B/W 1 operating at 2000 fps © RMA (2016)

4.3.8 Modified structural damage criterion

Finally, after having studied, evaluated and compared several models based on different hypotheses or experimental data, a tentative modification of the Flemish probit function is presented, integrating the strong points identified.

The basic idea behind the original AMINAL construction, to combine overpressure causing structural damage on the one hand to structural damage causing injury on the other hand, is adopted for reasons of simplicity. However quite some elements are borrowed from other sources, as explained below. Moreover, referring to the observations of the national energy consumption survey (ECS) conducted by Vito nv (2012) [79] and presented in section 3.3, the manifest presence of insulated glazing in Belgium is accounted for.

Low overpressure region

In the low overpressure region the argumentation from PGS1 part 2A (2003) [56] is adopted for the minor damage assessment. The skull fracture theory on the other hand, which characterises severe damage, is rejected.

The 2 kPa datum point accorded a $p_f \times p_i$ of 0.01 × 0.01 is taken over because it is frequently accepted in legislation as the lower threshold for minimal structural damage to windows. For instance, both in Walloon legislation [16] and French legislation [33, 34] this threshold is included. In Flanders, the well-known probit equation 4.10 by Dept LNE (2011) [22] returns a comparable value for $p_f \times p_i$ of $5 \cdot 10^{-4}$.

A new datum point for the average window breakage threshold is proposed. Knowing from equation 3.19 that the increase in static strength S will be found somewhere between 1 and 1.4, an average value of 1.2 is chosen, which is in line with the prescriptions of the Belgian construction federation (WTCB (1999) [80]). This value is used as a multiplier for the Flemish 40 mbar overpressure threshold accorded a minimal lethal response probability. From the observation that double glazing will result in a higher spatial density of trapped fragments ρ_D, the injury probability p_i is increased by means of a multiplier of 1.6. In conclusion, a 1.2 × 40 mbar overpressure, which is 5 kPa, is accorded a minimal lethal response probability of 0.50 × 1.6 × 0.01, which is 0.008. These calculations are in line with the methodology of PGS1.

With these two data points, probit equation 4.16a is established. Compared to the original probit, it is shifted to the right and has a stronger slope, as was intuitively predicted in the previous paragraph. Opposed to the PGS1 approach of extrapolation towards the high overpressure region, an upper limit of validity is set at 140 mbar. This overpressure is the 1 % threshold for lethal response from structural debris in the absence of windows accoring to Baker et al. (1983) [5] and is as such retained in the French legislation [33, 34]. Above this value, the effect of structural damage becomes evident and is thus added to the effect of window breakage.

Interestingly, the Dutch speaking part of Western Europe, i.e. the Netherlands and Flanders, seem to more or less agree upon the 40 mbar overpressure threshold required to break windows and subsequently create an exposure condition capable of causing a 1 % lethal response. The French speaking part on the other hand, including France and the Walloon region, as well as Germany, adhere to a threshold value of 50 mbar. NATO's AASTP-1 (2015) [1] also dictates a 50 mbar threshold towards third parties, be it in the context of storage of ammunition.[22] For the probit equation which is put forward here, a 1 % lethality is found for a peak (side-on) overpressure of 53 mbar.

High overpressure region

In the high overpressure region, the argumentation from AMINAL (1993) [3] is adopted that structural damage and the resulting crushing injuries will determine the lethal response.

It was already posited earlier that the datum point for severe damage chosen to construct the AMINAL probit is rather pessimistic about the extent of fatalities due to constructive failure. Therefore a new datum point is selected based on guidance on building collapse found in PGS1 part 2A (2003) [56]. In that reference it is attested that on average no more than 50 % of the occupants will be killed whereas everybody else will suffer injuries which are less severe. The lethal probability value is paired to an overpressure value of 300 mbar, which is a value numerously cited as a threshold for important structural damage (e.g. INERIS (2004) [33]). It is also mentioned in AMINAL (1993) [3] as the lower threshold for total destruction of houses.

The second datum point is found from the fact that both low and high overpressure regions should be joined to form a continuous criterion. The common response probability at 140 mbar found using the low pressure region probit is equal to some 17.5 %.

By means of these two data points, probit equation 4.16b is established. It is noted that at 700 mbar the probability for lethal response is 85 %.

Table 4.11: Overpressure versus casualty probability selection based on the structural damage observed

Source	Structural failure	P_{so^+}	$p_f \times p_i$
[16, 33, 56]	lower threshold for window breakage	20 mbar	10^{-4}
[16, 23, 33]	$>$ 50 % window panes broken	50 mbar	0.008
[5, 33, 34]	1 % lethality from building collapse	140 mbar	0.175
[3, 33]	important structural damage	300 mbar	0.50
[3]	all buildings totally destroyed	700 mbar	0.85

[22] Air blast overpressure threshold to determine the so-called IBD or inhabited building distance.

Probit relations

The resulting probit relations for the respective domains are given below in equations 4.16a and 4.16b for the low and high overpressure region respectively. The resulting bilinear is plotted on figure 4.14 on page 104 where it is compared to the current Flemish probit function and the PGS1 solution.

$$Pr = -9.59 + 1.43 \ln P_{so+} \quad \text{if} \quad P_{so+} \leq 0.14 \cdot 10^5 \text{ Pa} \tag{4.16a}$$

$$Pr = -7.64 + 1.23 \ln P_{so+} \quad \text{if} \quad P_{so+} > 0.14 \cdot 10^5 \text{ Pa} \tag{4.16b}$$

Combined criterion

If all five data points summarised in table 4.11 on page 103 are combined into one iteratively formed linear relation, probit equation 4.17 is found. Although preference is given to the bilinear solution, a blanket solution might be more practical to use. For reasons of clarity, this criterion is not plotted on figure 4.14 on page 104.

$$Pr = -8.85 + 1.34 \ln P_{so+} \tag{4.17}$$

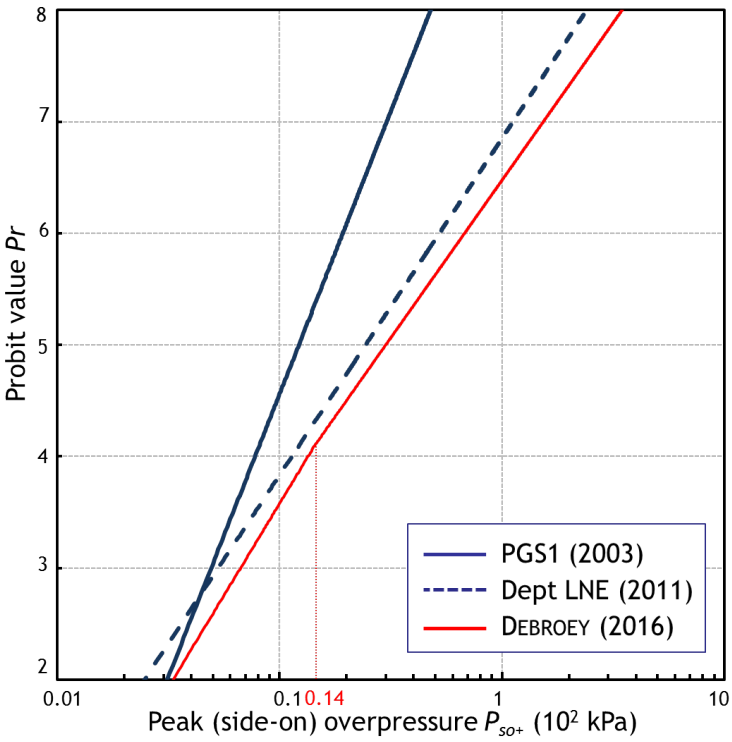

Figure 4.14: Modified structural damage criterion

4.4 Key point summary

This important chapter was dedicated to the indirect blast injuries related to overpressure that pose a threat to human beings outside the borders of a riskful establishment. It contains numerous elements found in literature that help to understand the history and pertinence of the Flemish 40 mbar overpressure criterion. For the rather low overpressures, generally expected at consequence distances relating to external human risk, the main threats that are considered relevant, are flying glass fragments after window breakage, and crushing debris after loss of structural integrity.

The parameters that matter for the assessment of the harm of fragments and debris are the projectile's mass m, its impact velocity v_0 and its presented area A_f. Different domains of fragment mass have been studied as it can be expected that this is the best parameter to predict which injury mechanism a victim will suffer from. It is noted that physical vulnerability and means of protection of the victim is usually given no consideration, which is of course a conservative approach.

Basically, three different injury mechanisms have been studied, namely skin penetration, blunt trauma and skull fracture. Because of the use and mutual overlap of multiple injury mechanisms, it has been a real endeavour to present the existing models in a clear and understandable way. The most significant models that have been discussed above are briefly resumed in the following paragraphs with comments on their strengths and weaknesses identified.

It is no surprise that this chapter is abounded with skin penetration models based on experiments with animal targets, gelatin or isolated human skin. A first category of models relies on experimental data obtained by means of ballistic, high density projectiles, developed to wound or to perforate. It includes models by Sperrazza & Kokinakis (1965, 1967) [5, 56, 65], Lewis et al. (1978) [41, 50] and McCleskey (1990) [44]. A second category of models relies on experimental data from glass fragments, projected as individual projectiles or originating from real scale blast testing on window systems using a shock tube or a realistic setting. It includes models by Glasstone (1962) [5] and Fletcher et al. (1980) [25].

Considering the context of the Flemish 40 mbar overpressure criterion, data should preferably be limited to the second category. From his investigation, the author acknowledges that the available data seem to show remarkably good correspondence. Nevertheless, attention is drawn to the approach described by Baker et al. (1983) [5] presented above, to combine data from both categories using the ratio A_f/m. The author has added new data from Fletcher et al. (1980) [25] which confirm that corresponding results are obtained through this methodology.

Intuitively, it seems rather difficult to associate window breaking with blunt trauma. Indeed, this type of injury is more likely to occur with fragments which are heavier and possess no real cutting potential, such as debris from structural

collapse. However, one could hypothetically imagine a complete sheet of safety glazing being thrown out of its frame into the interior space, causing blunt trauma. The kinetic energy incapacitation criterion, relying on the assumption that fragments with a kinetic energy of at least 58 ft-lbf ($\approx$ 79 J) are hazardous to human beings, although not specific regarding the adhered injury mechanism, is often encountered in literature to cope with this issue.

The author has presented several ambivalences on the interpretation and application of the 58 ft-lbf incapacitation criterion. From the fact that it was presumably developed for the military in the early 1900s, and due to the absence of the fragment parameter A_f, important to assess the cutting potential of a striking fragment, the author believes it should not be used to assess the injury potential of cutting glass fragments. It might have more significance for larger values of fragment mass and/or fragment density (e.g. fragments from a fragmentation grenade). Indeed, referring to the four-parameter blunt trauma model by Clare et al. (1976) as reported by Neades (1983) [50], underestimation of the fragment hazard in a range up to 100 g should be anticipated. It must yet be admitted that Clare's model is based on low density fragments ($\rho < 1.31$ g/cm^3).

Injuries from large pieces of debris, to be expected upon building collapse, have been put in relation with skull fracture threshold values in Baker et al. (1983) [5]. Tentative criteria for indirect blast effects from non-penetrating fragments with a mass of 10 lb ($\approx$ 4.54 kg) according to Clemedson et al. (1968) and White et al. (1968, 1971) have been presented. The threshold impact velocities reported as dangerous appear to be conservatively low. Moreover, further extrapolation for larger pieces of debris is not put in relation with other threshold values.

Continuously, four types of probit relations, particularly built for the injury estimation from glass fragments, have been reviewed, namely:

a. the Flemish probit relation, as prescribed by the Safety Reporting Division of the Department of Environment, Nature and Energy (2011) [22] in the frame of *Seveso-III* [61], which accords a 40 mbar overpressure to a 1 % lethality, and is based on structural damage criteria,

b. the Dutch probit relations found in the *Green Book* (1989) [17] and PGS1 part 2A (2003) [56], which are based on skull fracture criteria,

c. the Dutch probit relation found in PGS1 part 2A (2003) [56], which includes to solution b. the element of window breakage probability based on information from PGS1 part 2B (2003) [57], and

d. a probit relation by Gilbert et al. (1994) associated with experimental data on bare skin penetration by Lewis et al. (1978) as reported in Lees (2005) [41].

Both with solutions a. and c. the input variable of the probit equation is the peak (side-on) overpressure P_{so^+}. This is without any doubt the most practicable

form of operation in risk assessment calculations, where P_{so^+} follows from previously performed explosion modelling. The reader is invited to find the most important remarks with respect to the use of solution a. in chapter 5 on the main conclusions of this master's thesis. The recap of a tentative modification of the Flemish probit relation is further addressed as the ultimate end point of this research.

Solution b. seems to have become obsolete because solution c. covers its elements in a more readily usable manner. It is however noted that solution b. is able to implicitly include information on the duration of the dynamic load via the dynamic load factor (DLF). This is thus implicitly included into solution c. as well.

Finally, solution d. regroups the three fragment parameters into one causative factor χ. Two arguments have been brought forward by the author to shun this solution when dealing with glass fragments from broken windows. Firstly, strict independence of the fragment parameters, which is in theory required when a probit estimation is performed, is questionable. Secondly, the 1 % threshold value accepted by GILBERT et al. (1994) is tremendously high compared to the tentative value estimated by the author. This seems to be due to the fact that the fragment presented area A_f of glass fragments from shattered windows is several orders of magnitude higher compared to the military high density, point-on projectiles (flechettes) developed to wound or to perforate, that do fit GILBERT's definition.

This chapter ends how it started, by adducing the necessity to assess a combined probability of injury p_{tot}, dependent of three (or four) elements, namely:

p_f the probability of failure of a typical glass window, preferably estimated from window characteristics such as type and configuration of glazing, dimensions, and overall surface condition,

p_i the probability of injury from a glass fragment, preferably estimated from fragment characteristics such as mass, impact velocity, and cutting potential,

p_h the probability of being hit, preferably estimated from the spatial density ρ_D of the fragment cloud in relation to the danger zone behind the window, and the likelihood that a person is positioned in this zone, and

p_p a protective factor, indicating the influence of risk reducing measures, such as protective clothing, safety glazing or other physical mitigating elements.

For the Flemish 40 mbar overpressure criterion, p_f and p_i are mutually accounted for. p_h and p_p, however, cannot explicitly be discriminated.

References

[1, 3, 5, 10, 12, 13, 16, 17, 19, 22, 23, 25, 26, 30, 31, 33, 34, 41, 44, 56, 57, 58, 61, 65, 66, 70, 76, 79, 80]

Chapter 5

Conclusions and suggestions

In the final chapter of this work, the main discoveries with regard to the Flemish 40 mbar overpressure criterion and its associated probit relation are presented. In conclusion, the sources and hypotheses on the origin of their creation have been identified and adjustments have been suggested to improve their pertinence in modern circumstances.

Application of the Flemish 40 mbar overpressure criterion

Its application in Flanders as a pressure-based scenario selection criterion for subsequent full QRA investigation was elucidated in chapter 1. From the legal obligation for upper-tier establishments to present a report about the external human risk associated with their industrial activities in the context of the *Seveso-III* regulations (cf. Art. 10 of *Seveso-III* (2012) [61]), one understands that probit equations can offer important assistance as a consequence modelling tool for lethal response calculations related to a given physical effect.

For the Flemish probit equation 4.10, the chosen physical effect is the peak (side-on) overpressure P_{so^+}. With this probit relation, an input value of 40 mbar should logically correspond to a 1 % probability of lethality. Due to the influence of linear curve fitting in the construction process of the probit relation, the 1 % probability of lethality lies at 41.2 mbar peak (side-on) overpressure in reality.

Choice of the causative parameter

One could question why peak (side-on) overpressure P_{so^+} was selected as the explosion's physical effect to be associated with a certain likelihood of deadly injury. For the 40 mbar overpressure threshold specifically, it is known that focus lies with window breakage. Table 2.4 shows that literature abounds with references that confirm this relation. However, in section 3.5 it was noted that it is reflected pressure P_r a target is actually receiving.

Anyway, predictions about damage from an explosion are generally expressed in terms of P_{so^+}. This is very much so for structural damage which happens to be the cause of injury that lies at the origin of the Flemish probit relation. This was described in detail in section 4.3 and is yet to be resumed (cf. supra).

The available casuistic data mainly rely on damage reports from World War II, and on results from high yield (nuclear) experiments conducted in the era of the Cold War. Nowadays, they are more and more complemented by predictions from numerical simulations with computational methods such as Finite Element Method (FEM), which are preferably validated experimentally.

In an attempt to understand the physical injury potential of glass fragments, several injury models have been studied in section 4.2. In these models, fragment parameters (mass, impact velocity, and sharpness) have been brought in relation with skin penetration, blunt trauma and skull fracture. Referring to the difficulties identified to put them into practice as an alternative for the Flemish causative parameter, it is concluded that peak (side-on) overpressure is the best choice in the context of QRA.

Estimation of peak (side-on) overpressure

In section 2.3, an overview was given of the possibilities to predict P_{so^+} at any distance away from the epicentre of a free-air detonation of TNT, based on validated scaling laws. Existing techniques to correlate different types of explosions to TNT, a practice known as TNT equivalency, have been commented as well. Only the tip of the iceberg has been revealed, as it would require yet another master's thesis to thoroughly discuss this interesting topic.

The correlation techniques are argued for their low accuracy. Indeed, from section 2.1 it is known that explosions can behave quite differently, depending on their source and amount of energy, and on external conditions capable of influencing their nature. From a legislative perspective, this shouldn't be problematic, as the use of condensed phase detonation characteristics can be thought of as a worst-case approach. From the process industries' point of view, however, consequence modelling should lean as closely as possible to reality in order to avoid overestimation of consequences that could interfere with the safety targets that are prescribed by law.

What about impulse?

From the pressure-time history of a blast wave, presented in section 2.2, it is understood that the load duration should be given equal consideration when assessing the destructive potential of an explosion, as the additional effect of the continuous loading by overpressure for a longer period of time, expressed in terms of the specific impulse i_{s^+}, can increase the extent of damage significantly.

In section 3.6, a generic pressure-impulse or P-I diagram was presented. This diagram clearly demonstrates how brittle targets are vulnerable in the pressure-sensitive realm where low overpressures suffice to cause failure, as long as important impulses are registered. Unfortunately, this explosion semblance is precisely what is expected in the assessment of external human risk outside the installation's premises, where peak (side-on) overpressure P_{so^+} will surely have decreased but load duration t_d will have become large relative to the structure's natural frequency τ^{-1}. This (dynamic) loading situation is referred to as quasi-static opposed to impulsive loading where load duration is small compared to the natural response time of the structure.

Blast resistance of windows

Two different models, developed to predict blast resistance of windows, have been discussed in section 3.5. The first model, reviewed in PGS1 part 2B (2003) [57], was developed by The Netherlands Organisation of Applied Scientific Research (TNO). The second model, discussed in UFC 3-340-02 (2008) [72], was developed by the U.S. Department of Defence. Both of them rely on own experimental data to allow for dynamic response calculations using the SDOF approach by Biggs (1964) [8].

Some predicted results have been mutually compared as illustrated in the different charts of figure 3.17. This has lead to the ascertainment that thicker windows can cope with higher blast overpressures and larger windows are more prone to failure.

According to the U.S. model, windows with a larger aspect ratio fail more easily as well. As this appeared to be contradicted by the Dutch model, a specialist at TNO was contacted to clarify this discrepancy. In reply, TNO admitted that objections could be made regarding their 2003 model, reported in PGS1 part 2B, and that hence, TNO has meanwhile replaced it by a different one.

This comparative study has helped to understand that for large load durations relative to the structure's natural response time (i.e. quasi-static loading), the blast resistance of a window in terms of overpressure asymptotically reaches a lower limit value which can be used as a conservative threshold for QRA calculations. This is yet another argument to confirm how peak (side-on) overpressure alone could generally (and safely) suffice for damage prediction modelling, as prescribed in Flanders. The absence of information on impulse is thus obviated by associating lower limit values of overpressure of quasi-static events to window breakage. One can assume that this worst-case approach also covers the difficulties encountered when trying to predict the mechanical strength of window glass, discussed in section 3.2.

It was noted how unthoughtful application of the Flemish model can lead to odd results where very low yield explosion events and mere impulsive events would theoretically still predict some probability of injury even if there wouldn't be any structural damage at all. Therefore, standards for explosion-resistant glazing, presented in

section 3.4, do add requirements of specific impulse resistance to overpressure targets. Consequently, this type of safety glazing undergoes testing under quasi-static loading.

In fact, from his own experimental work in the impulsive loading domain, reported in a separate research document available for internal use at the RMA, the author has observed how window shedding is generally thrown towards the safe side (outside) of the structure. Whether this was mainly due to the subsequent negative phase of the blast wave, the negative vibrational response of the window at the moment of failure, or yet another phenomenon, such as the arrival of the incident wave at the rear side, requires further examination.

Origin of the Flemish 40 mbar overpressure criterion

At this point, the author feels that enough elements have been adduced to form a clear image of the reasons why the Flemish probit equation 4.10 exists in its current shape. Moreover, from literature review (of older data, cf. super) it is concluded that a peak (side-on) overpressure of 40 mbar is rather generally considered as a threshold for effective breakage of glass.

An influential paper by Harvey et al. (1979) [30] within the fold of the British Advisory Committee on Major Hazards (ACMH) is particularly cited as it is believed that it has played a predominant role in the determination of the Flemish threshold value. Logically, one cannot be 100 % sure of this assumption, as original documentation from the 1993 study conducted by Protec Engineering nv at the benefit of the Flemish Region (AMINAL back then, now Dept LNE) was not readily available to the author during his investigation.

Re-establishing the probit relation of Dept LNE (2011)

In order to be able to rebuild the entire probit linear, additional pinpoints were needed that connect overpressure to physical injury. This was elaborated in section 4.3. Analysis of the references cited in a more recent paper by Protec Engineering nv (2001) [58] lead to the conclusion that a higher overpressure, assumed to cause more severe building damage, had originally been related to the survival of the building's occupants. On this finding, the Flemish probit relation comes full circle as a lethal response criterion for overpressure based on structural damage.

Investigation of the available annex to the original paper by AMINAL (1993) [3] lead to the identification of a 70 kPa threshold, supposedly associated with a 90 % probability of lethality (i.e. a high number of casualties). This theory was presented to Em. Prof. dr. ir. Berghmans who was involved in the original development process of the probit relation in question. He confirmed it convincingly.

Suggested modification in the low overpressure region

Several arguments have been isolated to defend a possible need to revise the 40 mbar threshold value for effective window breakage.

Firstly, it is repeated that the criterion is based on tabled damage expectations from outdated casuistic data. In fact, the pertinence of this threshold was already openly questioned by the British Advisory Committee on Major Hazards (ACMH) in their 1979 report mentioned earlier [30]. Indeed, from the discussion on explosion energy in section 2.3, it could be argued whether high yield nuclear detonations comparable to several kilotons of TNT provide good reference data to assess the incident scenario's anticipated in the process industries.

Next, the positive evolution of the target material of study is highlighted. One can indeed trust that technology has continuously improved the quality of manufacture of window systems, making it plausible to expect that the overall resistance has improved and that the existence of flaws in the material has been brought down to a minimum.

Additionally, safety glazing is slowly setting in, stimulated by national standard NBN S 23-002 (2007) [49] that recommends the use of fully tempered glass (FTG) or laminated glass for a number of situations. However, this is not strictly of application to domestic houses and offices, where annealed glass (ANG) and heat-strengthened glass (HSG) are more current (cf. section 3.3).

From the observations of the national energy consumption survey (ECS), conducted by Vito nv (2012) [79], it was concluded that most of the dwellings in Belgium have insulated glazing installed. On the one hand, it is generally accepted that double glazing is more rigid, suggesting survival is more likely at 40 mbar overpressure. On the other hand, own experiments have clearly demonstrated that the presence of more mass in the glazing system will have a detrimental influence on the spatial density of the fragment cloud following blast rupture. Both these effects have been credited quantitatively.

Armed with these arguments, a TNO methodology, discussed in section 4.3, was elaborated upon to adjust the 40 mbar for 1 % lethality datum point. This resulted in the establishment of a 50 mbar for 0.8 % lethality datum point.

It was noted that this criterion approaches the 50 mbar for 1 % lethality criterion adhered to in quite some external safety publications found in literature, including the Walloon, French and German legislative documentation as well as the recently revised NATO publication AASTP-1 (2015) [1] on safe storage of ammunition.

Finally, two shortcomings from a victim's point of view were identified. Unfortunately they remain unaccounted for with the use of the Flemish probit relation.

Firstly, the work by Lewis et al. (1978) [50] and Fletcher et al. (1980) [25], presented in section 4.2, clearly gave proof of the significant protective nature of clothing against skin penetration.

Secondly, the combined probability of a person being injured by the breaking of a window should somehow include the fact that the presence of the victim inside the danger zone behind a window is stochastic as well.

Suggested modification in the high overpressure region

Recall from above that the high overpressure region is defined by a 700 mbar threshold, supposedly associated with a 90 % probability of lethality due to crushing injuries. Analysis of recent damage safety documentation and casuistic data on structural collapse have resulted in a growing belief that this datum point is too pessimistic nowadays.

Alternatively, the author has associated a 300 mbar threshold with a 50 % probability of lethality. The overpressure value was adopted for its numerous citations as a threshold for important structural damage (e.g. INERIS (2004) [33]). A decrease of the associated probability of lethality down to 50 % seemed to be valid from recent data presented in PGS1 part 2A (2003) [56].

The author's modified structural damage criterion

The low and high overpressure regions were split at an overpressure of 140 mbar. This overpressure is the 1 % threshold for lethal response from structural debris in the absence of windows according to Baker et al. (1983) [5]. Above this value, the effect of structural damage becomes evident and must as such be added to the effect of window breakage.

The complete set of selected data points is summarized in table 4.11. The resulting set of probit relations are given in equations 4.16a and 4.16b.

Although preference is given to the bilinear solution, a blanket solution is also derived, as it might be more practical to use. With the introduction of the author's combined criterion, given in equation 4.17, this interesting study has finally come to its conclusion.

Suggested future study

Because academic research can never be completed by means of a single master's thesis, some additional topics of study that would support the findings and assumptions of this research are identified.

As mentioned above, a through study of the current state-of-the-art on TNT equivalency of VCE's, BLEVE's and other types of explosions introduced in section 2.1 could be an interesting exercise to do, in order to investigate the conservativeness of the current approach.

With regard to blast resistance (and potential injury) of modern window systems, real-scale experiments have been conducted for the impulsive loading domain. Recommendations have been put onto paper that will be helpful when similar tests are organized in the quasi-static domain. During a future campaign, currently being prepared by the RMA, this could already be the subject of further investigation.

Specifically regarding the lethal response from window breakage based on bare skin penetration, a more fundamental research could be performed, that would allow to determine how GILBERT's thresholds for the causative factor χ, presented in section 4.3, should be shifted to a lower range. With the different tests and models for glass fragments mentioned in section 4.2, there is already quite some data available to investigate this further.

Excursuses throughout the text

Additionally, the author would like to explain why the scope of this master's thesis has clearly reached beyond the topic of study on numerous occasions. Indeed, the attentive reader will have encountered excursuses towards theory of explosions, materials science, standards for explosion resistance testing, modal analysis, and conventional weapons effects.

The author has in fact seized this opportunity to explore his subject in such a way that he would be able to benefit from it in his professional activities as a teaching assistant in military engineering and materials science, and as a range officer involved in experimental research on explosion effects on structures. By spending a great deal of time and intellect in the fundamental parts of his study, the author sincerely feels he has significantly enlarged his knowledge and understanding of these technical topics. Hopefully, the respected reader has not experienced the presence of these excursuses as an interfering factor with respect to the true aim of this study.

Bibliography

[1] AASTP-1. Allied Ammunition Storage and Transport Publication 1: NATO guidelines for the storage of military ammunition and explosives. NATO, 2015.

[2] AASTP-4. Allied Ammunition Storage and Transport Publication 4: Manual on explosives safety risk analysis. NATO, 2008.

[3] AMINAL. Richtlijn evaluatie veiligheidsrapportering. KU Leuven, 1993.

[4] ASTM F1642-04. Standard test method for glazing and glazing systems subject to airblast loadings. American Society for Testing and Materials, 1996.

[5] Baker et al. *Explosion Hazards and Evaluation.* Elsevier, 1983.

[6] Baker. *Explosions in Air.* Southwest Research Institute, 1973.

[7] Beveridge et al. *Forensic Investigation of Explosions*, 2nd ed. Taylor & Francis, 2012.

[8] Biggs. *Introduction to Structural Dynamics.* McGraw-Hill, 1964.

[9] Bjerketvedt et al. *Gas Explosion Handbook.* GexCon, 1992.

[10] Borgers. *Pyrotechniek en Beschermingsconstructies.* Nederlandse Defensie Academie, 2015.

[11] Bourgois. *Constructies onderworpen aan Explosiebelastingen.* Koninklijke Militaire School, 1999.

[12] Bowen et al. *Estimate of Man's Tolerance to the Direct Effects of Air Blast.* Lovelace Foundation for Medical Education and Research, 1968.

[13] Breeze et al. Perforation of fragment simulating projectiles into goat skin and muscle. *Journal of the Royal Army Medical Corps 159* (2013), 84–89.

[14] Bulson. *Explosive Loading of Engineering Structures.* E & FN Spon, 1997.

[15] Callister. *Materials Science and Engineering: An Introduction*, 7th ed. John Wiley & Sons, 2007.

[16] Cellule Risques d'Accidents Majeurs. *Vademecum*: Spécifications techniques relatives au contenu et à la présentation des études de sûreté, des notices d'identification des dangers et des rapports de sécurité. Département de l'Environnement et de l'Eau, 2015.

[17] CPR 16E. *Green Book*: Methods for the determination of possible damage to people and objects resulting from releases of hazardous materials. Committee for the Prevention of Disasters caused by Dangerous Substances, 1989.

[18] CPR 18E. *Purple Book*: Guideline for quantitative risk assessment. Committee for the Prevention of Disasters caused by Dangerous Substances, 1999.

[19] Debroey. *Analyse van de Interactie van Schokgolven met Gordijngevels*. Master's thesis, Koninklijke Militaire School, 2008.

[20] Dienst Veiligheidsrapportering. *Code Risicocriteria*. Departement Leefmilieu, Natuur en Energie van de Vlaamse overheid, 2006.

[21] Dienst Veiligheidsrapportering. *Handbook Failure Frequencies*. Departement Leefmilieu, Natuur en Energie van de Vlaamse overheid, 2009.

[22] Dienst Veiligheidsrapportering. *Richtlijn Probitfuncties*. Departement Leefmilieu, Natuur en Energie van de Vlaamse overheid, 2011.

[23] Duijm. *Acceptance Criteria in Denmark and the EU*. Danish Ministry of the Environment, 2008.

[24] FEMA 459. *Incremental Protection for Existing Commercial Buildings from Terrorist Attack*. U.S. Dept of Homeland Security, 2008.

[25] Fletcher et al. *Glass Fragment Hazard from Windows broken by Air Blast*. Lovelace Biomedical and Environmental Research Institute, 1980.

[26] Glasstone & Dolan. *The Effects of Nuclear Weapons*. U.S. Department of Defence, 1977.

[27] Gorrens. Lectures on quantitative risk analysis. KU Leuven, 2015.

[28] GSA-TSO1-2003. Standard test method for glazing and window systems subject to dynamic overpressure loadings. U.S. General Services Administration, 2003.

[29] Haldimann. *Fracture Strength of Structural Glass Elements*. PhD thesis, Ecole Polytechnique Fédérale de Lausanne, 2006.

[30] Harvey et al. *Second report*. Advisory Committee on Major Hazards, 1979.

[31] HSE. The effects of explosions in the process industries. *Loss Prevention Bulletin, Issue 068* (1986).

[32] Hubbard & Hamilton. Studies of the chemical durability of glass by an interferometer method. *Journal of Research of the National Bureau of Standards 27* (1941), 143–157.

[33] INERIS. Guide technique relatif aux valeurs de référence de seuils d'effets des phénomènes accidentels des installations classées. Ministère de l'Ecologie et du Développement Durable, 2004.

[34] INERIS. La résistance des structures aux actions accidentelles. Ministère de l'Ecologie et du Développement Durable, 2007.

[35] ISO 16933. Glass in building - explosion-resistant security glazing - test and classification for arena air-blast loading. International Organisation for Standardization, 2007.

[36] ISO 16934. Glass in building - explosion-resistant security glazing - test and classification by shock tube loading. International Organisation for Standardization, 2007.

[37] Janovsky et al. Small-scale physical explosions in shock tubes in comparison with condensed high explosive detonations. *Journal of Loss Prevention in the Process Industries 26* (2013), 1590–1596.

[38] Kingery & Bulmash. *Air Blast Parameters from TNT Spherical Air Burst and Hemispherical Burst.* U.S. Army Ballistic Research Laboratory, 1984.

[39] Kinney & Graham. *Explosive Shocks in Air*, 2nd ed. Springer-Verlag, 1985.

[40] Krauthammer et al. *Structural Design for Physical Security.* Structural Engineering Institute of the American Society of Civil Engineers, 1999.

[41] Lees. *Loss Prevention in the Process Industries*, 3rd ed. Elsevier, 2005.

[42] Marchand. *Blast-resistant and Anti-terrorism Design.* Protection Engineering Consultants, 2011.

[43] Mays et al. *Blast Effects on Buildings*, 2nd ed. Thomas Telford, 2009.

[44] McCleskey. A comparison of two personnel injury criteria based on fragmentation. *24th DoD Explosives Safety Seminar* (1990).

[45] NBN EN 13123-1. Windows, doors and shutters - explosion resistance - requirements and classification - part 1: Shock tube. Belgisch Instituut voor Normalisatie, 2001.

[46] NBN EN 13123-2. Windows, doors and shutters - explosion resistance - requirements and classification - part 2: Range test. Belgisch Instituut voor Normalisatie, 2004.

[47] NBN EN 13124-1. Windows, doors and shutters - explosion resistance - test method - part 1: Shock tube. Belgisch Instituut voor Normalisatie, 2001.

[48] NBN EN 13124-2. Windows, doors and shutters - explosion resistance - test method - part 2: Range test. Belgisch Instituut voor Normalisatie, 2004.

[49] NBN S 23-002. Work in glass. Belgisch Instituut voor Normalisatie, 2007.

[50] Neades. *An Examination of Injury Criteria for Potential Application to Explosive Safety Studies.* U.S. Army Ballistic Research Laboratories, 1983.

[51] Ngo et al. Blast loading and blast effects on structures - an overview. *Electronic Journal on Structural Engineering Special Issue: Loading on Structures* (2007), 76–91.

[52] Nowee & Harmanny. *De Invloed van het Glaskozijn op de Dynamische Bezwijkbelasting van Ruiten.* Prins Maurits Laboratory, TNO, 1983.

[53] NSG Nippon Sheet Glass. ATS-129: Properties of soda-lime silica float glass. Pilkington, 2013.

[54] Overend et al. Diagnostic interpretation of glass failure. *Structural Engineering International*, 2 (2007), 151–158.

[55] Peugeot et al. *TNT Equivalency: Misconceptions and Reality.* Limited report L-132. Munitions Safety Information Analysis Center, 2006.

[56] PGS1. Deel 2A: Effecten van explosie op personen. Ministerie van Verkeer en Waterstaat, 2003.

[57] PGS1. Deel 2B: Effecten van explosie op constructies. Ministerie van Verkeer en Waterstaat, 2003.

[58] Protec Engineering nv. *Schademechanismen & -criteria - Inschatting t.b.v. de Externe Veiligheidsrapportage.* BVR 002, 2001.

[59] Scholze. Chemical durability of glasses. *Journal of Non-Crystalline Solids*, 52 (1982), 97–103.

[60] Sedlacek et al. Glass in structural engineering. *The Structural Engineer 73* (1995), 17–22.

[61] *Seveso-III-Directive 2012/18/EU.* On the control of major-accident hazards involving dangerous substances. *Official Journal of the European Union*, 2012.

[62] Smith & Renfroe. *Glazing Hazard Mitigation.* Whole Building Design Guide resource page, Applied Research Associates Inc., 2010.

[63] Smith & Hetherington. *Blast and Ballistic Loading of Structures.* Butterworth-Heinemann, 1994.

[64] Solomos & Karlos. Report EUR 26456 EN: *Calculation of Blast Loads for Application to Structural Components*. EC Joint Research Centre - Institute for the Protection and Security of the Citizen, 2013.

[65] Sperrazza & Kokinakis. *Criteria for Incapacitating Soldiers with Fragments and Flechettes*. U.S. Army Ballistic Research Laboratories, 1965.

[66] Stewart. Blast injuries: Preparing for the inevitable. *Emergency Medicine Practice 8*, 4 (2006).

[67] Timoshenko. *Theory of Plates and Shells*, 2nd ed. McGraw-Hill, 1959.

[68] TM 5-0855-1. Design and analysis of hardened structures to conventional weapons effects. Joint Departments of the Army, Air Force, and Navy and the Defence Special Weapons Agency, 1997.

[69] TM 5-1300. Structures to resist the effects of accidental explosions. Joint Departments of the Army, Air Force, and Navy, 1990.

[70] Trbojevic. *Risk Criteria in EU*. Risk Support Limited, UK, 2005.

[71] UFC 3-340-01. Design and analysis of hardened structures to conventional weapons effects. U.S. Department of Defence, 2002.

[72] UFC 3-340-02. Structures to resist the effects of accidental explosions. U.S. Department of Defence, 2008.

[73] UFC 4-010-01. DoD minimum antiterrorism standard for buildings. U.S. Department of Defence, 2007.

[74] Van de Vyver & Vande Mergel. *Behaviour of Laminated Glass under Impact and Blast Loading*. Master's thesis, UGent, 2015.

[75] van den Berg. The multi-energy method: A framework for vapour cloud explosion blast prediction. *Journal of Hazardous Materials*, 12 (1985), 1–10.

[76] Van den Schoor. Lectures on quantitative risk analysis. KU Leuven, 2014.

[77] Van den Schoor. Lectures on explosion safety. KU Leuven, 2015.

[78] Verplaetsen. Lectures on explosion safety. KU Leuven, 2015.

[79] Vito nv. *Energy Consumption Survey for Belgian Households*. EUROSTAT, 2012.

[80] WTCB. Technische voorlichting 214: Glas en glasproducten, functies van beglazing, 1999.

[81] Yadav. *Nuclear Weapons and Explosions: Environmental Impacts and Other Effects*. SBS Publishers, 2007.